# INVESTIGATIONS OF THE LARGE IMPACT OF RELATIVELY SMALL TEMPERATURE GRADIENTS ON REGIONAL CLIMATE IN THE TROPICS

by

Alexandria M. Russell

A dissertation submitted to Johns Hopkins University in conformity with the requirements for the degree of Doctor of Philosophy.

Baltimore, Maryland

April, 2017

# Abstract

Near-term impacts of climate change on regional climates are uncertain due to the complex dynamics of internal climate oscillations. In the tropics where climate change is expected to be most intense, these dynamics continue to modulate decadal variability and play a major role in the manifestation of climate trends regionally. For this reason not all areas of the Tropics have been warming to the same extent and small gradients in temperature trends manifest throughout the Tropics. In particular, the tropical Andes Mountains of South America stand out as a hot-spot of recent mid-tropospheric warming relative to Pan-Tropical land areas due to the interactions between local dynamics, regional oscillations and global anthropogenic change. Regional trends in mid-atmospheric temperatures over the Andes Mountains may be driven by changes in the radiative balance. These regional changes in free-atmospheric temperatures and radiation are poorly captured by global climate models. However, this dissertation demonstrates that simulations with a regional climate model improve upon these deficiencies by increasing resolution and better parameterizing local physical processes. Furthermore, relatively small changes in sea surface temperatures associated with internal modes of variability within the Atlantic and Pacific Oceans appear to contribute to local changes in radiative balance over the Andes Mountains. Not only do the small temperature gradients in and across the oceans modulate the influence of anthropogenic climate change on a regional scale, but they also drive long time period variability in the Pacific Ocean. In

fact, the multidecadal responsiveness of the atmospheric wind stress to oceanic temperatures in the equatorial Pacific is shown to be stronger when sea surface temperature gradients are relatively small. These studies reveal the importance of small temperature gradients set up by internal climate oscillations in modulating long time period variability on a regional level in the Tropics.

Primary Reader, Thesis advisor: Dr. Anand Gnanadesikan

Secondary Reader: Dr. Benjamin Zaitchik

# Acknowledgements

Dr. Anand Gnanadesikan and Dr. Benjamin Zaitchik of the Department of Earth and Planetary Sciences at Johns Hopkins University made essential contributions to the work in this dissertation and are co-authors on many potions of the work herein. Funding for Alexandria Russell was provided by the Johns Hopkins University Department of Earth and Planetary Sciences and the National Science Foundation Water, Climate and Health IGERT at Johns Hopkins University (Grant # 1069213).

# Dedication

This thesis is dedicated to my father Steve Russell who pushed me to work hard and never be satisfied with anything, and my mother Gwyn Russell who taught me how to stay positive and keep perspective.

# Contents

# List of Figures

# List of Tables

# Chapter 1. Introduction

The Earth System is very complex and is characterized by dynamically coupled processes that drive the circulation of the atmosphere and oceans on a variety of spatial and temporal scales. There are several internal modes and patterns of variability which modulate the global climate on interdecadal to multidecadal timescales. For example, the El-Nino Southern Oscillation (ENSO) – a primary mode of variability in the tropical Pacific Ocean with teleconnections to weather and climate patterns around the world – has been shown to vary in amplitude on multidecadal to centennial timescales (e.g. Wittenberg et al. 2009). Interactions between the various climate modes affect the transport of mass, momentum and energy within the Earth System and create highly inhomogeneous trends in sea surface temperatures and other climatic parameters on short time-scales.

Even in the presence of the well-documented and highly certain increases in the heat content of the global climate due to anthropogenic activities, internal climate oscillations have a large influence on the manifestation of climate change on a regional level. In particular, atmospheric and sea surface temperature increases are expected to be higher in the tropics than in the midlatitudes relative to the natural internal variability and therefore the impacts of and changes in tropical oscillations will play a huge role moving into the near-future. It is anticipated that the average warming of the climate will continue to fluctuate with the internal modes of variability and vary by location based on regional interactions on multidecadal timescales (IPCC, 2013). In fact, natural decadal

fluctuations in the eastern equatorial Pacific Ocean have acted to slow the early 21st century rise in global mean surface air temperatures, contributing to a temporary "hiatus" in global warming (e.g. Meehl et al. 2013, Kosaka and Xie 2013, England et al. 2014). However, the influence of natural decadal climate variations on global mean temperatures is gradually decreasing relative to the anthropogenic warming signal (e.g. Wantanabe et al. 2014).

While the predicted future warming of the atmosphere and oceans are relatively consistent across global climate models on average, the near-term impacts of warming on regional climate are less certain (IPCC, 2013). In addition, due to the natural long time period variability of the Earth System, it is often difficult to distinguish externally forced changes in climate due to anthropogenic activities from the natural fluctuation in the system (e.g. Stevenson et al. 2012). As such, characterizing the impact of both internal variability and externally-forced climate change is extremely challenging, especially on a regional level for the reasons stated above. In particular, the manifestation of and driving factors of regional trends on multidecadal timescales in the Tropics are not well characterized. This dissertation describes and works toward an understanding of multidecadal climate variability in the Tropics and demonstrates that relatively small horizontal temperature gradients in both the atmosphere and the ocean are major drivers of regional climate variability.

Due to the fact that the Coriolis parameter near the equator is small, horizontal temperature gradients in the tropical atmosphere are also very small – often less than a few degrees across the entire globe. As such, it is possible to dynamically derive tropical circulation as a result of only the near-surface temperature and humidity and the free-

tropospheric relative humidity, while holding free-tropospheric temperatures fixed (Sobel et al. 2001, Sobel and Bretherton, 2000). This so-called "weak temperature gradient (WTG) approximation" is a highly useful simplifying assumption that can be used to accurately represent tropical circulation in idealized models. However, relatively small horizontal gradients in both free atmospheric temperatures and sea surface temperatures in the Tropics have been shown to play an important role in setting processes ranging from tropical cyclone formation (Vecchi and Soden 2007, Gnanadesikan et al. 2010) to the decadal variability of droughts (Seager and Ting 2017). Hence, this dissertation describes the impact of relatively small temperature gradients in both the free atmosphere and in sea surface temperatures on modulating regional climate variability on multidecadal timescales, in particular over South America and in the tropical Pacific Ocean. In addition, it examines the ability of models and model-based products to adequately capture these effects.

In Chapter 2, I demonstrate evidence for an enhanced multidecadal warming signal in the tropical free atmosphere. Global climate model simulations project that the tropical Andes Mountains of South America, which are particularly vulnerable to climate change due to a reliance on snow/glacial melt for freshwater resources, will experience enhanced warming in the near future, with both higher rates of warming at higher elevations within the mountain range itself and localized enhancement of warming exceeding surrounding areas of the globe. Yet recent surface temperature changes in the tropical Andes do not show evidence for either elevation dependent warming or regional enhancement of warming on average. However, it remains a possibility that the expected warming trends in this region have begun to manifest in other ways, for example in the free atmosphere

or at intermediate mountain elevations. This chapter proposes evidence from several reanalysis products that there has indeed been a regional enhancement of mid-tropospheric warming around the Central Andes over the past few decades which makes this region stand out as a hot spot within the broader Pan-Tropics. This trend is generally not reproduced by historical AMIP climate model simulations, which suggests that the mechanisms through which the atmosphere is warming over the Central Andes are not adequately captured by climate models. Possible explanations for the enhancement of warming in this region are considered. One particularly intriguing mechanism involves an increase in the Outgoing Longwave Radiation (OLR), which is seen in observations but not in models, and would correspond to a decrease in cloudiness. Overall, the enhanced free-atmospheric warming over the tropical Andes Mountains of South America demonstrates the importance of horizontal gradients in tropical free-atmospheric temperatures on long time scales.

In Chapter 3 I show that multidecadal trends in outgoing longwave radiation (OLR) and free-atmospheric temperatures over tropical South America, and over the Andes Mountains in particular, which AGCMs generally fail to capture, can be simulated by a regional climate model forced with reanalysis boundary conditions. Correlation analysis further demonstrates that the recent changes in regional climate over tropical South America may be influenced by trends in sea surface temperatures in the adjacent oceans, with strong links to shifts in the Atlantic Multidecadal Oscillation, as well as shifts in the positioning and/or intensity of the midlatitude jet. It is clear from this study that model simulations of the impacts of SST gradients (and trends) on regional climate can be improved through increased model resolution and better physical parameterizations.

Chapter 4 presents an investigation of the coupling strengths between the ocean and atmosphere on multidecadal timescales in the tropical Pacific. Sea surface temperatures (SSTs) in the tropical Pacific vary as a result of the coupling between ocean and atmosphere driven largely by the El Niño – Southern Oscillation (ENSO). ENSO amplitude is known to vary on long timescales, which makes it difficult to quantify its response to climate change and constrain the physical processes that drive it. In order to characterize the long-period variability in ocean-atmosphere coupling strengths, a linear regression of local SST changes is applied to the GFDL 4000-yr CM2.1 model and 500-yr CM2Mc model pre-industrial control runs, while also comparing to the observationally-constrained ECDA dataset. This analysis reveals that the amplitude of ENSO is strongly modulated by the response of the atmosphere to sea surface temperature gradients on multidecadal timescales.

In sum, I examine observational evidence for tropical temperature gradients in the free atmosphere, describe the role of SST gradients in driving regional OLR trends, and thoroughly demonstrate the impact of SST gradients on ENSO amplitude, all on multidecadal timescales. This work makes progress towards a better understanding of the impact of tropical oscillations on regional climate and an improvement of the modelling of these effects. This dissertation concludes with a discussion of the current advances in the field, some challenges for modeling the impacts of relatively small temperature gradients in the Tropics and suggestions for future progress.

# Chapter 2. Are the Central Andes a warming hotspot?

**The work in this chapter has been published as a manuscript in the *Journal of Climate* (Russell et al. 2017) and is reproduced here.**

## 2.1 INTRODUCTION

Future global climate model simulations indicate that mountain regions will experience high rates of warming by the end of this century, with the most dramatic temperature changes at high northern latitudes and at the highest elevations within respective mountain ranges (Bradley et al. 2004; Bradley et al. 2006; Nogues-Bravo et al. 2007). The tropical Andes Mountains of South America appear as a potentially localized hot spot of warming compared to other areas of the world in terms of both surface temperatures (Nogues-Bravo et al. 2007) and free-atmospheric temperatures (Bradley et al. 2004; Bradley et al. 2006). Additionally, the first regional climate modeling study devoted to future changes over the tropical Andes Mountains indicated that the largest warming is expected to occur at the highest elevations (Urrutia and Vuille 2009). Note that the word "tropical" here is used in the broadest sense. However there is often a distinction in the literature between the inner tropical Andes and the outer tropical (a.k.a. subtropical or extratropical) Andes. There are no consistent definitions for these terms throughout the literature – in the strictest sense, the inner tropics are defined as equatorial regions between about 5°N and 5°S (e.g., Rabatel et al. 2013), while in the broadest sense

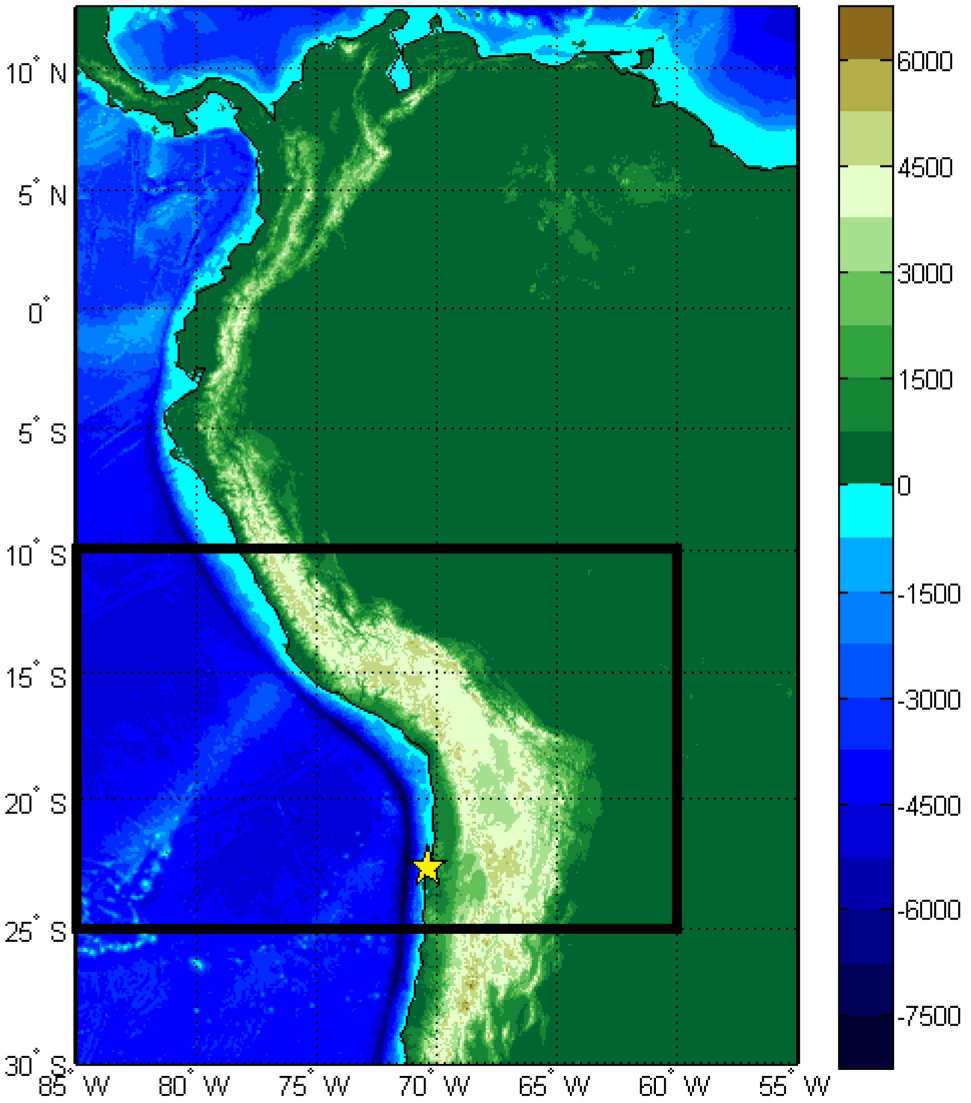


**Figure 2.1:** ETOPO1 elevation of study area in meters above sea level. Yellow star indicates the location of the SCFA sounding station. Black box indicates the Central Andes Mountains.

they indicate areas between about 15°N and 15°S (e.g., Vuille et al. 2008; Garreaud 2009).

The tropical Andes Mountains (Figure 2.1) will be heavily impacted by these projected changes because they rely heavily on snow/glacial melt for freshwater and play

host to very specialized ecosystems and biodiversity niches. In the inner tropical Andes Mountains glaciers act as major natural reservoirs of fresh water. In fact, the strong and minimally varying solar radiation in the inner tropical Andes inhibits the persistence of seasonal snow cover outside of the highest glaciated peaks, unlike in midlatitude mountain ranges like the Rockies or the Alps. Even as far south as La Paz, Bolivia (~16°S) snow cover does not endure for more than a few days (LeJeune et al. 2007; Soruco et al. 2015). Therefore, the glaciers are the only water reservoirs that change on a seasonal timescale in the inner tropical Andes (Kaser et al. 2003; Kaser et al. 2005) and are therefore the primary natural buffers to the highly seasonal rainfall cycle and key indicators of climate change in this region (e.g. Mark et al. 2005). Meanwhile, seasonal snowpack plays an increasingly important role in controlling river runoff in the outer tropical and midlatitude Andes Mountains (Masiokas et al. 2006). Yet while some local sites have exhibited extreme surface temperature trends, the average surface temperature rise over recent decades in the high elevation tropical Andes of 0.1 to 0.2°C/decade over the time frame 1981-2010 reported by Vuille et al. (2015) does not exceed the average trend over tropical land-areas of 0.3°C/decade as calculated from the Climate Prediction Center (CPC) GHCN+CAMS global land surface air temperature analysis (Fan and van den Dool 2008). In addition, although several studies have documented recent intensification of warming with elevation in other mountainous regions of the world (Mountain Research Initiative EDW Working Group 2015), surface observations in the tropical Andes Mountains do not show evidence for stronger warming at higher altitudes (e.g., Vuille et al. 2003; Vuille et al. 2015).

This is perhaps not surprising given that the manifestation of climate change in mountain regions is not necessarily a linear increase in temperatures with elevation. In fact, there have been reports of warming only at intermediate elevations in other mountain ranges, such as near the freezing line (e.g., Pepin and Lundquist 2008). Hence it may be that the manifestations of enhanced warming in the tropical Andes are simply not captured by the current available surface observations. Therefore, two questions arise: first, have we seen any other evidence of enhanced warming in the tropical Andes in recent decades, either in the free atmosphere or at intermediate mountain elevations and second, to what extent can we have confidence in model projections of future warming in this area?

Interestingly, the long-term Met Office SCFA radiosonde station – World Meteorological Organization (WMO) station # 85442 located in coastal Antofagasta, Chile at 23.43°S, 70.44°W (yellow star in Figure 2.1) with an elevation of 137.0 meters above sea level (Met Office 2006), exhibits a surface cooling trend and an off-surface elevated warming trend over the time period 1979-2008 (Figure 2.2). The characteristic contrast between coastal cooling and warming aloft has been attributed by others to the strong modulating effect of the Pacific Ocean which creates a sharp vertical thermal stratification in the atmosphere on the western side of the Andes (Falvey and Garreaud 2009). Nonetheless, the off surface warming of about 0.4°C/decade (Figure 2.2) is notable and could suggest that the free atmosphere over the adjacent mountains to the east could be experiencing similarly high rates of warming. While this observed warming is not actually at the surface, it is within the range of high elevation surface warming reported by Vuille et al. (2015) for nearby areas in the Andes. This radiosonde

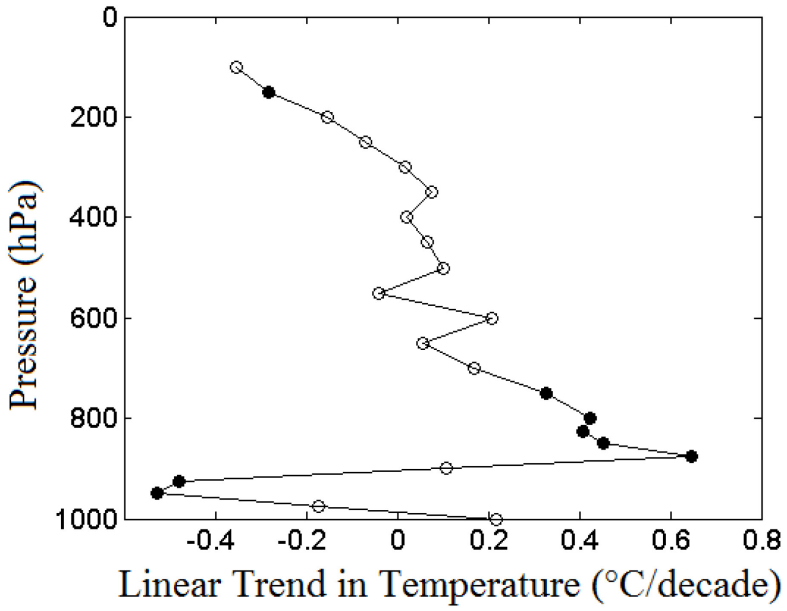


**Figure 2.2:** Linear trend over the time period 1979-2008 SCFA vertical profile sounding station temperatures (°C/decade), where filled dots indicate that the trend is significant to the 0.05 alpha level and empty dots indicate that the trend is insignificant.

record is relatively unique because it is the only observation to our knowledge that is in close proximity to the tropical Andes Mountains which profiles vertical temperatures consistently over the past 30+ years.

In the face of such limited in-situ information, one often turns to reanalysis products to provide an interpolated model-driven yet data-constrained picture of climate. For example, Schauwecker et al. (2014) showed that there are strong warming trends in the 500mb temperature field over the Andes Mountains around 20°S between 1979 and 2012 in two reanalysis products. Yet it is unclear whether this recent warming trend is consistent across products or reliable compared to in-situ data and whether these trends are indicative of the elevated warming that is expected to occur in coming decades. Due to the scarcity of in-situ observations in and over the high elevation tropical Andes and the seeming inconsistency between recent observations and future climate projections,

both a methodical examination of the available data-based and model-driven products and a thorough investigation of common signals and inter-product inconsistencies are needed in this region.

Therefore, this paper considers whether reanalysis products exhibit recent manifestations of enhanced warming in the free atmosphere above or at intermediate elevations within the tropical Andes Mountains of South America and whether historical climate model simulations are consistent with reanalysis products. The following section describes the methodological approach. Section 3 describes the datasets used in this analysis. Section 4 shows the results of the analysis. Section 5 considers potential mechanisms which may be driving recent regional temperature changes. Section 6 discusses the implications of our work for the understanding of climate change in this area.

## 2.2 METHODS

In order to better understand temperature changes in and around the tropical Andes Mountains of South America, this study first explores changes in key parameters in reanalysis products. Specifically, linear trends in the monthly mean 500mb temperature and the freezing level height (FLH) time series are examined to determine whether there has been enhanced warming in the free atmosphere or at intermediate elevations in the tropical Andes over recent decades. The specific details of trend analysis are outlined at the end of this section. The altitude of the 0°C isotherm (FLH) was calculated by linearly interpolating the pressure-level geopotential height data for each product (either

reanalysis or climate model) to the pressure level at which the corresponding pressure-level temperature data equals 0°C. We limit our analysis to the time frame 1979-2008 in order to allow direct comparison with historical climate model simulations.

Although reanalyses use a fixed model and a stable data-assimilation system (Kalnay et al. 1996), it is important to be aware that changes in the global observing system with time can create inhomogeneities, most dramatically in 1979 with the dawn of the satellite era, but even in recent decades, for example with the addition of the SSM/I and NOAA-15 satellites (Santer et al. 1999; Trenberth et al. 2001; Bengtsson et al. 2004; Fasullo 2012). In fact homogenization efforts are ongoing in multiple reanalysis products. Owing to the fact that most reanalyses are not well suited to trend analysis due to frequent changes in data sources, it is recommended that trend analysis be performed on multiple reanalyses at once; if trends are robust across reanalyses then it is more likely, though still not completely certain, that trends are genuine (Kistler et al. 2001).

Therefore in this paper several reanalyses are analyzed in order to identify similarities between them which may be indicative of real trends. It is also for this reason that we include the National Oceanic and Atmospheric Administration (NOAA) Twentieth Century Reanalysis Version V2 (20CR), which is specifically designed to be used for trend analysis due to its consistency of integrated data sources (primarily surface pressure station readings) throughout time. One caveat of 20CR however is that it does not assimilate radiosonde observations, which means that the free atmospheric temperatures are largely dependent on the base model's vertical dynamics. Another caveat is that although 20CR maintains consistent data source *types*, it does not maintain consistent data *points* – that is, data stations are added and removed at various times in the historical

record. However, this is less of a problem in recent decades when the locations and number of contributing stations have not changed drastically (e.g. Oliver 2015).

From the results of the trend analysis, there appears to be an enhanced mid-tropospheric warming signal in the greater vicinity of the Altiplano – a region henceforth referred to as the Central Andes which is defined as areas within the bounding box 10°S–25°S, 85°W–60°W (black box in Figure 2.1) that are greater than 1500 m.a.s.l. – in many of the reanalysis products. Therefore, trends in 500mb temperatures and FLH in the Central Andes are compared to the average trends over Pan-Tropical land areas – areas 30°N-30°S, > 0 meters above sea level (m.a.s.l.) – as a means to see if changes in this area have been disproportionately intense. The Central Andes are assessed as a tropical warming "hot spot" by testing whether this area has experienced average rates of change that are greater than 1 standard deviation above the global tropical over-land area average. Longitude-Pressure cross sections of tropospheric temperature trends across the Central Andes are also examined in order to see how the vertical distribution of recent warming compares to future projections of warming in the area.

In the interpretation of results from reanalysis products, it is often difficult to separate the effects of actual data vs. data-assimilation methodologies and model dynamics. Therefore, we perform a synonymous trend analysis and "hot spot" assessment of tropical tropospheric temperature and FLH changes in several Coupled Model Intercomparison Project phase 5 (CMIP5) simulations (Taylor et al. 2012) from the Atmospheric Model Intercomparison Project (AMIP) which are constrained only by observational records of sea surface temperatures (SSTs) and sea ice. A comparison to AMIP simulations allows us to distinguish the effects of SST forcing on atmosphere-only models and gives us a

sense for how well the AMIP simulations capture recent climate change in the area of interest. Results may differ across reanalyses and AMIP simulations, for a number of reasons namely: 1) the assimilation of data, particularly satellite-based temperatures, 2) the potentially different SST datasets utilized, and 3) differences in the physical parameterization in the underlying models, which will be especially important in areas that are poorly constrained by observations. Note that there is a well-documented tendency for GCMs to overestimate historical upper tropospheric (~200mb) tropical temperature trends compared to observations (e.g., Fu et al. 2011; Po-Chedley and Fu 2012). While there is some evidence that constraining atmospheric GCMs (AGCMs) with prescribed SSTs reduces this discrepancy (Mitchell et al. 2013), it is still an important issue to be aware of when analyzing tropospheric temperature trends.

### 2.2.1 TREND ANALYSIS

To calculate the trend with time, a linear fit is calculated for the raw monthly time series data at each product/model grid cell or station. All time series data are truncated at whole year intervals; so that a reported trend from 1979-2008 is computed including all months from January 1979 through December 2008. Note that because we are working only with whole years, the slope of the linear fit line for the deseasonalized monthly time series is negligibly different from the slope for the raw monthly time series. The slope of the linear fit line yields the annual rate of change in units/year. The total change over the time period of interest is simply the unit trend multiplied by the number of years (e.g., 1979-2008 → 30 years). Throughout the paper we report the total trend in 500mb

temperature and OLR because the annual rates of change would be quite small, whereas we report the annual rate of change in FLH because the total trend would be quite large. The symbol Δ is used to indicate either the total change or the rate of change depending on the variable – note the reported units to differentiate the two. Trends are only computed if at least 75% of the time series is complete (non-missing).

In order to determine whether trends are significant, we apply the Mann–Kendall test (Mann 1945; Sen 1968), a nonparametric, distribution-free method, which tests the null hypothesis of trend absence against the alternative of trend. This test has been shown to work well even with non-normal and incomplete time series (Yue and Pilon 2004). Throughout this paper we use a significance level of 0.05, meaning that the time series has a linear slope that has a 95% chance of being different from zero.

## 2.3 DATA / PRODUCTS

### 2.3.1 ELEVATION DATA

We use ETOPO1 elevation data at 1 arcminute (1/60th of a degree) resolution (Amante and Eakins 2009), averaged in a simple manner to determine the approximate model or product-based grid cell elevations. For spatial longitude-latitude plots, the average elevation of the product-based grid cells is determined by averaging all ETOPO1 points within each grid cell (not including points along the edges of the cells). A thin yellow contour is shown on all spatial plots to denote grid cells with average elevations above 1500 meters, which indicates mountainous regions. For meridionally-averaged

longitude-pressure plots, a red line shows the maximum ETOPO1-derived average product/model grid cell elevation within that meridional range and is also not a real feature, but rather a guide for the maximum product/model topography within that meridional range.

### 2.3.2 REANALYSIS PRODUCTS & AMIP CLIMATE MODELS

Monthly mean output is examined in a suite of 6 reanalysis products, the details of which, including abbreviations which are used throughout this paper, are outlined in Table 1. This is an adapted version of the table provided on the University Corporation for Atmospheric Research (UCAR) Climate Data Guide Website (Dee et al. 2015). Most of the reanalyses examined here are based on AGCMs, except for CFSR which is based on a coupled atmosphere-ocean-land surface-sea ice model. Although all of the models underlying the reanalyses use terrain-following coordinates, there are some differences in the interpolation rules to convert to pressure surfaces in the final product. Therefore, some products/models (e.g., MERRA) have missing information at low altitude pressure levels which may happen to intersect with high elevation land, while other products (e.g., CFSR) generate output at all pressure levels. Monthly mean output is also examined for a suite of 6 AGCMs, the details of which are outlined in Table 2, which were run for the 30-year historical time period 1979–2008 in accordance with the AMIP time-varying SST protocol. The results for the AMIP models are ensemble averages over all available realizations for each model.

**Table 2.1:** Details of reanalysis products utilized in this analysis (abbreviations in parentheses), including their data assimilation scheme and model vintage (column 2), data output resolution (column 3), atmospheric model and resolution (column 4), data assimilation scheme (column 5), and citation (column 6).

| **Reanalysis Product** | **Data Assimilation Scheme & Model Vintage** | **Data output Resolution** | **Atmospheric Model & resolution** | **Data Assimilation Scheme** | **Citation** | **Source** |
|---|---|---|---|---|---|---|
| NCEP-NCAR Reanalysis I (R1) | 1995 | 2.5° x 2.5° x 28 vertical levels, 3 hPA top | NCEP operational global spectral model, T62 | Spectral Statistical Interpolation, 3D-VAR, Climate Data Assimilation System (CDAS-1) | Kalnay et al. (1996) | NOAA/OAR/ESRL PSD http://www.esrl.noaa.gov/psd/ |
| NCEP-DOE Reanalysis 2 (R2) | 2001 | 2.5° x 2.5° x 28 vertical levels, 3 hPA top | NCEP operational global spectral model, T62 | 3D-VAR | Kanamitsu et al. (2002) | NOAA/OAR/ESRL PSD http://www.esrl.noaa.gov/psd/ |
| NOAA Twentieth Century Reanalysis Version V2 (20CR) | 2009 | 2° x 2° x 28 levels 10 hPA top | NCEP GFS08ex atmosphere/land model, T62 | Ensemble Kalman Filter | Compo et al. (2011) | NOAA/OAR/ESRL PSD http://www.esrl.noaa.gov/psd/ |
| NASA GSFC Modern Era Retrospective- | 2009 | 0.5° x 0.667° x 72 vertical | GEOS v5.2.0 | 3D-VAR, with Incremental | Bosilovich et al. (2008) | GMAO and the GES DISC http://gmao.gsfc.nasa.gov/merra/ |

| | | | | | | |
|---|---|---|---|---|---|---|
| Analysis for Research and Applications (MERRA) | | levels, 0.01 hPA top | | Analysis Updates | | |
| ECMWF ERA-Interim (ERA-Int) | 2006 | 0.75° x 0.75° x 60 vertical levels, 0.1 hPA top | IFS cycle 31r2 (CY31r2), T255 | 4D-VAR | Dee et al. (2011) | ECMWF http://apps.ecmwf.int/datasets/ |
| NCEP Climate Forecast System Reanalysis (CFSR) | 2009 | 0.5° x 0.5° x 64 vertical levels, 0.266 hPA top | CFS, T382 | 3D-VAR | Saha et al. (2010) | NCAR CISL RDA http://rda.ucar.edu/datasets/ds093.2/ |

**Table 2.2:** Details of the AMIP climate models utilized in this analysis (abbreviations in parentheses), including the number of ensemble members (column 2), the atmospheric model output resolution (column 3), and citation (column 4).

| **AMIP Climate Model** | **Number of Ensemble Members** | **Atmospheric Model Output Resolution (Lon x Lat)** | **Citation** |
|---|---|---|---|
| Flexible Global Ocean-Atmosphere-Land System model, Grid-point Version 2 (FGOALS-G2.0) | 1 | 2.8125° x irregular (6 - 2°) | Li et al. (2013) |
| Goddard Earth Observing System Chemistry-Climate Model (GEOSCCM) | 3 | 2.5° x 2° | Garfinkel et al. (2015) |
| Institute for Numerical Mathematics Climate Model 4 (INMCM4) | 1 | 2° x 1.5° | Volodin et al. (2010) |
| Model for Interdisciplinary Research on Climate v5 (MIROC5) | 2 | 1.40625° x irregular (~1.4°) | Wantanabe et al. (2010) |
| Centro Euro-Mediterraneo sui Cambiamenti Climatici Climate Model (CMCCCM) | 3 | 0.75° x irregular (~0.75°) | Scoccimarro et al. (2011) |
| GDFL High Resolution Atmospheric Model (GDFL HiRAM) C180 | 3 | 0.625° x 0.5° | Zhao et al. (2009) |

## 2.4 RESULTS

### 2.4.1 REANALYSIS PRODUCTS

Since in-situ measurements of surface temperatures do not yet support the idea that the tropical Andes Mountains are experiencing regionally enhanced warming (Vuille et al. 2015), we turn to reanalysis products to determine how free atmosphere temperatures and the FLH have been changing in the tropical Andes. In an extension of the analysis done by Schauwecker et al. (2014), total trends in the 500mb temperature field ($\Delta$T500mb) are examined over the global Tropics in 6 reanalysis products over the time period 1979–2008. Looking at the spatial distribution of mid-tropospheric temperature changes in the different reanalyses, we see that the Central Andes Mountains – specifically around the Bolivian Altiplano – stand out when compared to the rest of the Pan-Tropics (Figure 2.3), though the spatial extent and magnitude of warming trends vary between the different reanalysis products. In fact, the average $\Delta$T500mb over the Central Andes is greater than 1 standard deviation above the Pan-Tropical land-area average trends in most of the reanalyses examined here, except for CFSR and 20CR, the latter of which still comes very close to that threshold (Table 3). Note that due to the wide range of values between the various products (e.g. Table 3), the subpanels displaying the spatial distribution of trends throughout this paper (e.g. Figure 2.3) may have different contour scales which is necessary to make regional differences more visually apparent. It is also evident from looking at the area-averaged time series of 500mb temperatures that the trend over the Central Andes is much steeper – with an inter-product average $\Delta$T500mb

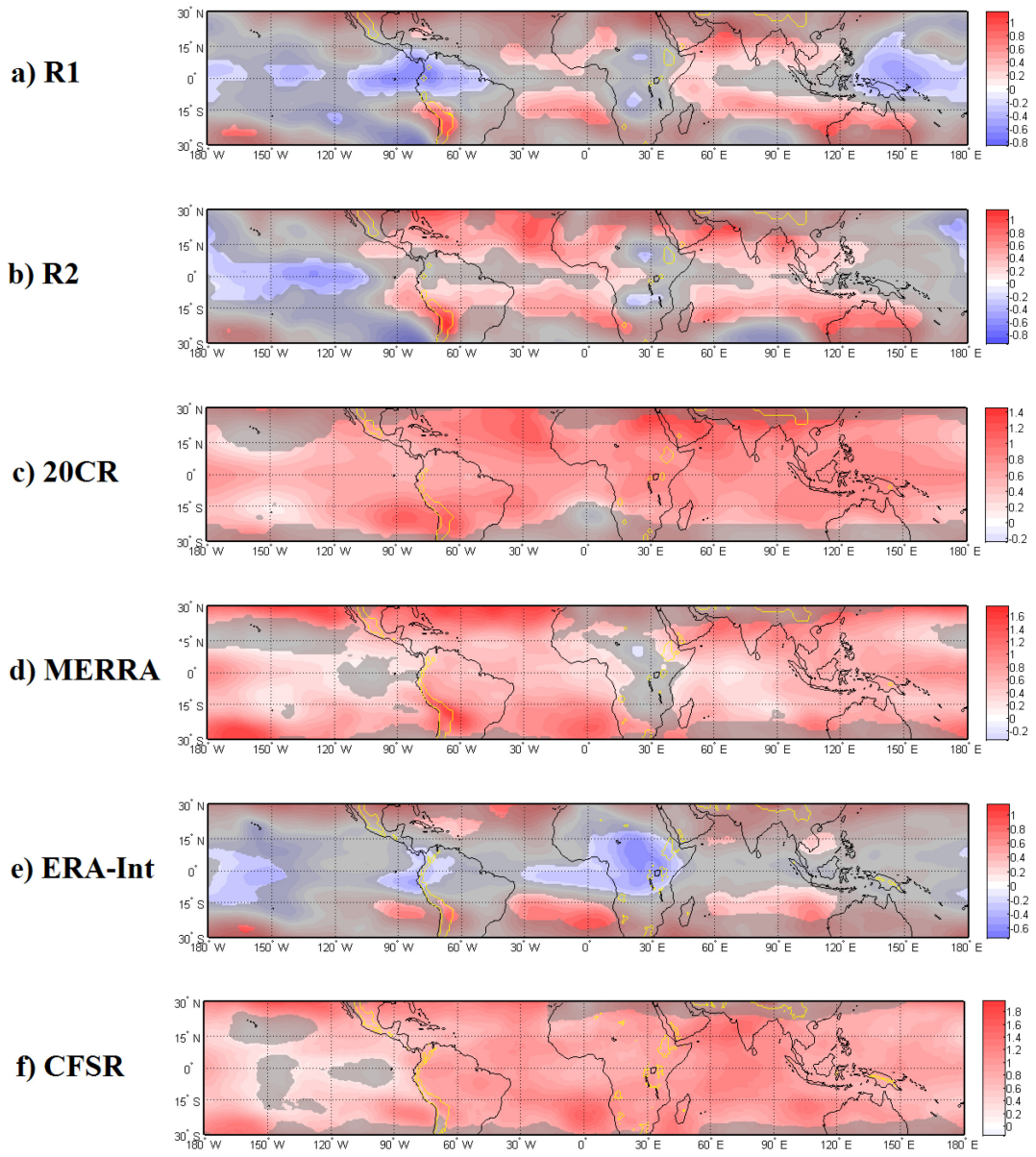


**Figure 2.3:** Total change in 500 mb temperature (°C) over the time period 1979-2008 in each reanalysis product: a) R1, b) R2, c) 20CR, d) MERRA, e) ERA-Int, and f) CFSR. Note that each spatial plot has different color bar limits. The yellow contour outlines areas with mean ETOPO1 elevation greater than 1500 meters. Insignificant trends are grayed-out.

of 0.84°C compared to 0.50°C over Pan-Tropical land areas – and is much more uniform across the different reanalysis products (Figure 2.4). Therefore the Central Andes

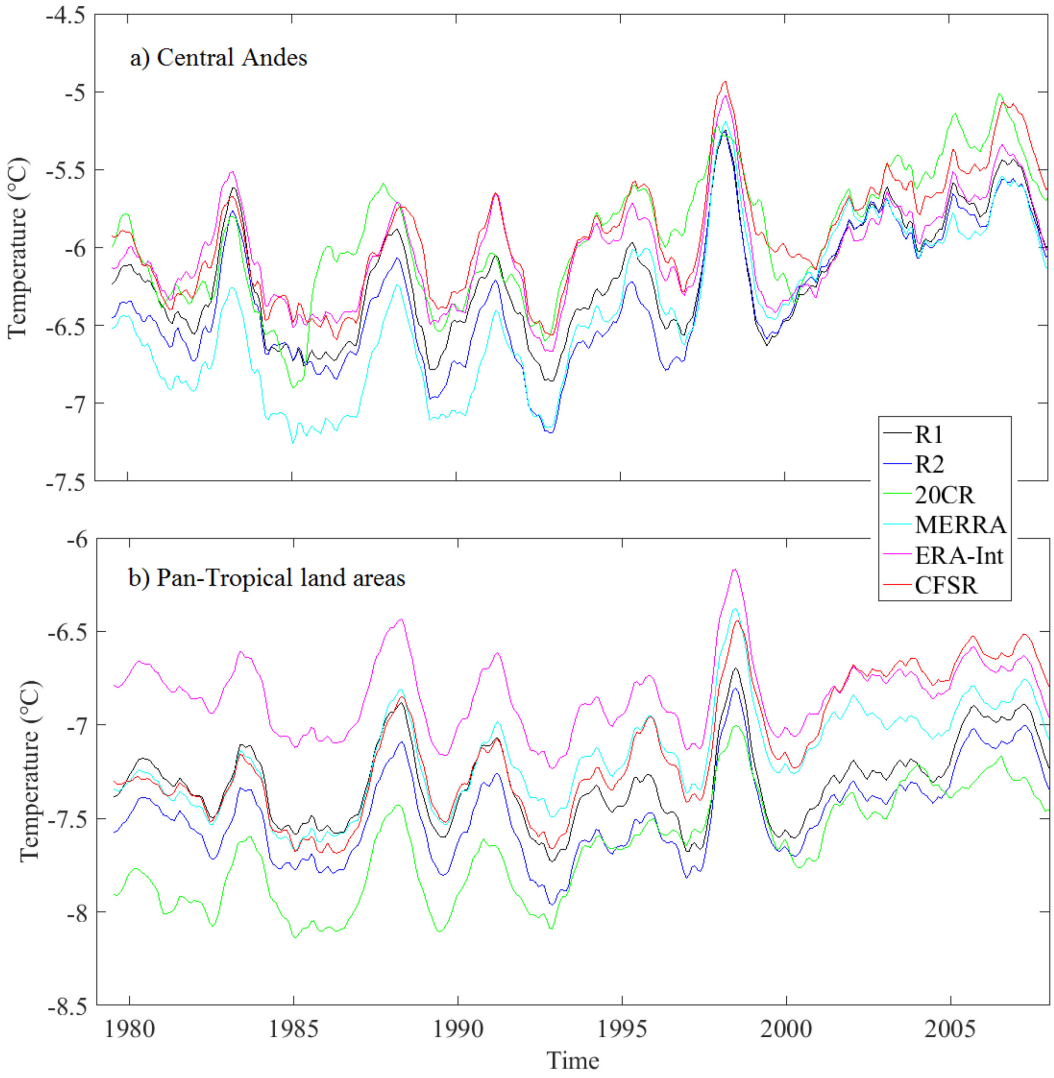


**Figure 2.4:** Deseasonalized time series of the 500 mb temperatures (°K) averaged over a) the Central Andes and b) Pan-Tropical land areas in several reanalysis products: R1 (black), R2 (blue), 20CR (green), MERRA (cyan), ERA-Int (magenta), and CFSR (red).

Mountains have likely been a hot spot in recent decades in terms of mid-tropospheric warming.

On the other hand, the majority of reanalyses do not show the Central Andes as being a hot spot in terms of FLH. The reanalyses examined here indicate an average rate of change in the FLH (ΔFLH) over the Central Andes Mountains ranging anywhere from about 2 to 7 m/yr over the 30-year timeframe 1979-2008 (Table 4). R1 is the exception

to this because it shows negative (though insignificant) changes in FLH. Overall, the Andes Mountains do not stand out as an area of enhanced FLH change with respect to the rest of the Tropics (Figure 2.5), except in CFSR where there are extremely local rises in FLH in the Central Andes Mountains. Upon close inspection of Fig. 2.5f, the CFSR product shows both the high Central Andes and the high Himalayas as being areas of extremely local FLH rise. In fact, if we adjust the minimum mountain elevation from 1500 m.a.s.l. to 3000 m.a.s.l., both the Central Andes and the tropical Himalayas (30°N-25°N) qualify as hot spots of FLH change in CFSR. It is however worthwhile to note that there is not a strong correlation between elevation and FLH rise in those mountain ranges – rather local dynamics appear to determine the locations of the strongest changes in FLH.

Yet in the majority of reanalyses, the Central Andes display ΔFLH that are within 1 standard deviation of the Pan-Tropical land-area average (Table 4) and therefore do not meet this paper's qualification for hot spot. Note that while MERRA does indicate that the Central Andes qualify as a hot spot of FLH change, the center of FLH rise activity is actually located over the Chaco lowlands and not in the Andes Mountains themselves (Figure 2.5). Nonetheless, although the Central Andes have not likely been a hot spot of FLH activity, moderate rises are still very important in this region because the FLH determines the extent of snow packs and/or glaciers (e.g., Bradley et al. 2009), as well as potentially how much precipitation is received as snow vs. rain (e.g., Shook and Pomeroy 2012).

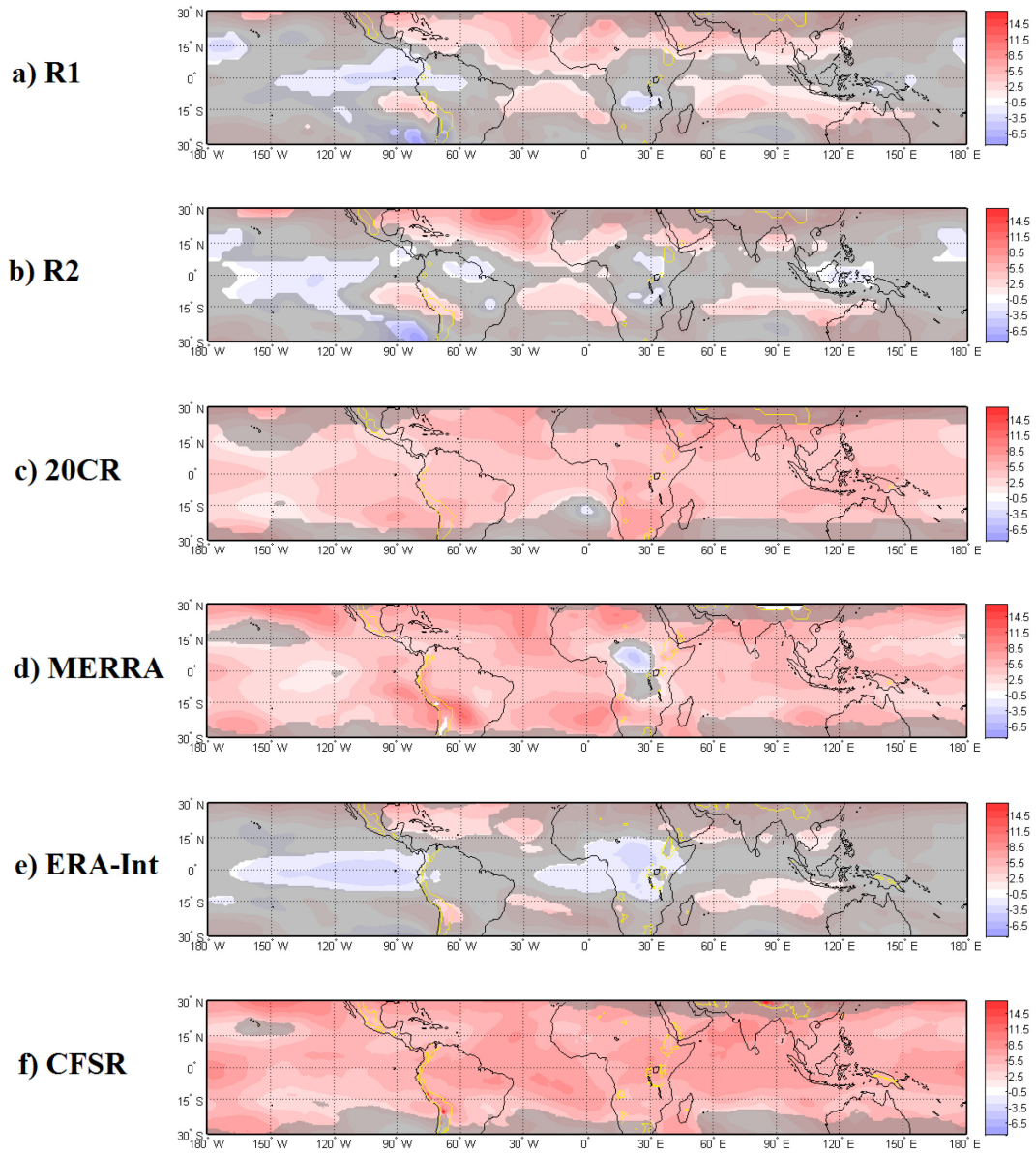


**Figure 2.5:** Annual trend in FLH (m/yr) over the time period 1979-2008 in each reanalysis product: a) R1, b) R2, c) 20CR, d) MERRA, e) ERA-Int, and f) CFSR. All plots have the same color bar limits. The yellow contour outlines areas with mean ETOPO1 elevation greater than 1500 meters. Insignificant trends are grayed out.

When we look at the longitude-pressure cross sections of the temperature trends over the Central Andes (meridionally averaged from 10°S-25°S), it is clear that the vertical distribution of warming also varies greatly between the different reanalyses (Figure 2.6).

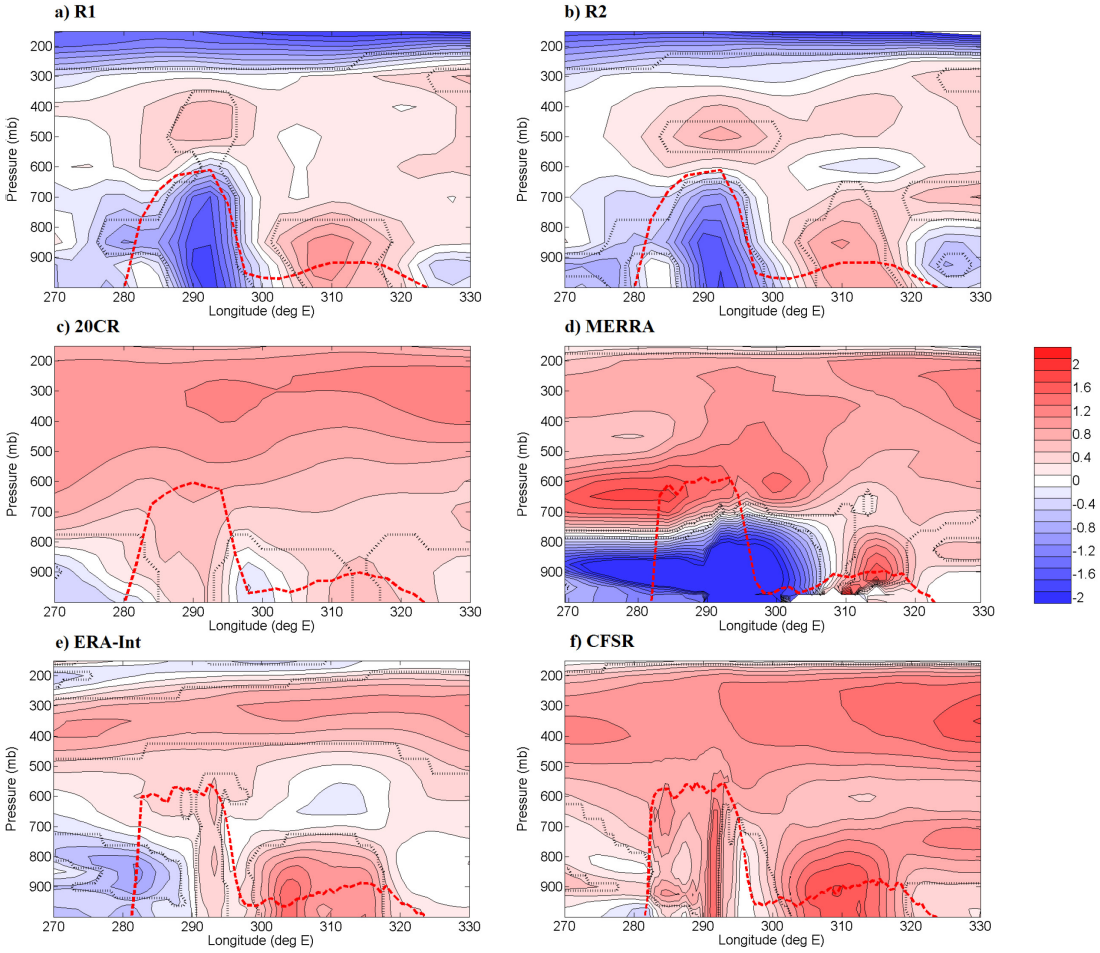


**Figure 2.6:** Vertical profile of total temperature change (°C) over the time period 1979-2008 averaged meridionally over 10°S-25°S in each reanalysis product: a) R1, b) R2, c) 20CR, d) MERRA, e) ERA-Int, and f) CFSR. White blocked out areas appear where all the values in the meridional range were missing – note that these are not real features. The bold red dashed line shows the maximum ETOPO1-derived average product/model grid cell elevation within that meridional range and is also not a real feature, but rather a guide for the maximum product/model topography within that meridional range. The hatched black contour line separates significant areas from insignificant areas – (weaker) stronger trends are always (in)significant.

Whereas R1, R2, and MERRA show an elevated hot spot of warming above or around the mountains, CFSR & 20CR show more of an altitudinal downward extension of upper-level warming over the mountain peaks. The latter behavior more closely resembles the vertical profile of warming projected by climate model simulations of the future (Bradley et al. 2004; Bradley et al. 2006). It is worthwhile to note that the results from 20CR must

be interpreted with caution considering that the free atmospheric temperatures are not heavily influenced by data because 20CR does not assimilate radiosondes. Although there are very few radiosonde observations to assimilate in this region, the other reanalysis products have the advantage of assimilating satellite-retrieved temperature profiles. Still, it is interesting that 20CR produces similar spatial patterns in temperature trends to the other reanalysis products that do assimilate radiosondes. This could indicate that 20CR actually does a good job of simulating free atmosphere temperature trends in the absence of the assimilation of satellite and radiosonde data.

Regarding radiosondes, the SCFA sounding record does not show significant warming around 500mb (Figure 2.2) as one might expect from the reanalyses (Figure 2.3). To the best of our knowledge, this particular radiosonde record is assimilated into all of the reanalysis products, except for 20CR of course. Therefore, the discrepancy between this station and the reanalysis products that assimilate it could be due to a few different possibilities. First, it could be that the base models underlying the reanalysis products are generating spurious middle tropospheric warming that is not in alignment with reality. Second, the off-surface warming seen at this coastal station could extend up and along the mountains, such that there is middle tropospheric warming localized only to the mountains, while the reanalysis products produce a pattern of warming that is too broad. Finally, it could be that other data (particularly satellite-derived temperature profiles) exhibit warming trends that override this particular station in the data assimilation schemes of the reanalyses. Although the SCFA station is certainly a contributor to the trends, there are a multitude of other data-based contributors (short-term radiosonde records in other areas, satellite records, surface observations, etc.) and

model-based factors (e.g., the ability of the base-models to advect temperature anomalies) that could be driving the trends that manifest in the reanalyses. Therefore, the SCFA radiosonde record *alone* cannot support the idea of a regional warming hot spot and we caution against in-depth interpretation of this record when comparing to reanalysis products. Furthermore, since even 20CR shows regional mid-tropospheric warming in the vicinity of the Central Andes, it is unlikely that the SCFA station is causing major differences between 20CR and the other products.

It is likely that the elevated warming portrayed in Figure 2.6 contributes to the rising FLH in the Central Andes Mountains. With the exception of ERA-Interim, rises in FLH are generally larger in the higher resolution, with CFSR exhibiting extreme local rises in FLH of close to 30 m/yr (Table 4). However, the maximum FLH change should be interpreted with caution because extreme values could be the result of grid-scale numerical artifacts. Furthermore, such extreme rises in FLH are likely unrealistic and would outpace glacier recession trends in the region (e.g., Vuille et al. 2008; Rabatel et al. 2013). Nonetheless, the general theme of higher, more local rises in FLH in the higher resolution products suggests that higher resolution base models may be required to resolve the feedback between the high topography of the mountains and the regional atmospheric circulation patterns that are important for driving climate change in this region. It also suggests that we should probably see higher rates of warming at higher elevations within the Andes Mountains. However, the surface station data available from the local environmental agencies of Andean countries does not provide evidence for elevation dependent warming, except perhaps on the lower elevation eastern slopes (Vuille and Bradley 2000; Vuille 2003; Vuille et al. 2015).

**Table 2.3:** Total change in 500mb temperature in °C (ΔT500mb) in the various reanalysis products and AMIP climate models over the time period 1979-2008. Column 3 gives the average ΔT500mb over the Central Andes region, which is defined as grid cells that fall within the bounding box 10°S–25°S, 85°W–60°W with an average ETOPO1 elevation greater than 1500 meters. Column 4 gives the average ΔT500mb over Pan-Tropical land areas which are defined as grid cells that fall within the latitude range 30°N-30°S with an average ETOPO1 elevation greater than 0 meters. Column 5 gives the standard deviation of ΔT500mb over Pan-Tropical land areas. Column 6 indicates whether the Central Andes qualify as a tropical warming hot spot in terms of ΔT500mb as described in the text.

| Product Type | Product Name | Average of change in T500mb over Central Andes (°C) | Average of change in T500mb over Pan-Tropical land areas (°C) | Standard deviation of change in T500mb over Pan-Tropical land areas (°C) | Hot Spot? |
|---|---|---|---|---|---|
| Reanalysis Products | R1 | 0.695 | 0.248 | 0.367 | YES |
| | R2 | 0.833 | 0.379 | 0.292 | YES |
| | 20CR | 0.942 | 0.783 | 0.232 | NO |
| | MERRA | 1.243 | 0.594 | 0.324 | YES |
| | ERA-Int | 0.487 | 0.093 | 0.345 | YES |
| | CFSR | 0.844 | 0.910 | 0.152 | NO |
| AMIP Climate Models | FGOALS-G2.0 | 0.622 | 0.735 | 0.218 | NO |
| | GEOS-CCM | 0.560 | 0.603 | 0.156 | NO |
| | INMCM4 | 0.685 | 0.700 | 0.162 | NO |
| | MIROC5 | 0.687 | 0.821 | 0.209 | NO |
| | CMCCCM | 0.675 | 0.735 | 0.155 | NO |
| | GFDL HiRAM C180 | 0.542 | 0.690 | 0.237 | NO |

**Table 2.4:** Same as Table 2.3 except that values are reported for the rate of change in the FLH in m/yr (ΔFLH) and an addition column was added which gives the maximum ΔFLH over the Central Andes region (Column 3).

| Product Type | Product Name | Maximum rate of change in FLH over Central Andes (m/yr) | Average rate of change in FLH over Central Andes (m/yr) | Average rate of change in FLH over Pan-Tropical land areas (m/yr) | Standard deviation of change in FLH over Pan-Tropical land areas (m/yr) | Hot Spot? |
|---|---|---|---|---|---|---|
| Reanalysis Products | R1 | 2.658 | -0.060 | 1.930 | 2.311 | NO |
| | R2 | 3.427 | 2.347 | 1.604 | 2.148 | NO |
| | 20CR | 5.521 | 4.742 | 4.905 | 1.329 | NO |
| | MERRA | 11.166 | 7.335 | 5.037 | 1.685 | YES |
| | ERA-Int | 5.457 | 2.658 | 0.720 | 2.005 | NO |
| | CFSR | 27.163 | 6.754 | 5.853 | 1.354 | NO |
| AMIP Climate Models | FGOALS-G2.0 | 3.173 | 3.137 | 3.574 | 1.147 | NO |
| | GEOS-CCM | 3.668 | 2.745 | 3.478 | 0.871 | NO |
| | INMCM4 | 3.821 | 2.832 | 3.947 | 1.511 | NO |
| | MIROC5 | 4.403 | 3.752 | 4.840 | 1.118 | NO |
| | CMCCCM | 4.445 | 3.612 | 4.309 | 0.791 | NO |
| | GFDL HiRAM C180 | 3.826 | 2.404 | 3.905 | 1.291 | NO |

This discrepancy between the observational data and reanalysis products could be due to several different factors. For example, it could be that the assimilation of new data sources over time into reanalyses produces an artificial temperature rise at higher elevations. However, it is difficult to determine whether the reanalysis products exhibit strong biases related to changes in the observing system. While the time series of reanalysis mid-tropospheric temperatures (Figure 2.4) do not show any clear jumps that would indicate assimilation of drastically new data sources, there is a gradual change in both the trend and the range of variability during and after the 1990s which is present on both a regional (Fig. 2.4a) and a Pan-Tropical (Fig. 2.4b) scale. Nonetheless, the 20CR product, which maintains consistent data sources over time, also shows a localization of warming trends, which gives more confidence that the regional enhancement of warming is not simply an artifact of data assimilation.

The lack of elevation dependent signals in the station data presented in the aforementioned studies may also be simply due to averaging over large areas. For instance, this study finds evidence for possible elevated warming in the region centralized around the Altiplano, while the results of Vuille et al. (2015) were an average of stations over a large meridional extent. It may be that some sub-regions do in fact exhibit elevation-dependent temperature trends, but that they are outweighed by the surrounding areas that go into the overall average. This is not surprising given than prior studies have shown that temperature trends in the Andes Mountains are highly dependent on the both the geographic location (latitude, elevation, & aspect) and the time period analyzed (e.g., Vuille et al. 2015). There is also the possibility that the surface stations have simply not

felt the effects of elevated warming yet due to natural interannual variability and local insulating mechanisms.

One caveat of this study is that it is challenging to validate the elevated warming trends exhibited by the reanalysis products with data because there are few long term sounding readings in the tropical Andes Mountains and most individual satellite observations are not long enough to span a 30-year climatological time period. For instance, the Atmospheric Infrared Sounder (AIRS) satellite data (which plays an important role in the MERRA reanalysis) is only available from 2003. However, the consistency of a qualitative trend in the reanalysis products examined here, the presence of a dipping down of warming in the most internally consistent product with time (20CR), and the evidence of extreme elevated warming from the Antofagasta sounding station, gives us confidence that that there is a real elevated warming trend above the mountains in the central tropical Andes.

### 2.4.2 HISTORICAL AMIP CLIMATE SIMULATIONS

Since it is difficult to tease apart the model-driven aspects of reanalysis products, we investigate temperature trends in several AMIP climate model simulations. Figure 2.7 shows the spatial pattern of $\Delta$T500mb in all the AMIP models. In contrast to the reanalyses there is no localized hot spot of warming around the Central Andes Mountains in any of these simulations (Table 3). The rates of mid-tropospheric warming in the Central Andes are highly comparable to the rates of change over other Pan-Tropical land areas and are often even lower than the surrounding areas. In terms of FLH, the AMIP

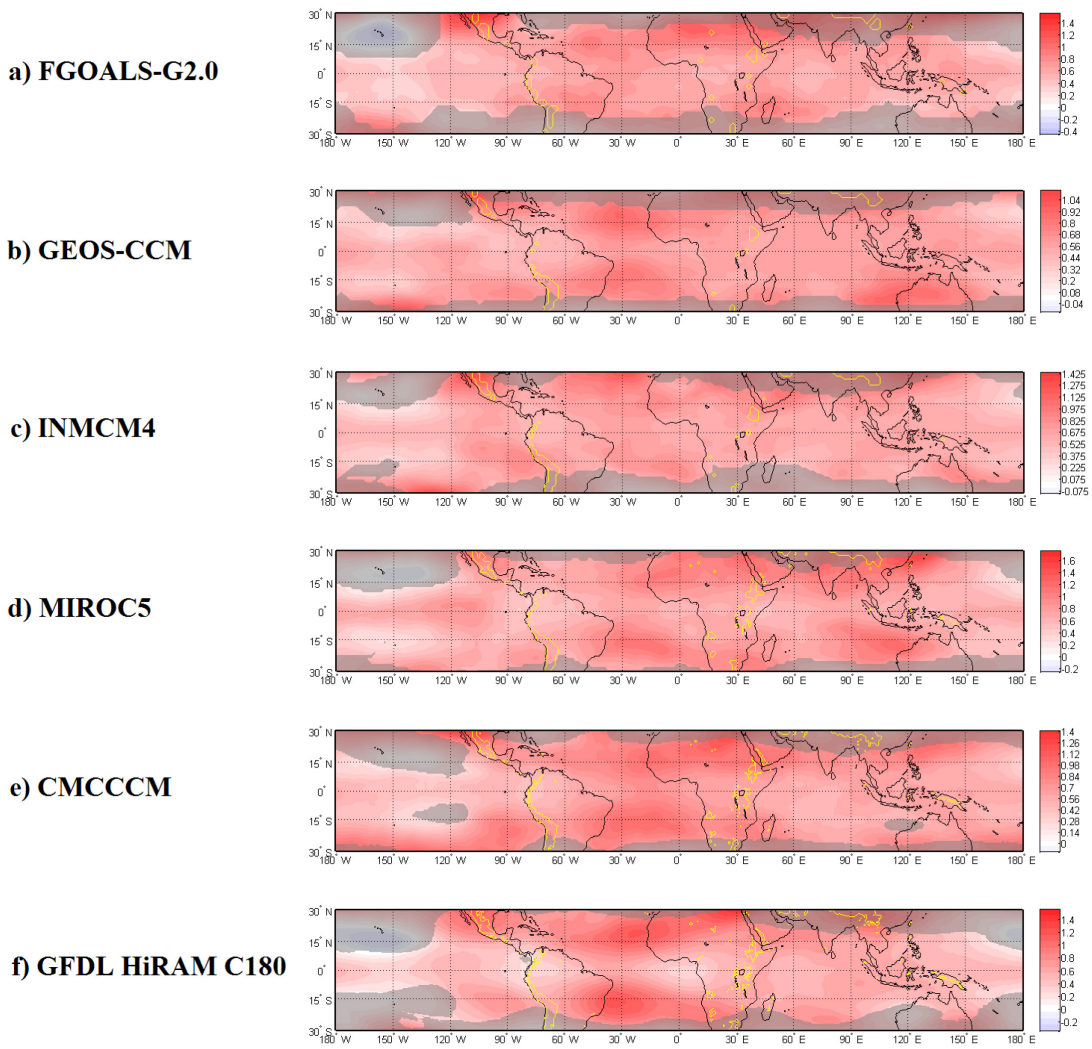


**Figure 2.7:** Same as Figure 2.3 ($\Delta T_{500mb}$ in °C) except for the ensemble average of each AMIP climate model: a) FGOALS-G2.0, b) GEOS-CCM, c) INMCM4, d) MIROC5, e) CMCCCM, and f) GFDL HiRAM C180.

models examined here also do not show any hot spot type behavior around the Central Andes (Table 4) and they tend to underestimate trends in FLH on the whole as shown by the smaller colorbar range in Figure 2.8. And while the AMIP simulations do show elevation dependent warming, with stronger warming at higher elevations and cooling at lower elevations over the western Andean slopes, consistent with observations (Falvey and Garreaud 2009), they do not show a prominent localized warming over the Central

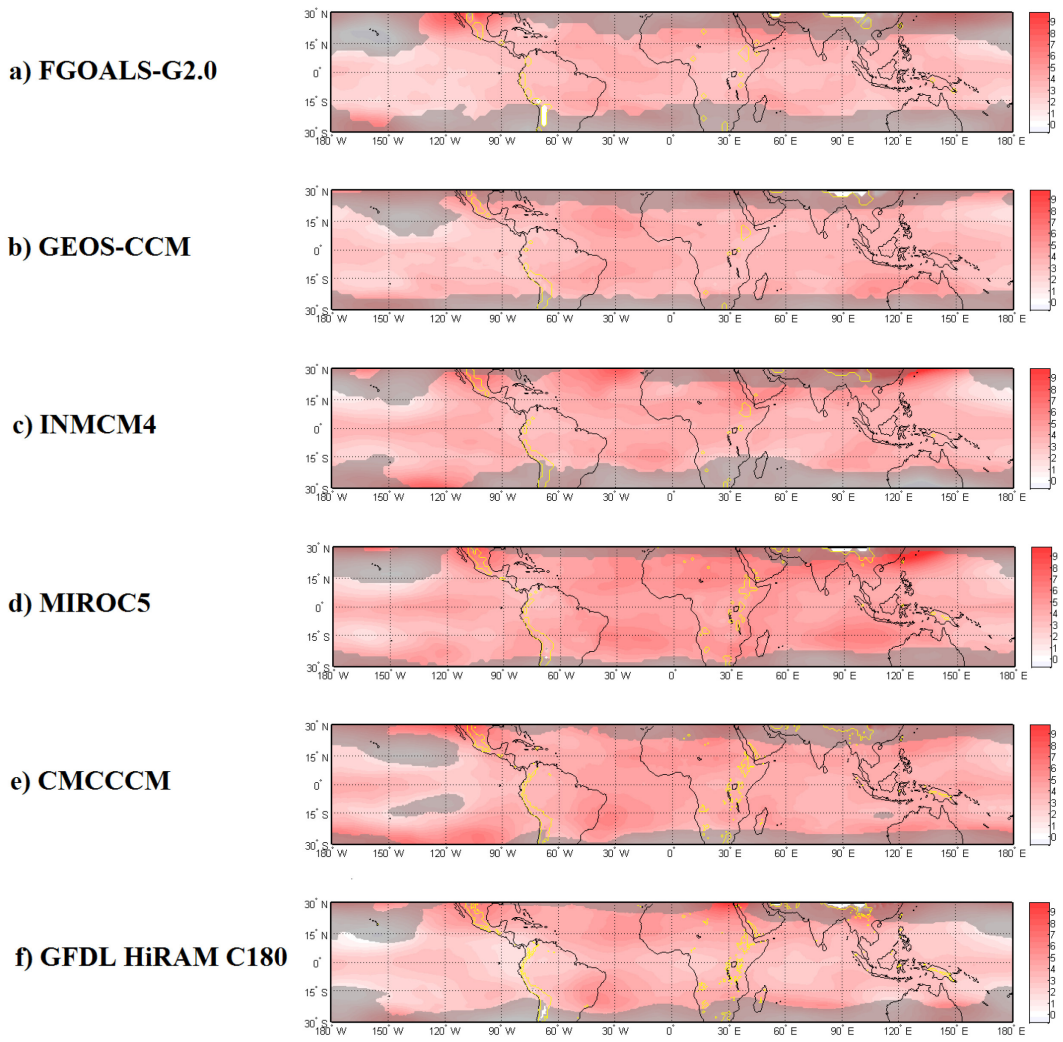


**Figure 2.8:** Same as Figure 2.5 (ΔFLH in m/yr) except for the ensemble average of each AMIP climate model: a) FGOALS-G2.0, b) GEOS-CCM, c) INMCM4, d) MIROC5, e) CMCCCM, and f) GFDL HiRAM C180.

Andes Mountains in the middle troposphere (Figure 2.9). In GEOS-CCM and CMCCCM there are slight indications of a dipping down of the upper-level warming over the mountain peaks (Figure 2.9), but not to the extent that we might expect given the future climate model projections.

Hence, in contrast to the fact that GCMs reasonably represent the *global average* tropical middle tropospheric warming (Fu et al. 2011; Po-Chedley and Fu 2012; Mitchell

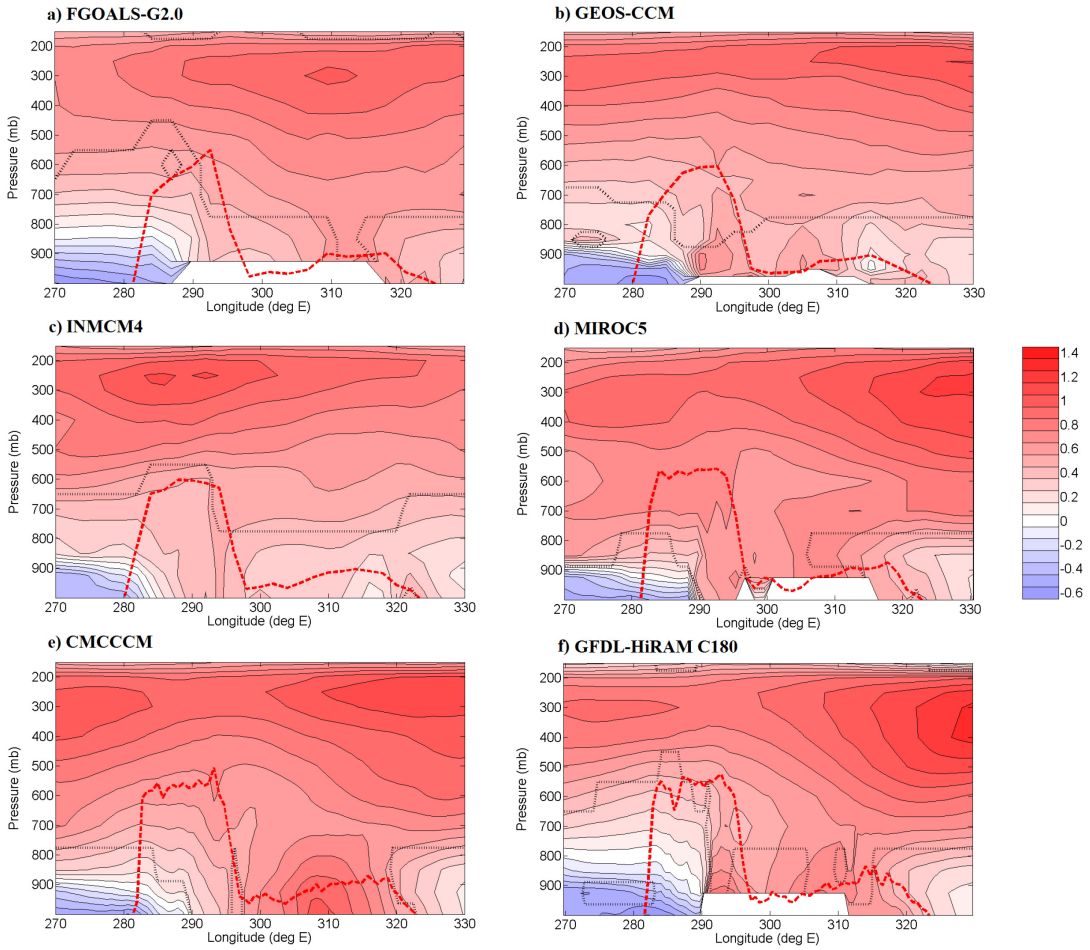


**Figure 2.9:** Same as Figure 2.6 (ΔT in °C) except for the ensemble average of each AMIP climate model: a) FGOALS-G2.0, b) GEOS-CCM, c) INMCM4, d) MIROC5, e) CMCCCM, and f) GFDL HiRAM C180.

et al. 2013), the AGCMs examined here fail to capture the *regional* enhancement of free atmospheric temperature changes over the Central Andes in comparison to reanalyses. This could indicate that the regional manifestations of elevated warming are not well captured by the GCMs, meaning that future projections may be underestimating the amount of change in this area, which could be very problematic for water resources. Or perhaps the shortcomings of the AMIP simulations are due to the very tendency of GCMs to exaggerate upper tropospheric temperature change on average. A full exploration of these possibilities lies outside the scope of this paper because the AMIP models

examined here are not the same as the ones which were shown to predict enhanced tropospheric warming over the tropical Andes (Bradley et al. 2004) or the ones which were examined for assessing historical tropical tropospheric temperature trends (Fu et al. 2011; Po-Chedley and Fu 2012; Mitchell et al. 2013).

Those theories aside, the discrepancy between the AMIP simulations and reanalyses in mid-tropospheric hot spot type warming could be due to uncertainties or deficiencies in the observational SST data sets used to force the AGCMs (e.g., Flannaghan et al. 2014). It could also be due to differences of model resolution (e.g., Mitchell et al. 2013). However, in contrast to the general pattern in the reanalysis products, the higher resolution AMIP climate models do not necessarily show more localized warming or even higher magnitudes of mid tropospheric warming over the Central Andes (Table 3). Alternatively, it could indicate that the AGCMs examined here either respond too slowly to observed SST forcings or diffuse anomalous sea surface heating too quickly throughout the tropical troposphere.

## 2.5 POTENTIAL MECHANISMS FOR ENHANCED WARMING

Assuming that the elevated warming exhibited in the reanalysis products is not a spurious trend (which still remains a possibility, though unlikely), the question then becomes: what is driving localized enhancement of warming in the Andes and why don't the AMIP climate models capture it? Below, we consider several possible mechanisms and suggest areas for future research and more rigorous testing across reanalyses, models, and observations based on the plausibility of each potential driver.

### 2.5.1 SEA SURFACE TEMPERATURES

One might hypothesize that the broad pattern of mid-tropospheric warming seen in several of the reanalysis products (Figure 2.3) is due to changes in the mean state and/or internal variability of large-scale SSTs. On interannual timescales El Niño–Southern Oscillation (ENSO) is known to play a major role in the interannual variability of temperature and precipitation in the tropical Andes (Vuille et al. 2000a,b). However, Vuille et al. (2015) show a low correspondence between tropical Andean station temperature trends and ENSO over recent decades. Furthermore, a quick look into 20CR shows that the spatial patterns of seasonal $\Delta$T500mb do not resemble the ENSO composite maps (not shown). So it is not simply the case that a shift in ENSO behavior (say a shift towards more El Niño like conditions) has resulted in the recent pattern of mid-tropospheric warming over the Central Andes.

Alternatively, the Pacific Ocean has recently entered a negative phase in both its decadal variability and its multidecadal variability (Trenberth and Fasullo 2013; England et al. 2014; Meehl et al. 2014; Steinman et al. 2015), which is likely to play some role in changing temperatures over the tropical Andes. Vuille et al. (2015) argued that the shift of the Pacific Decadal Oscillation (PDO) into a negative phase drives much of the temperature variability in coastal and low elevation (<2000m) sites along the western slopes of the tropical Andes, which have exhibited insignificant temperature trends over recent decades. They also point out that the higher elevation sites seem to be insulated from the effects of Pacific Ocean variability due to the high thermal vertical stratification

of the atmosphere along the western Andean slopes (e.g., Falvey and Garreaud 2009) because they continue to warm at a rate of anywhere from 0.1 to 0.2°C/decade. This may partly explain why the Andes stand out as a hot spot of warming over recent decades because they are relatively insulated from the effects of the long-term variability in the Pacific Ocean which modulates temperatures in much of the surrounding regions. It is also possible that the remote effect of changes in the Pacific Ocean's mean state or internal variability could be felt by the tropical Andes via other teleconnections. For example, a decrease in the cross-Pacific temperature gradient could result in a weakening of Walker circulation (e.g. Vecchi and Soden 2007) which would likely increase tropospheric temperatures over the Andes.

### 2.5.2 REGIONAL ATMOSPHERIC CIRCULATION PATTERNS

It is also possible that changes in regional circulation patterns and/or water vapor flux are driving temperature changes in the Andes Mountains. According to the NOAA Interpolated Outgoing Longwave Radiation product (Liebmann and Smith 1996) the subtropical Andes Mountains and the Chaco lowlands have been experiencing increases in outgoing longwave radiation (OLR) over recent decades (Figure 2.10f – black box panel) which could potentially indicate decreases in water vapor and/or cloudiness. One possible explanation for this trend could be the recent intensification and southward shift of the South Pacific Anticyclone (SPAC) as documented in Falvey and Garreaud (2009). This change, which is a consistent feature of future climate model simulations (Stocker et al. 2013), acts to cool the western coast of South America and may induce moisture

divergence from the Andes Mountains. Another explanation could be a weakening of the Chaco low pressure system to the east of the Bolivian Altiplano resulting in less uplift over the Chaco lowlands and less moisture transport to the subtropical Andes.

Each of these theories is difficult to validate in the reanalysis products examined here because most show OLR trends that are at odds with or spatially inconsistent with the NOAA OLR product (Figure 2.10). For example, MERRA shows the exact opposite trend in the area of interest (enhanced Chaco low pressure system due to a westward shift of the South American Low Level Jet). In the case of MERRA, this suggests that the internal model dynamics generate an incorrect mechanism in order to match the observed warming trends. This may be because MERRA exhibits negative biases in the overall climatological representation of precipitation during this time period (that is, MERRA is much too dry) as compared to observations (Quadro et al. 2013), which might cause it to develop a runaway positive feedback between precipitation, atmospheric stability, and temperature changes.

### 2.5.3 ELEVATION DEPENDENT WARMING MECHANISMS

It is worth coming back to the general theme that higher resolution reanalyses produce more localized and stronger trends in FLH over the tropical Andes Mountains in addition to the extremely local FLH rises exhibited by CFSR (Table 4). This combined with the fact that future climate model simulations project more warming at higher elevations in the Andes, leads us to believe that local elevation dependent feedbacks cannot be entirely discounted. A recent review by the Mountain Research Initiative

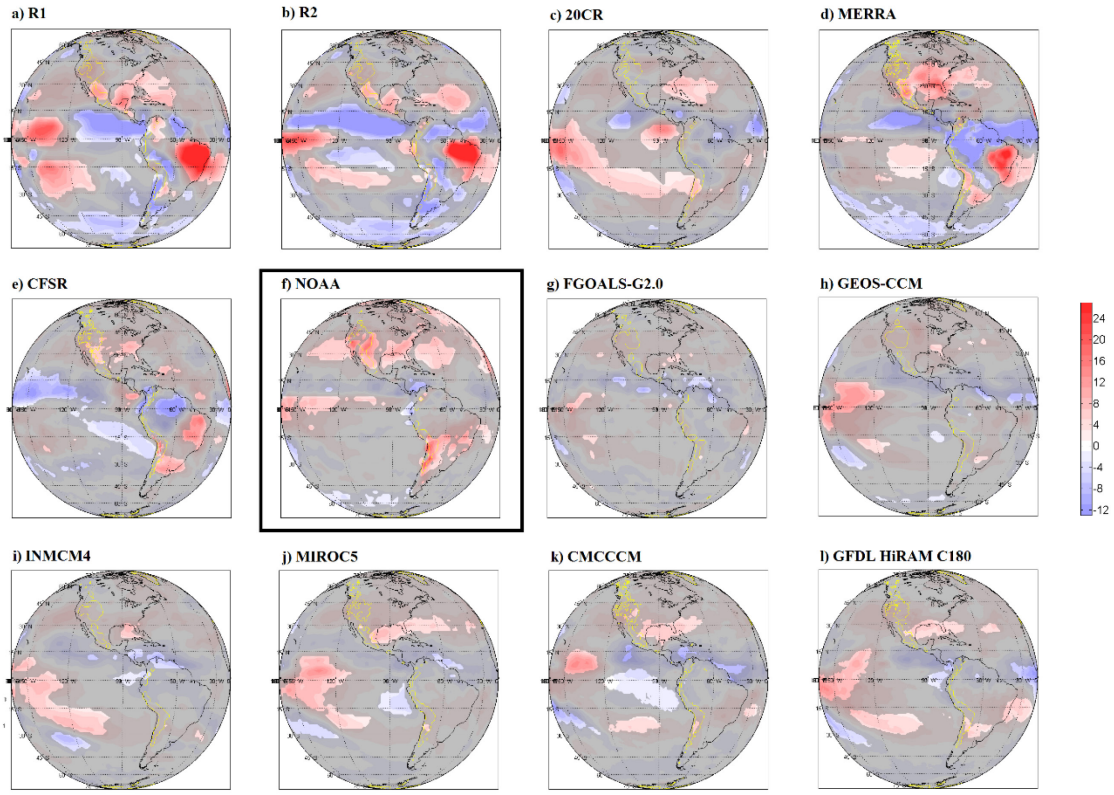


**Figure 2.10:** Total change in OLR ($W/m^2$) over the time period 1979-2008 in all reanalysis products (a) - (e), except ERA-Interim which was unavailable, the NOAA satellite product (f), and all the AMIP climate models (g) - (l). Insignificant trends are grayed-out. The yellow contour outlines areas with ETOPO1 mean elevation greater than 1500 meters.

EDW Working Group (2015) found evidence for elevation dependent warming (EDW) in many different mountain systems around the world and outlined several different mechanisms that explain why higher elevation areas might experience more warming than lower elevation areas. We examine a few of these mechanisms here and discuss whether and/or to what extent they may contribute to warming in the Andes Mountains.

#### 2.5.3.1 ALBEDO-RADIATIVE FEEDBACK

One such mechanism is the albedo-radiative feedback mechanism whereby melting of snow and ice reduces the albedo of the surface causing more radiation to be absorbed at the surface which increases melt rates and results in a positive feedback loop. This is unlikely to be a major actor in the inner tropical Andes because the strong and minimally varying solar radiation inhibits the persistence of snow cover on seasonal timescales (Kaser et al. 2003; Kaser et al. 2005; LeJeune et al. 2007). On the other hand, long-term changes in snow cover may be important in the subtropical Andes Mountains where snowpacks cover more surface area and last longer. There have been a few studies of changes in snow cover in the extratropical Andes Mountains (south of about 30°S), though most report insignificant trends over the past century (Prieto et al. 2001; Masiokas et al. 2006; and Masiokas et al. 2012). More recently, Vuille et al. 2015 report that surface temperatures in the extratropical Andes (defined in their analysis as 18°S–42°S) have been decreasing at an average rate of -0.05°C/decade over the time period 1981-2010 which could suggest that snow cover changes have been minimal over recent decades in this region. Nonetheless, a comprehensive analysis of snow cover trends over recent decades in the vicinity of the warming exhibited by the reanalysis products seems warranted in order to better understand the potential for albedo feedbacks in this region.

#### 2.5.3.2 DLR-WATER VAROR FEEDBACK

Another possible candidate that could be responsible for the elevated warming we see in the tropical Andes is the feedback between downward longwave radiation (DLR) and water vapor. Both observations and models have shown that changes in absolute humidity at high elevations can result in a greatly enhanced greenhouse effect due to the nonlinear relationship between humidity and DLR (Philipona et al. 2005; Rangwala et al. 2009; Rangwala et al. 2010; Rangwala 2013). In the 20CR product, there is some evidence for this mechanism playing a role because the eastern slopes of the Central Andes show an extremely high correlation of >0.9 between 500mb omega and DLR. Increasing vertical motion could lead to more convergence and uplift of water vapor thereby trapping of longwave radiation which is consistent with warming temperatures. Although the NOAA satellite OLR product (Figure 2.10f) shows this to be an area of increasing OLR, this does not necessarily contradict the mechanism in question because increases in OLR do not necessarily indicate decreases in clouds/water vapor (e.g., Vuille et al. 2003). Hence this feedback mechanism is still a viable candidate for contributing to rising temperatures in the region.

#### 2.5.3.3 CLOUD-RADIATIVE FEEDBACKS

Changes in clouds associated with changes in regional circulation are a strong candidate for inducing elevated warming over the mountains. Yet the complexity of cloud feedbacks and the lack of long term observations in the Andes make this a difficult

mechanism to test. According to the NOAA interpolated satellite OLR product, most of the central and southern part of the continent, including the central/subtropical Andes, has been experiencing increases in OLR (Figure 2.10f), which could indicate decreases in cloudiness and therefore less precipitation. However, changes in OLR could also be influenced by changes in surface temperature and water vapor content, perhaps even to a greater extent than changes in clouds (especially in non-convective regions and seasons), which means that this mechanism is heavily linked to the previous mechanism.

The broad region of increased OLR is captured to some extent in the reanalysis products except for an incorrect band of increased cloudiness or no significant change on the eastern slopes of the Andes and into the Chaco lowlands (Figure 2.10). The AMIP climate models on the other hand generally show insignificant OLR trends or trends which are too weak in this region. This inconsistency may indicate that the climate models do not correctly simulate decreases in cloudiness and or water vapor that are associated with less blocking of intense solar radiation which heats up the middle troposphere. At the same time, the tendency of reanalyses to produce an OLR trend that is at odds with observations on the eastern slopes of the Andes and into the Chaco lowlands requires an explanation.

While each of these aforementioned EDW mechanisms are likely drivers of the enhanced mid-tropospheric warming over the Central Andes that is exhibited by reanalyses, it is important to be aware that changes in radiation emissions/absorptions, water vapor, clouds and winds are all intertwined. Therefore, it may be that some combination of these mechanisms is at play. In addition, although future climate model simulations predict both free atmosphere warming and EDW in the tropical Andes, it is

not clear which is the primary driver and how closely the two are linked. Furthermore, the lack of recent EDW signals in surface station data (Vuille et al. 2015) does not necessarily preclude the possibility that free atmospheric warming will drive EDW in the near future. These points need to be more thoroughly examined and will be the subject of future work.

## 2.6 CONCLUSIONS AND DISCUSSION

This paper presents evidence from multiple reanalysis products that the Central Andes Mountains of South America have experienced rates of mid-tropospheric warming that are much higher than the rates exhibited by other Pan-Tropical land areas over the past few decades. This behavior is consistent with and perhaps a prelude to the projected enhanced warming in this region (Bradley et al. 2004; Bradley et al. 2006; and Nogues-Bravo et al. 2007). Whether the vertical structure of warming is also localized or is more of a regional drawdown of upper level warming as projected by future climate model simulations (Bradley et al. 2004; Bradley et al. 2006) is still unclear. In addition, this paper reveals that there is no consistent evidence that warming is enhanced at intermediate mountain elevations around the FLH in the Central Andes compared to Pan-Tropical land areas. Nonetheless, it seems that the Central Andes have been and will likely continue to be a hot spot for global climate change.

Historical AMIP climate model simulations generally do not exhibit the same regional enhancement of mid-tropospheric warming over the Central Andes Mountains which ties into the greater issue of GCMs' ability to simulate free-atmosphere

temperature changes and leads us to suspect that the models do not adequately capture the mechanisms which have enhanced warming in this area over recent decades. When we examine possible mechanisms which might be responsible for elevated warming over the Central Andes, we find that a variety of both large-scale and local mechanisms are likely drivers. In particular, large-scale SST patterns and changes in regional atmospheric circulation patterns could result in the broad pattern of warming exhibited in many of the reanalyses, while EDW-type feedback mechanisms may drive more localized enhancement of warming along the mountain peaks. Moving forward, it is important that we work towards a better understanding of the mechanisms which enhance warming in this region in order to improve their representation in climate models.

Although there has been a recent surge in the amount of regional climate modeling efforts over South America (see Solman 2013 for a review), to our knowledge there has only been one regional climate model simulation over the historic timeframe of interest here – the Swedish Meteorological and Hydrological Institute (SMHI) Rossby Centre ran a regional atmospheric model RCA4, which is based on the numerical weather prediction model HIRLAM (Unden et al. 2002), with approximately 50km resolution for the CORDEX (COordinated Regional climate Downscaling EXperiment) South America domain over the time period 1979-2005. A preliminary examination of the trends in the 500mb temperatures (not shown) indicates that this model does not show the Central Andes Mountains as a hot spot for warming over that time period. This reinforces the conclusion that increased resolution alone is not enough to rectify the inability of models to capture recent Andean warming. Nonetheless, there is certainly added value to increasing resolution in this area due to the dramatic topography which is over-smoothed

in global climate models. Improving the resolution will likely improve the representation of the low-level jet and the upslope winds. Since this is but one regional climate model, it is impossible to know whether other regional climate models might be better able to represent the physical dynamics that contribute to the recent temperature trends. It also highlights the need for additional historical regional climate modeling efforts over South America.

In sum, this study reveals how much remains to be done to properly understand recent Andean temperature changes. These efforts are important because the impacts of climate change in mountain regions are far reaching, including everything from shifts in vegetation and biodiversity belts to the loss of cryospheric environments (i.e. glaciers and/or seasonal snowpack). The disappearance of many low altitude Andean glaciers (e.g. Rabatel et al. 2013) is a sobering testament to this. The decline of these natural runoff buffers is expected to have dramatic economic consequences for Andean countries where rapid population growth and resource exploitation are placing extra demands on fresh water resources (e.g., Vergara et al. 2007). The loss of wetland areas (e.g., Bury et al. 2013) poses an additional challenge to water resources management in the tropical Andes. At the same time, there have been clear shifts in ecosystem and species distributions in the tropical Andes which cannot always keep pace with the dramatic changes in climate (Feeley et al. 2011; Rapp et al. 2012; Forero-Medina et al. 2011; Bury et al. 2013). Therefore, a better understanding of recent climate change and better representation in models is essential because it will ultimately help regional agriculture and water resources managers plan for the future in this highly vulnerable area.

*Acknowledgements*

Met Office SCFA radiosonde station – World Meteorological Organization (WMO) station # 85442 – data is collected by the Met Office. We use a version of the data record provided by the University of Wyoming, Department of Atmospheric Science (http://weather.uwyo.edu/upperair/sounding.html). The authors acknowledge the World Climate Research Programme's Working Group on Coupled Modelling, which is responsible for CMIP, and we thank the climate modeling groups (listed in Table 2 of this paper) for producing and making available their model output. The authors thank Dr. Valentina Aquila, NASA GSFC, for providing the GEOSCCM AMIP output. A. Russell acknowledges support from NSF through the Water, Climate and Health IGERT at Johns Hopkins University (Grant # 1069213).

# Chapter 3. Clearing skies in the tropical Andes

## 3.1 INTRODUCTION

Changes in global climate, such as alterations to surface temperatures, cloud distributions and precipitation are often associated with changes in the radiative balance of the Earth. While observations of temperatures, clouds and precipitation are limited and/or associated with high levels of uncertainty, there are relatively accurate and consistent observations of reflected shortwave radiation and outgoing longwave radiation from satellites since about the mid 1970's. However, cloud-radiative feedbacks are very poorly constrained by global climate models (e.g. Bony 2006), which makes it difficult to determine the impacts of changes in clouds on a regional level, not to mention in predicting future implications of these feedbacks (e.g. Andrews et al. 2012).

A region where this may be particularly important is the tropical Andes Mountains of South America. Recent work by Russell et al. (2017) showed that this region is a "hotspot" of free-atmospheric warming relative to the rest of the tropics in many reanalysis products and that historical AGCMs from the Atmospheric Model Intercomparison Project (AMIP) which are driven only by observed sea surface temperatures do not capture this regional enhancement signal. Additionally, the mechanism behind this change remains elusive, as mechanisms driving the change in reanalysis products do not always agree with observations. A particularly intriguing area

of disagreement is in outgoing longwave radiation (OLR) which was found to increase in the NOAA observationally-based OLR dataset (Liebmann and Smith 1996) at the same time that free-atmospheric temperatures increased. Russell et al. (2017) show that the observed OLR trends are only partially captured in reanalysis products while historical global climate model simulations generally show no significant trend in OLR over this timeframe. The later fact may help to explain why the models also produce less atmospheric warming than the reanalysis products in this region. For this reason, as well as the fact that global climate models and reanalysis products are often too course in resolution to resolve the important regional circulation patterns in areas of complex topography (e.g. Feser et al. 2011), global climate models appear to be ill-suited to simulate regional trends in temperatures and radiation. Therefore, this study uses controlled numerical experiments with a regional climate model to investigate drivers of the observed OLR trend, which is likely associated with decreased cloud cover.

The implications of rising temperatures and decreased cloud cover could be devastating for the Andes Mountains where many cities rely heavily on snow and glacial melt during the dry season. For example, in the Santa River watershed of the Cordillera Blanca mountain range in Peru, it is estimated that glacial melt water provides up to 40% of the dry season runoff (Mark et al. 2005). The availability of fresh water during dry periods is critical to the productivity of regional agriculture and the stability of local economies (e.g., Vergara et al. 2007). Rising temperatures are also associated with an increase in the average freezing level height (FLH) – the altitude of the 0°C isotherm – an important geophysical threshold which determines the extent of snow packs and/or glaciers (e.g., Bradley et al. 2009), as well as potentially how much precipitation is

received as snow vs. rain (e.g., Shook and Pomeroy 2012). Hence it is important that we understand why the radiative balance is changing in the Andes Mountains.

In order to further examine this issue, this study considers two potential drivers for increasing OLR in the subtropical and extratropical Andes Mountains. Considering that there are broad patterns of change in OLR across central and southern South America, large scale changes in sea surface temperatures (SSTs) may be driving changes in the regional radiative balance. A correlation analysis between seasonal mean OLR over the subtropical Andes and seasonal mean global SST anomalies (Figure 3.1) reveals that there is a spatial pattern of correlation which strongly resembles the Atlantic Multidecadal Oscillation (AMO) sea surface temperature signature (e.g. Li et al. 2014), especially during the austral winter. Figure 3.1 may also indicate that regional OLR trends are linked impacted by the contrast between the Pacific and Atlantic mean states. Alternatively, atmospheric boundary conditions may play a role. The extratropical and midlatitude Andes Mountains are regions where wintertime storms are spawned from frontal systems originating in the midlatitude Pacific (Garreaud 2009). The recent poleward shift of midlatitude westerlies (e.g. Seidel et al. 2008) may have some influence on the local radiative balance.

The Weather Research and Forecasting model (WRF) will be used to examine changes in the radiative balance over the Andes Mountains of South America and determine methods for improving the simulation of regional cloud-radiative feedbacks. WRF is used here because it offers several advantages over global models, including higher resolution, multiple physics parameterization options, and the capability to manually manipulate boundary conditions. This study aims to determine whether the use

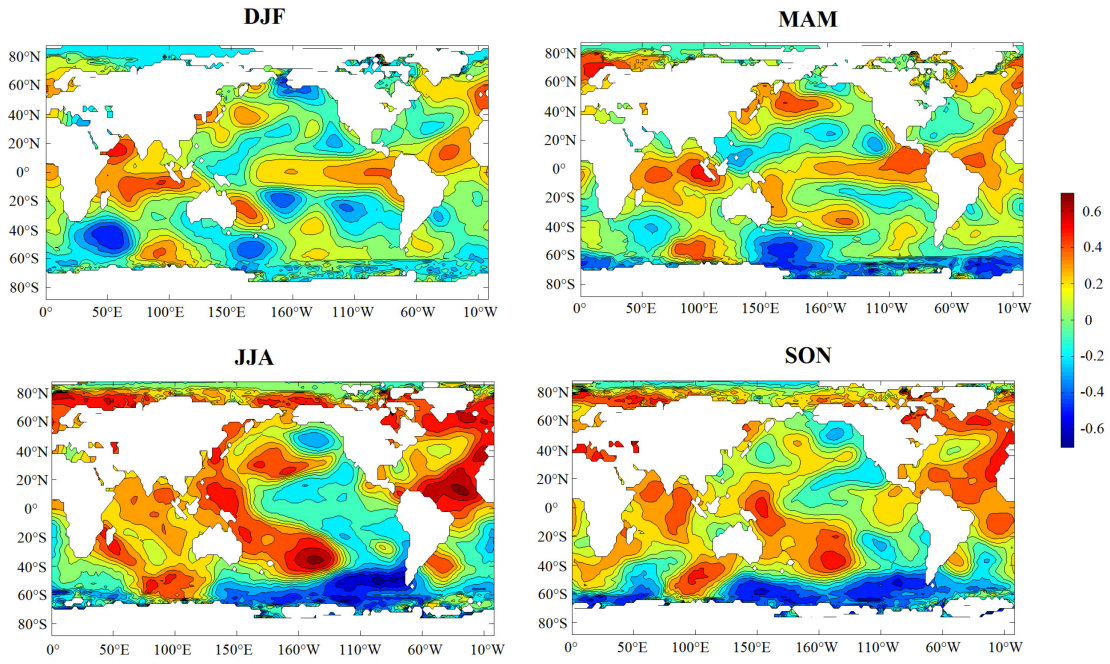


**Figure 3.1:** Seasonal correlation between ERSST sea surface temperature anomalies and the Subtropical Andes domain average (75°W–60°W, 15°S–22.5°S, >1500 m.a.s.l.) NOAA OLR for each season – a) December-January-February, b) March-April-May, c) June-July-August, and d) September-October-November – over the time period 1979 to 2013.

of a high resolution regional climate model improve the representation of OLR trends over the past few decades.

## 3.2 DATA, MODELS, AND METHODS

In order to answer these questions, an investigation of multiple observational products is conducted and compared to numerical modeling results from the WRF model. Linear trends in observational records of important parameters are compared to the mean difference between WRF model results from an earlier portion of the time period of interest and a later portion of the time period of interest. The details of the observational

products, linear trend analysis techniques and model setup and validation are outlined below.

### 3.2.1 NOAA OUTGOING LONGWAVE RADIATION

The NOAA Interpolated Outgoing Longwave Radiation product (Liebmann and Smith 1996) is examined to characterize both the climatology and the trends in regional OLR. Monthly NOAA OLR data at a resolution of 2.5° are provided by NOAA ESRL at their website http://www.esrl.noaa.gov/psd/. As evidenced by Figure 3.2 the subtropical Andes Mountains are characterized by low seasonal mean OLR during the austral summer – December-January-February (DJF) – and moderate seasonal mean OLR during the austral winter – June-July-August (JJA) – in close alignment with the hydrological seasons experienced by this region, while the extratropical Andes Mountains exhibit the opposite pattern.

### 3.2.2 ISCCP CLOUD COVER

This study also analyzes the International Satellite Cloud Climatology Project (ISCCP) D2 dataset which provides satellite-based monthly cloud cover information at a resolution of 2.5° (Schiffer and Rossow 1983, Rossow and Schiffer 1999). The ISCCP D2 data are available at the ISCCP web site isccp.giss.nasa.gov, which is maintained by the ISCCP research group at the NASA Goddard Institute for Space Studies, New York,

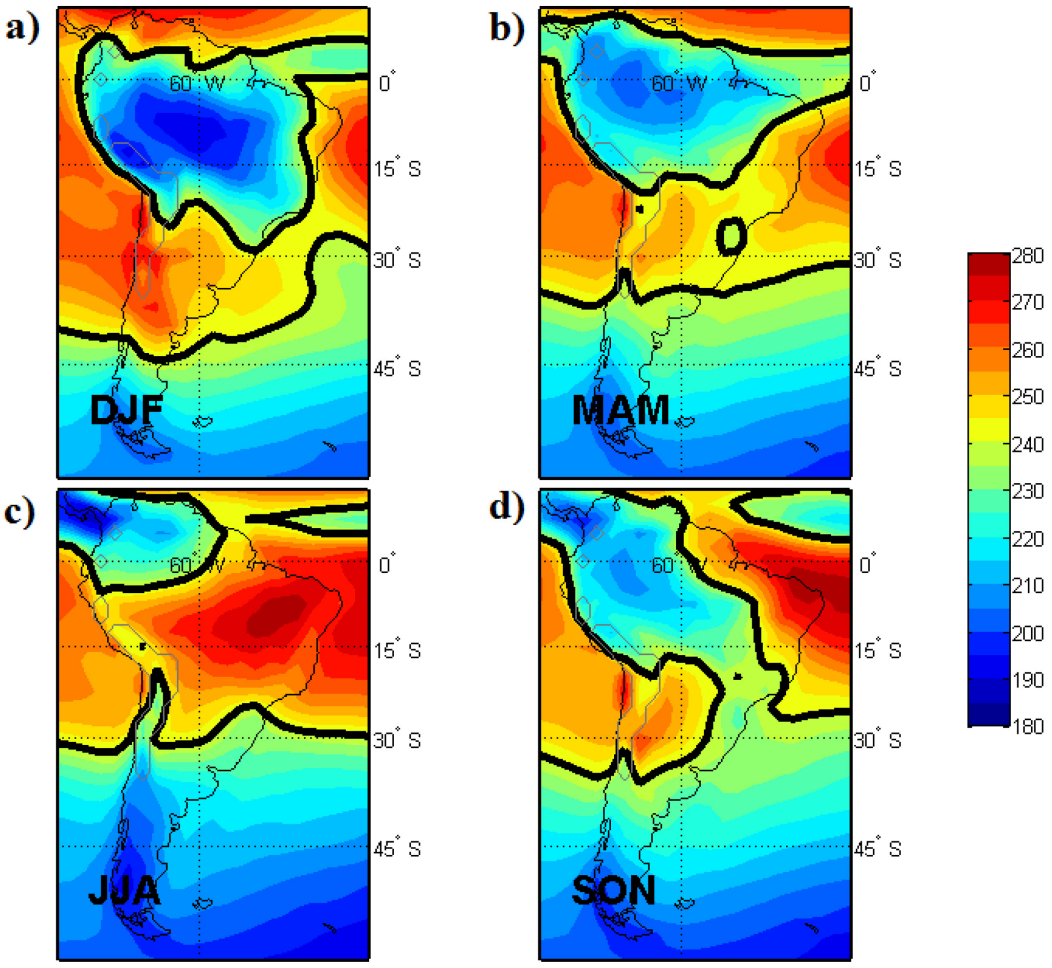


**Figure 3.2:** Mean NOAA outgoing longwave radiation (OLR) over the time period 1979 to 2013 (W/m$^2$) and broken down by season: a) December-January-February, b) March-April-May, c) June-July-August, and d) September-October-November. The gray contour outlines areas with mean ETOPO1 elevation greater than 1500 meters. The bold black line indicates the 240 W/m$^2$ contour – a general cutoff between convective vs. non-convective regions (Morrissey 1986).

NY. This dataset is analyzed to determine the changes in cloudiness over the Andes

Mountains during the time period 1984 to 2009.

### 3.2.3 LINEAR TREND ANALYSIS

We use the same methodology as in Russell et al. (2017) and reproduce the description from that paper here for the reader's convenience. Linear trend analysis on relevant climatic parameters such as OLR was performed by calculating the linear trend with time for the raw monthly time series data at each product/model grid cell. All time series data are truncated at whole year intervals; so that a reported trend from 1979-2013 is computed including all months from January 1979 through December 2013. Note that because we are working only with whole years, the slope of the linear fit line for the deseasonalized monthly time series is negligibly different from the slope for the raw monthly time series. The slope of the linear fit line yields the annual rate of change in units/year. The total change over the time period of interest is simply the unit trend multiplied by the number of years (e.g., 1979-2013 → 35 years). The symbol Δ is used to indicate either the total change or the rate of change depending on the variable – note the reported units to differentiate the two. Trends are only computed if at least 75% of the time series is complete (non-missing).

In order to determine whether trends are significant, the Mann–Kendall test (Mann 1945; Sen 1968), a nonparametric, distribution-free method, which tests the null hypothesis of trend absence against the alternative of trend is applied. This test has been shown to work well even with non-normal and incomplete time series (Yue and Pilon 2004). Throughout this paper the Mann-Kendall test is applied at a significance level of 0.05, meaning that if the trend is reported as significant then the time series has a linear slope that has a 95% chance of being different from zero.

### 3.2.4 MODEL SET UP AND VALIDATION

In order to determine the ability of regional climate models to capture trends in temperatures and radiation over the tropical Andes Mountains, a series of climate simulations were performed using the Weather Research and Forecasting model version 3.7 (Skamarock et al. 2008). First, two 5-year time periods were simulated at the beginning and end of the recent 30-yr timeframe. The time blocks 1980-1984 and 2006-2010 were chosen because they exhibit no significant trend in OLR over the subtropical and extratropical Andes Mountains and there is a strong difference between the mean region-averaged OLR of these two 5-year timeframes. The difference between the mean OLR of these 2 time periods is examined in order to see whether WRF correctly simulates the magnitude and spatial distribution of observed changes in OLR. Only the austral winter and spring are simulated making for a total of ten 8-month long integrations. Each year is simulated independently and only part of the year is simulated in order to optimize computational resources (as opposed to running two 5 year integrations with yearly restarts). The simulations start in April and run through November but only the austral winter and spring months (June through November) are analyzed because they are the months of strongest OLR trends in the observed record. The first 2 months of the simulation are performed to allow model variables (particularly soil moisture and temperature) to reach dynamical equilibrium with the boundary conditions.

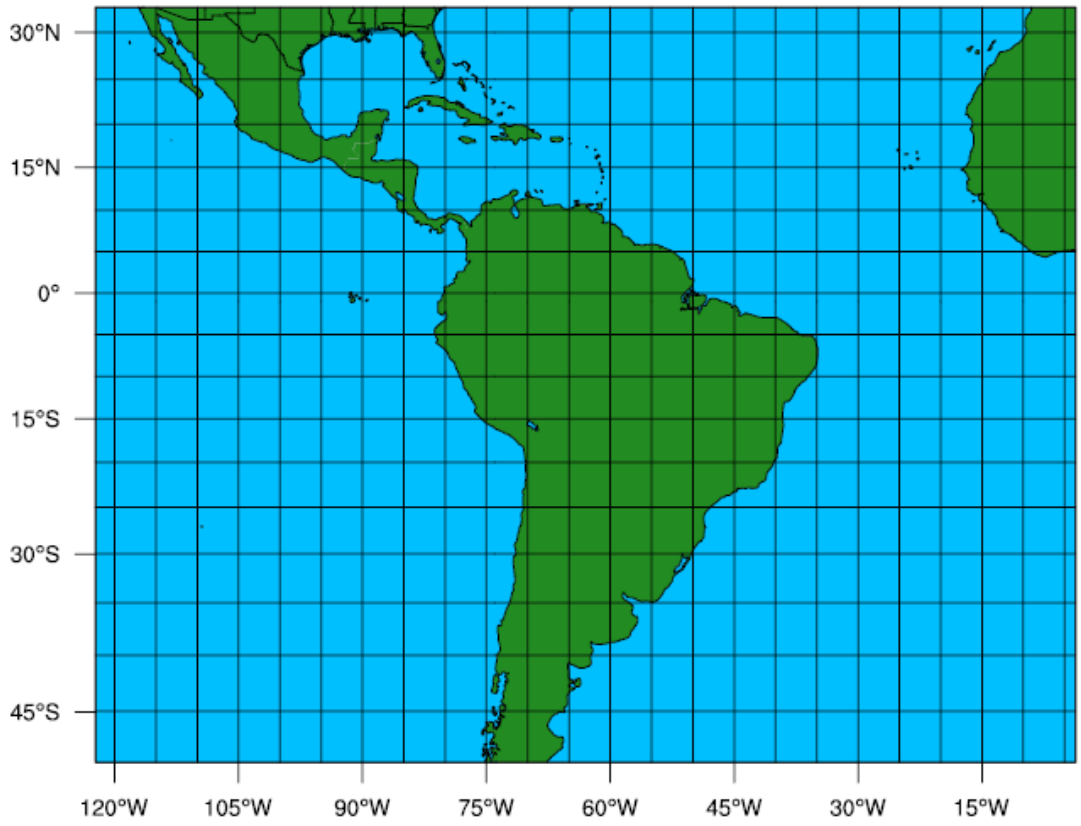


**Figure 3.3:** WRF Domain Extent

The 50-km WRF simulation domain composed of 260 x 200 grid points, which is displayed in Figure 3.3, encompasses most of the South American continent, the tropical Atlantic Ocean and the eastern tropical Pacific Ocean, which is an expanded version of the CORDEX South America domain. The model was driven by ERA-Interim, the boundary conditions from which were provided every 6 hours over a relaxation zone of 4 grid points with an exponentially decaying ramp. The physics options (shown in Table 3.1) were selected based on a series of in-house parameterization sensitivity tests as well as a personal communication with a member of the Atmospheric and Climate Dynamics Group at the Federal University of Alagoas who have done a comprehensive set of WRF sensitivity tests over the CORDEX South America Domain (Dr. Helber Barros Gomes,

**Table 3.1:** WRF simulation physics parameterization selections

| Parameterization Option | Scheme |
|---|---|
| Microphysics | WRF Single-Moment (WSM) 6-class |
| Longwave radiation | RRTMG |
| Shortwave radiation | Dudhia |
| Surface Layer | Monin-Obukhov (Janjic Eta) |
| Planetary Boundary Layer | Mellor-Yamada-Janjic (Eta) TKE |
| Cumulus | Grell 3D |

personal communication, October 24, 2016). A sample WRF namelist for these simulations is provided in the Appendix. The performance of the model using the final parameterization options shown in Table 1 is demonstrated in Figure 3.4 which shows the seasonal mean error of the WRF model compared to the NOAA OLR observationally-based product for the 10 simulation years. The final WRF model setup does reasonably well in simulating seasonal OLR in the subtropics and throughout the Andes Mountains in general. While the erros may seem high in places like northwestern South America, this final model setup produces average RMSEs that are far lower than alternate model setups. For example, Figure 3.5 shows the performance of the final WRF model set up as compared to a worse-performing simulation using a different set of parameterizations in the simulation of OLR on a single day. On this day, the spatial root mean square error (RMSE) of WRF model set up 1 was 20.5 $W/m^2$, while the spatial RMSE of WRF model set up 2 was 45.1 $W/m^2$. It is clear that the final model setup (Fig. 3.5a) produces a much more realistic representation of both the spatial extent and magnitude of convection – depicted by areas enclosed within the 240 $W/m^2$ bold contour line which indicates a general cutoff between convective vs. non-convective regions (Morrissey 1986) – as compared to the NOAA satellite-based OLR product (Fig. 3.5c). Note that although it has often been demonstrated that an ensemble of physics parameterization options

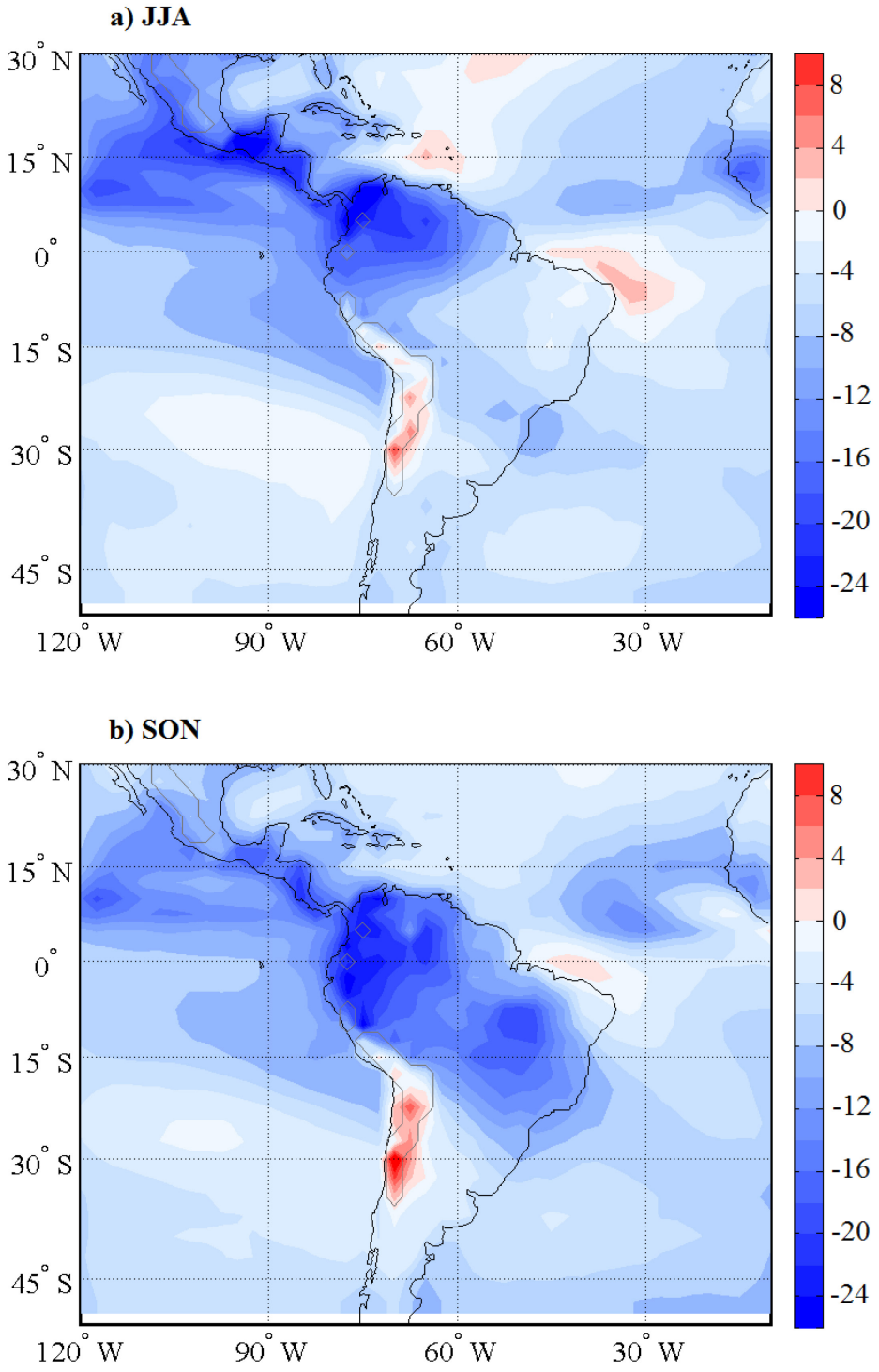


**Figure 3.4:** Seasonal mean error of the WRF-simulated outgoing longwave radiation (OLR) compared to the NOAA observationally-based OLR product for years 1980-1984 and 2006-2010 in a) June-July-August (JJA) and b) September-October-November (SON).

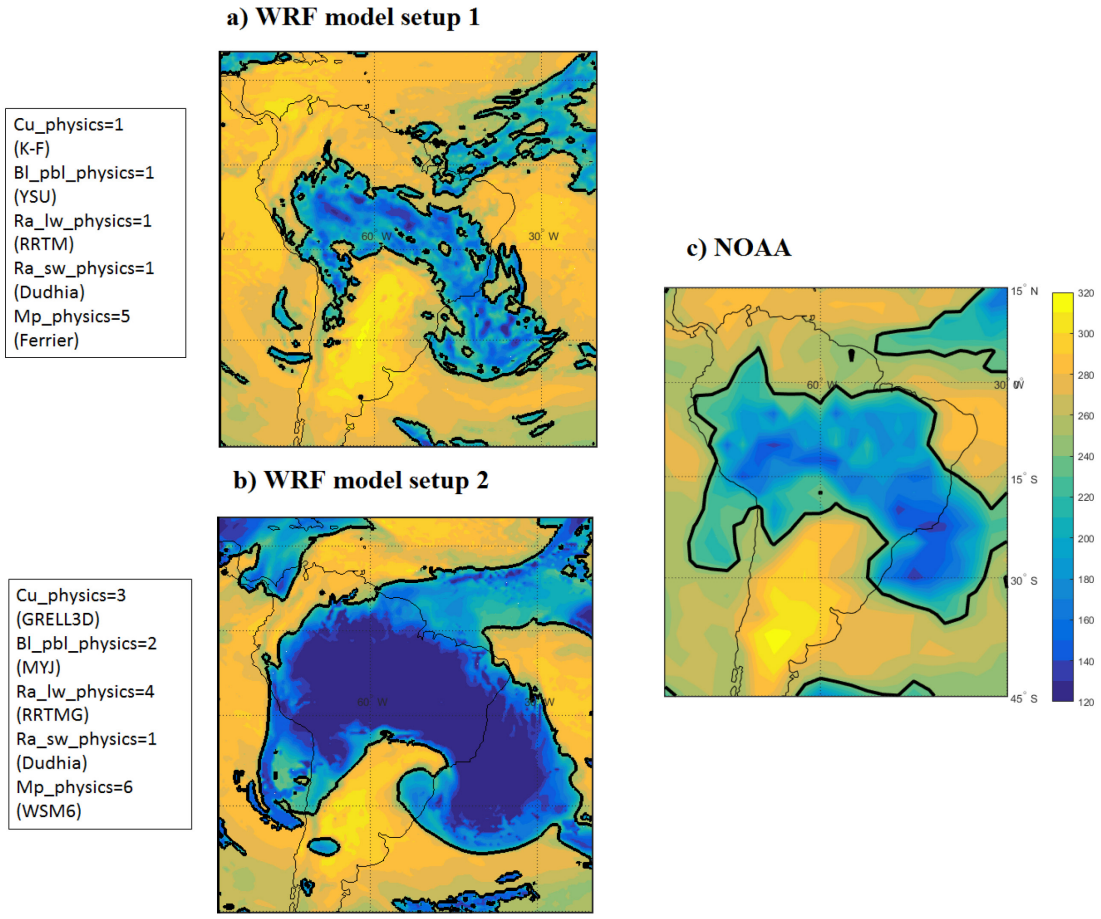


**Figure 3.5:** WRF simulations of mean daily OLR using 2 different model physics parameterization setups (a) and (b) as compared to NOAA OLR ($W/m^2$) on January 2nd, 2012.

outperforms any one set of physics options for regional climate modeling applications (Fernandez et al. 2007, Ruiz et al. 2010, Solman et al. 2013a, Solman et al. 2013b, Solman and Pessacg 2012), such an ensemble simulation for 10 consecutive years would be prohibitively computationally expensive givens the resources available.

## 3.3 RESULTS

A linear trend analysis of the NOAA OLR product indicates that there have been strong increases in OLR over many parts of subtropical and midlatitude South America over the past few decades (Figure 3.6). In areas and/or seasons that are dominated by deep convection (as denoted by the 240 $W/m^2$ contour line in Figure 3.2), such as in the Amazon Basin during the austral summer, increases in OLR are usually indicative of a reduction in the water vapor content of the atmosphere which tends to manifest as a reduction in high clouds, and potentially low level clouds (e.g. Schulz et al. 2012). In areas and or seasons dominated by clear skies, increases in OLR correspond closely to increases in surface temperature (e.g. Schutz et al. 2012).

Figure 3.6 indicates that there are particularly intense increases in OLR in the subtropical & southern Andes Mountains during most of the year. These areas are highly vulnerable to climate change due to the reliance on glacial melt for dry-season runoff (Soruco et al. 2015). Considering the climatology of OLR in this region (Figure 3.2), one might hypothesize that increases in OLR in the subtropical Andes which occur mainly during the dry season and into the start of the rainy season are likely due to changes in surface temperature, while increases in OLR in the extratropical Andes which occur during the rainy season are likely due to decreases in cloudiness.

Figure 3.7 shows the NOAA OLR time series broken down by season over the last few decades averaged over the subtropical Andes (Figure 3.7a) – here defined as areas that fall within the geographic bounding box 15°S-22.5°S, 75°W-60°W, and have an elevation greater than 1500 m.a.s.l. – and over the extratropical Andes (Figure 3.7b) –

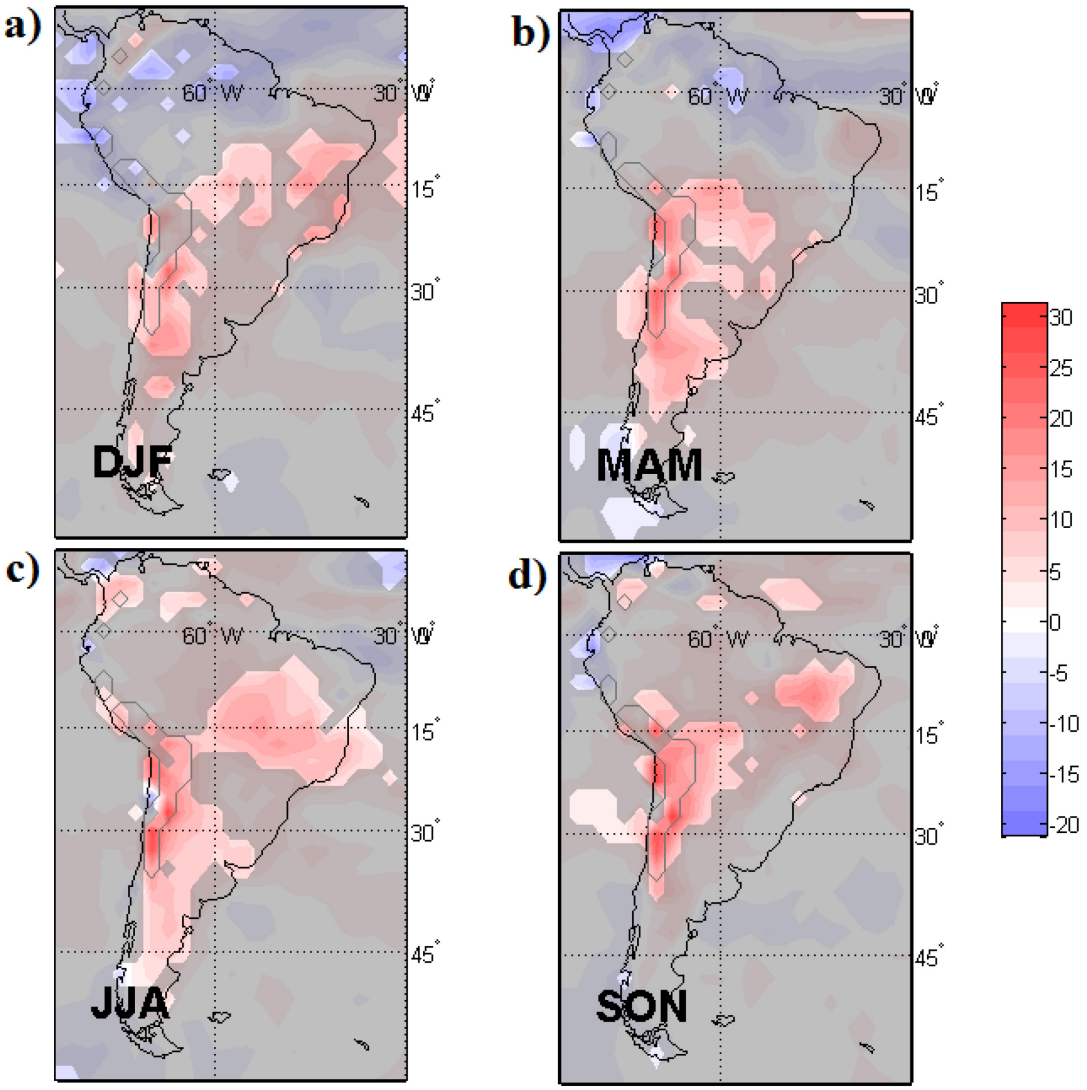


**Figure 3.6:** Total change in mean seasonal NOAA outgoing longwave radiation (OLR) over the time period 1979 to 2013 (W/m$^2$) for a) December-January-February (DJF), b) March-April-May (MAM), c) June-July-August (JJA), and d) September-October-November (SON). The gray contour outlines areas with mean ETOPO1 elevation greater than 1500 meters. Insignificant trends are grayed-out.

here defined as areas that fall within the geographic bounding box 22.5°S-35°S, 80°W-60°W, and that have an elevation greater than 1500 m.a.s.l.. The trends in OLR over both regions of the Andes Mountains are strongest during the austral winter – June-July-August (JJA) – and during the austral spring – September-October-November (SON).

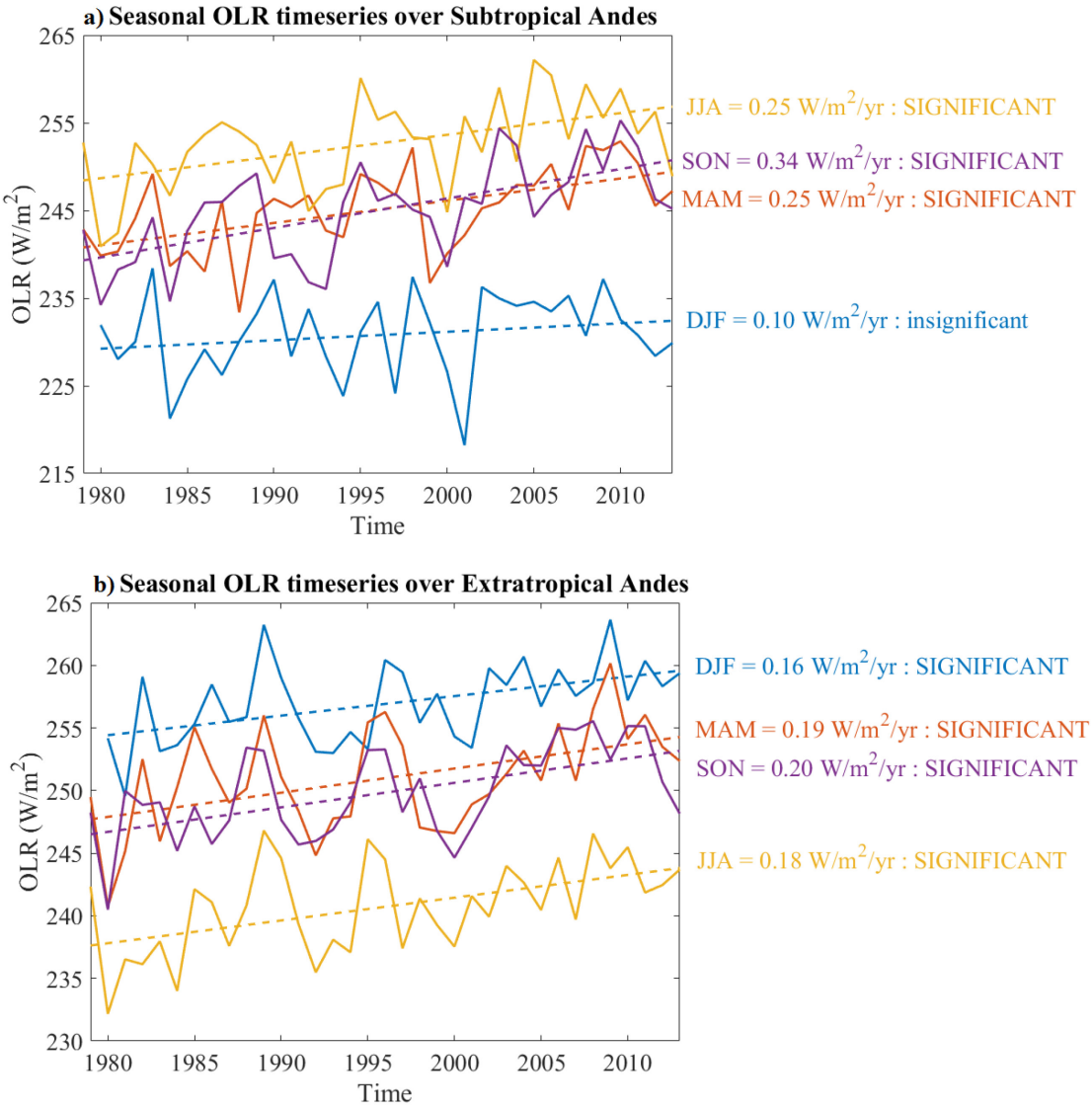


**Figure 3.7:** Seasonal NOAA OLR time series from 1979 to 2013 averaged over the subtropical Andes (a) and the extratropical Andes (b). The blue line shows the seasonal mean December-January-February time series, the red line shows the seasonal mean March-April-May time series, the yellow line shows the seasonal mean June-July-August time series, and the red line shows the seasonal mean September-October-November time series. The linear trend line and indications of significance of trend are reported for each time series in the matching color.

Depending on how far south the region is and which side of the mountains are examined,

JJA/SON may rainy or dry – see Garreaud et al. (2008) for a detailed review of the local

variations in Andean climate. It is important to take these local variations in regional climate into consideration when evaluating the meaning of trends in the radiative balance.

It has been suggested that changes in OLR associated with changes in cloud cover and/or regional atmospheric circulation in the subtropical and extratropical Andes Mountains may have a direct impact on rising free-atmosphere temperatures in the region (Russell et al. 2017). Yet it remains unclear what factors could be driving these trends in OLR. Figure 3.8, which shows the deseasonalized time series of NOAA OLR and The International Satellite Cloud Climatology Project (ISCCP) total cloud cover for the two regions of the Andes Mountains, reveals that increases in OLR are heavily related to decreases in total cloud cover in both regions on an annual scale. Note that while both the NOAA OLR product and the ISCCP cloud cover product are susceptible to generation of artificial trends due to periodic repositioning of satellites (e.g. Allan and Slingo 2002, Norris 2005), it is unlikely that the trends or correlations in these regions are spurious due to the fact that the two products exhibit the opposite trend and they are derived from a different set of satellites. Therefore in both regions, while NOAA OLR is increasing at significant rates, the ISCCP total cloud cover is decreasing at significant rates, and the two variables are highly correlated.

It is important to note that both variables' time series appear to exhibit a somewhat stepwise behavior in their trends such that the trend is dominated by changes in the mid 1990's and early 2000's, which may be due to primary shifts in the climatic drivers that are forcing these variables. In addition, Vuille et al. (2015) show that station records from local meteorological agencies indicate warming surface temperatures in the subtropical Andes over recent decades, but there is a significant lack of data in the

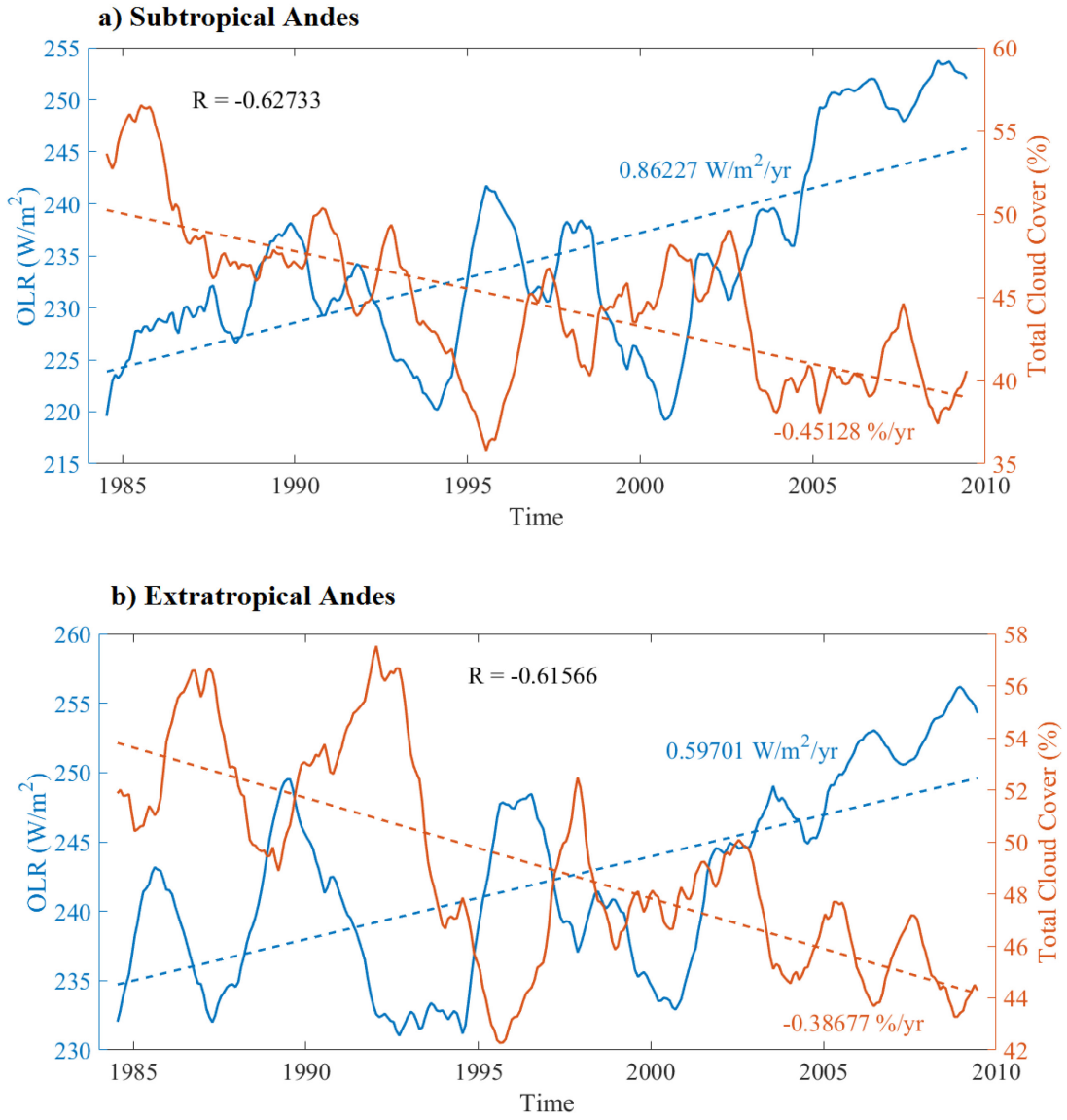


**Figure 3.8:** Deseasonalized time series of NOAA OLR in W/m$^2$ (blue lines corresponding with the left-hand axes) and ISCCP total cloud cover in % (red lines corresponding with the right-hand axes) averaged over the Subtropical Andes (a) and the Extratropical Andes (b). Dashed lines indicate linear trend fit lines with reported slopes. The correlation values (R) between the OLR and cloud cover time series are also reported.

Central Andes Mountains between about 20°S and 30°S. Therefore it appears that changes in OLR in the subtropical and extratropical Andes correspond to both an increase in surface temperatures and/or water vapor in the boundary layer and a decrease in cloud

cover. These changes in cloudiness, surface temperatures and surface water vapor over the subtropical Andes may in fact be contributing to increases in atmospheric temperature as suggested by Russell et al. (2017).

Given that the NOAA OLR observationally-based product indicates that much of central and southern South America have experienced large increases in OLR over the past few decades, with the Andes Mountains exhibiting particularly high increases, and that historical AMIP climate model simulations fail to capture these trends, it is worth examining whether the regional climate model WRF can simulate such trends during the seasons of strongest OLR trends over the Andes Mountains (JJA and SON). Figure 3.9 shows the difference in mean seasonal OLR generated by WRF between the two time periods 2006-2010 and 1980-1984 in order to represent the trend over the last few decades. In general, WRF captures not only the general spatial pattern of changes in OLR over South America, but the direction of those changes in many locations is more accurate than the ERA-Interim forecast of OLR (Figure 3.10) as compared to the observational NOAA OLR product (Figure 3.6). Although the magnitudes of OLR trends are underestimated by WRF, the model captures some regionally enhanced increases in OLR within and around the Andes Mountains, which suggests that this regionally downscaled mesoscale model is better suited to capture long term changes in OLR. WRF also simulates local deceases in cloud cover within the subtropical and extratropical Andes Mountains during both JJA and SON (Figure 3.11) which is consistent with ISCCP observationally based cloud cover trends over that area (Figure 3.8), though the magnitude of those changes is underestimated.

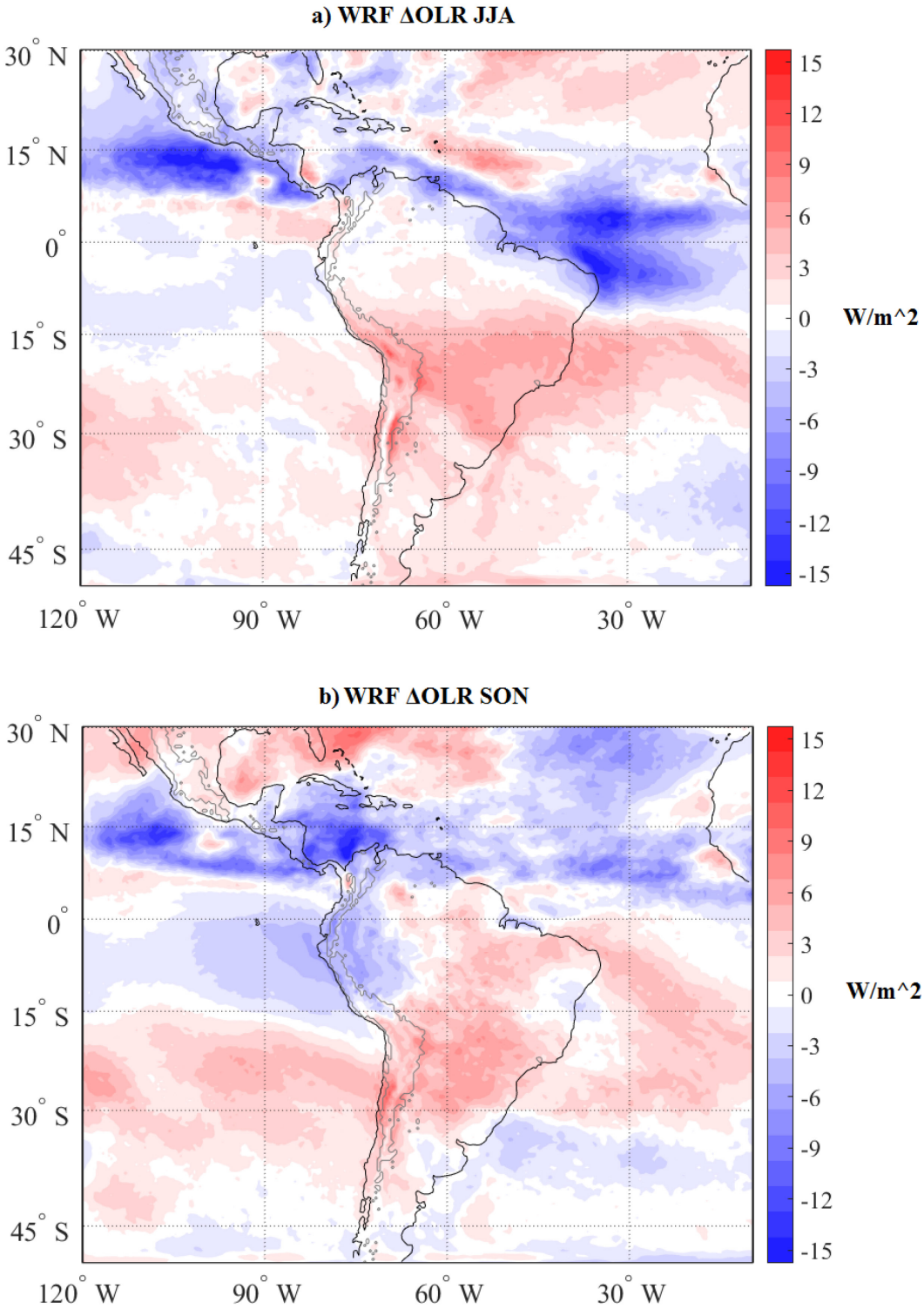


**Figure 3.9:** Difference in mean seasonal OLR generated by WRF between the two time periods 2006-2010 and 1980-1984 for the JJA season (a) and the SON season (b).

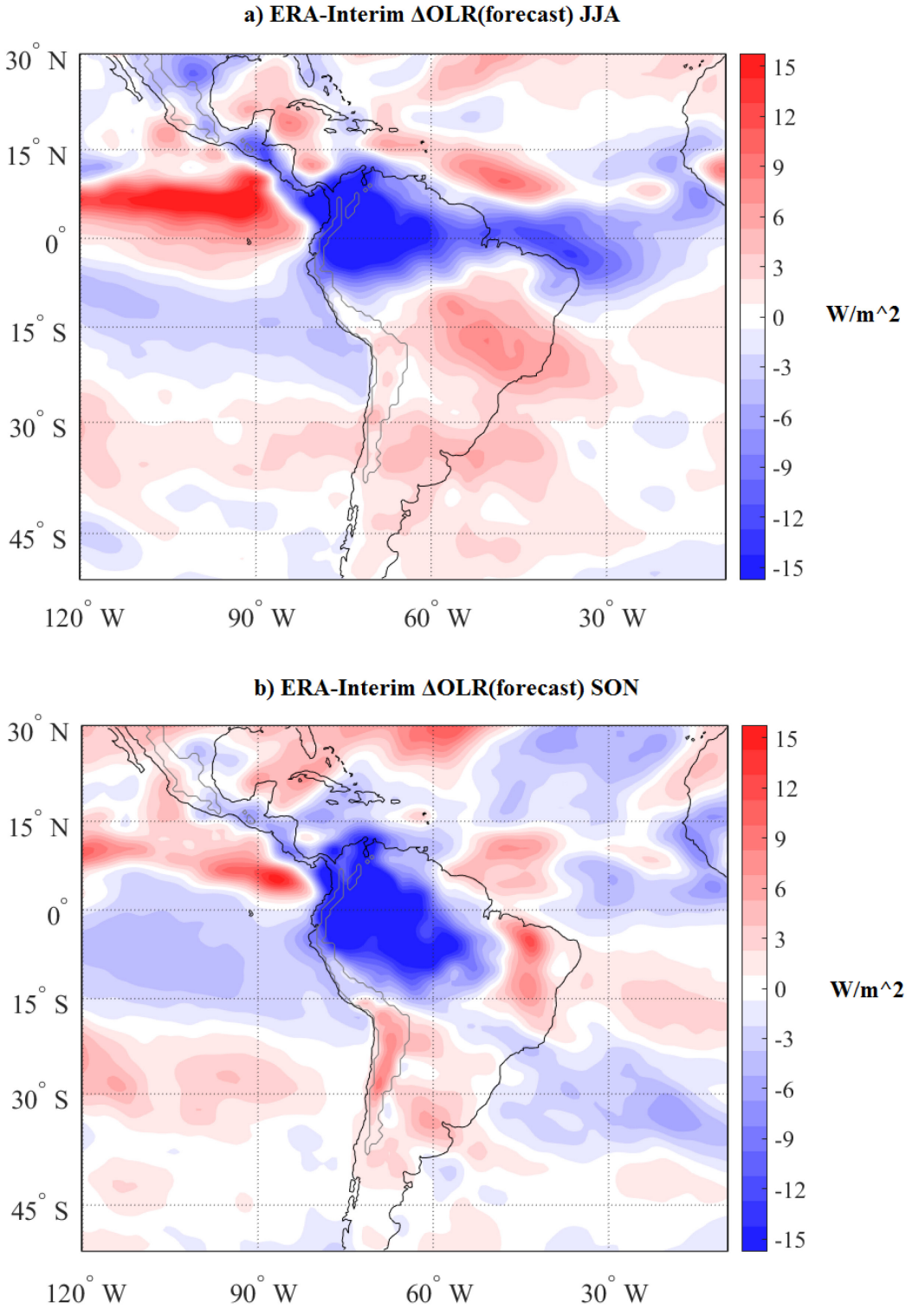


**Figure 3.10:** Difference in mean seasonal 6-hourly forecasts of OLR generated by ERA-Interim between the two time periods 2006-2010 and 1980-1984 for the JJA season (a) and the SON season (b).

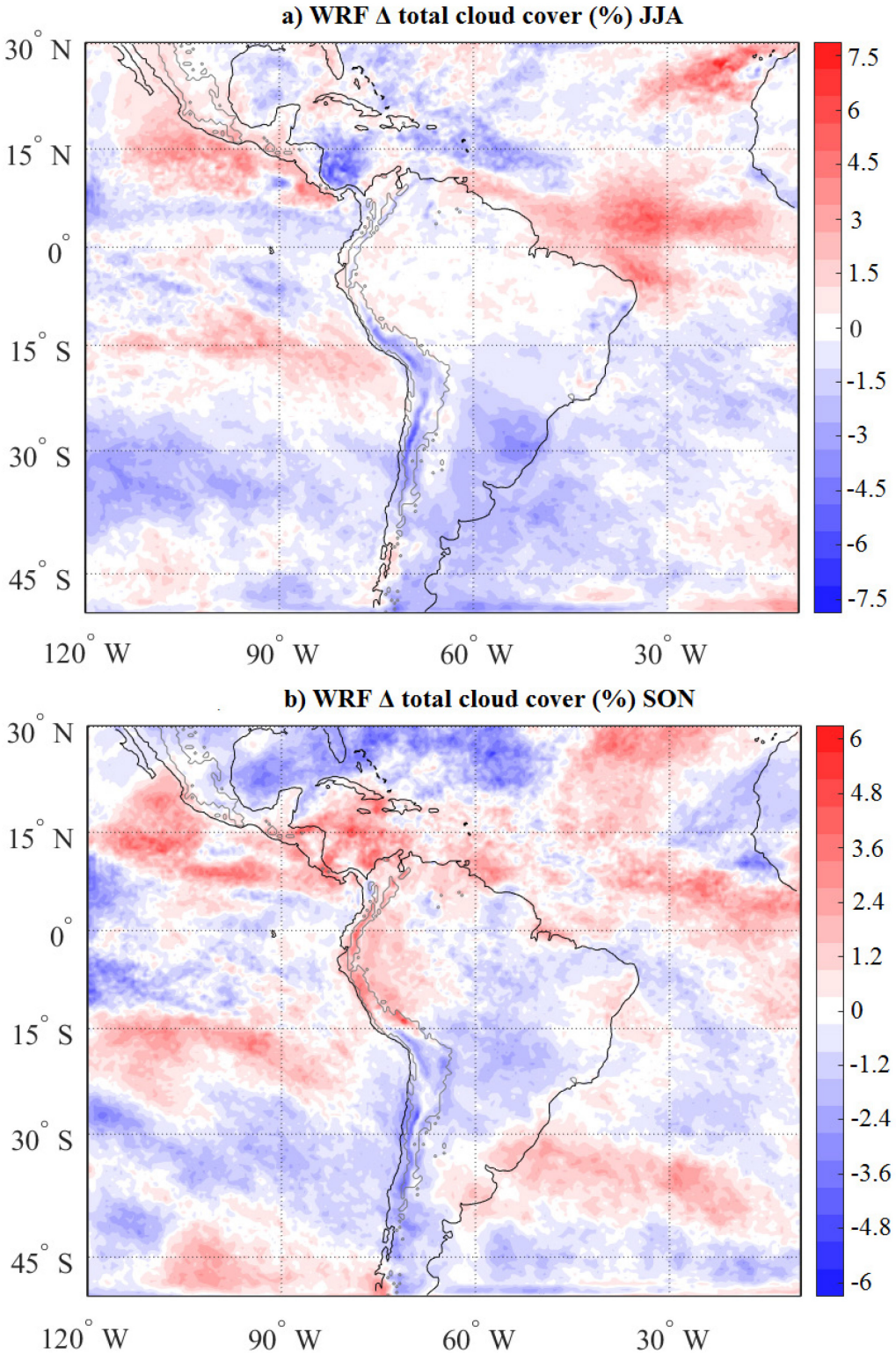


**Figure 3.11:** Difference in total cloud cover in % generated by WRF between the two time periods 2006-2010 and 1980-1984 for the JJA season (a) and the SON season (b).

This study expands further upon the work of Russell et al. (2017) by examining the WRF-simulated changes in free-atmospheric temperatures. Russell et al. (2017) determined that the Central Andes of South America exhibit rises in mid-tropospheric temperatures that exceed one standard deviation above the mean of Pan-Tropical land areas. In order to compare the regional model simulations performed here to the results of Russell et al. (2017), Figure 3.12 shows the WRF-simulated changes in mean 500mb temperatures over the domain between the time periods 1980-1984 and 2006-2010. In JJA (Figure 3.12a), the Andes Mountains do not exhibit accelerated rates of mid-tropospheric warming compared to the other land areas in the simulated WRF domain, but in SON (Figure 3.12b) the Andes Mountains do appear to exhibit relatively high rates of mid-tropospheric warming compared to the neighboring land areas. It is difficult to determine whether this local enhancement of warming exceeds rates of warming across Pan-Tropical land areas due to the limited domain, but this does suggest that the WRF model may be able to capture regional enhancement of mid-tropospheric warming in some seasons.

In terms of the relationship with regional radiative trends, it is difficult to determine whether the enhanced free atmospheric temperature trends over the Andes Mountains are in fact driven by changes in OLR and regional circulation patterns as suggested by Russell et al. (2017) because the centers of action in warming and radiation in WRF are actually quite different. Interestingly, WRF-simulated 2 meter temperatures show enhanced localized trends in the Andes Mountains relative to the rest of the continent in both austral winter and spring (Figure 3.13), which have strong spatial correlations with

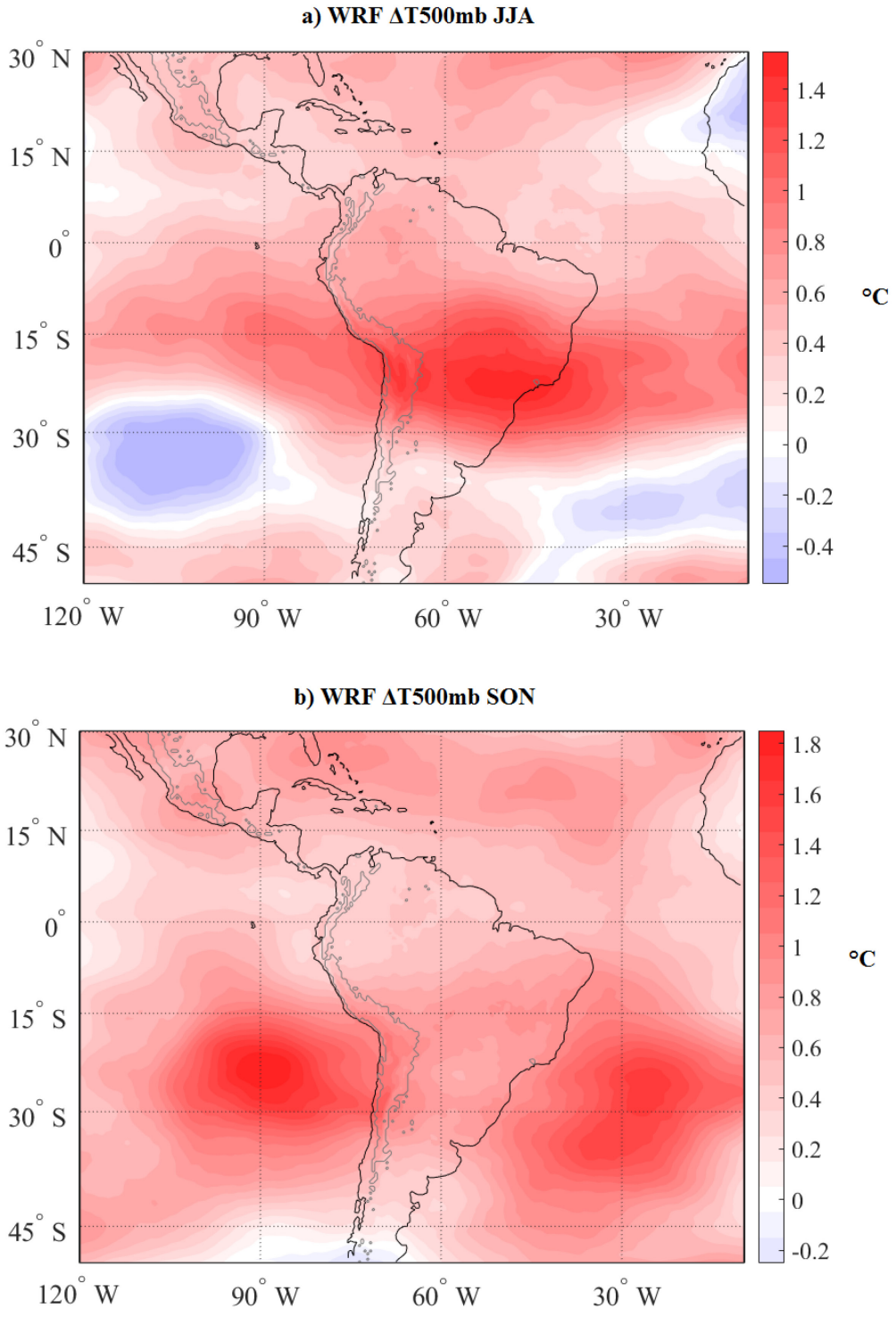


**Figure 3.12:** Difference in mean seasonal T500mb generated by WRF between the two time periods 2006-2010 and 1980-1984 for the JJA season (a) and the SON season (b).

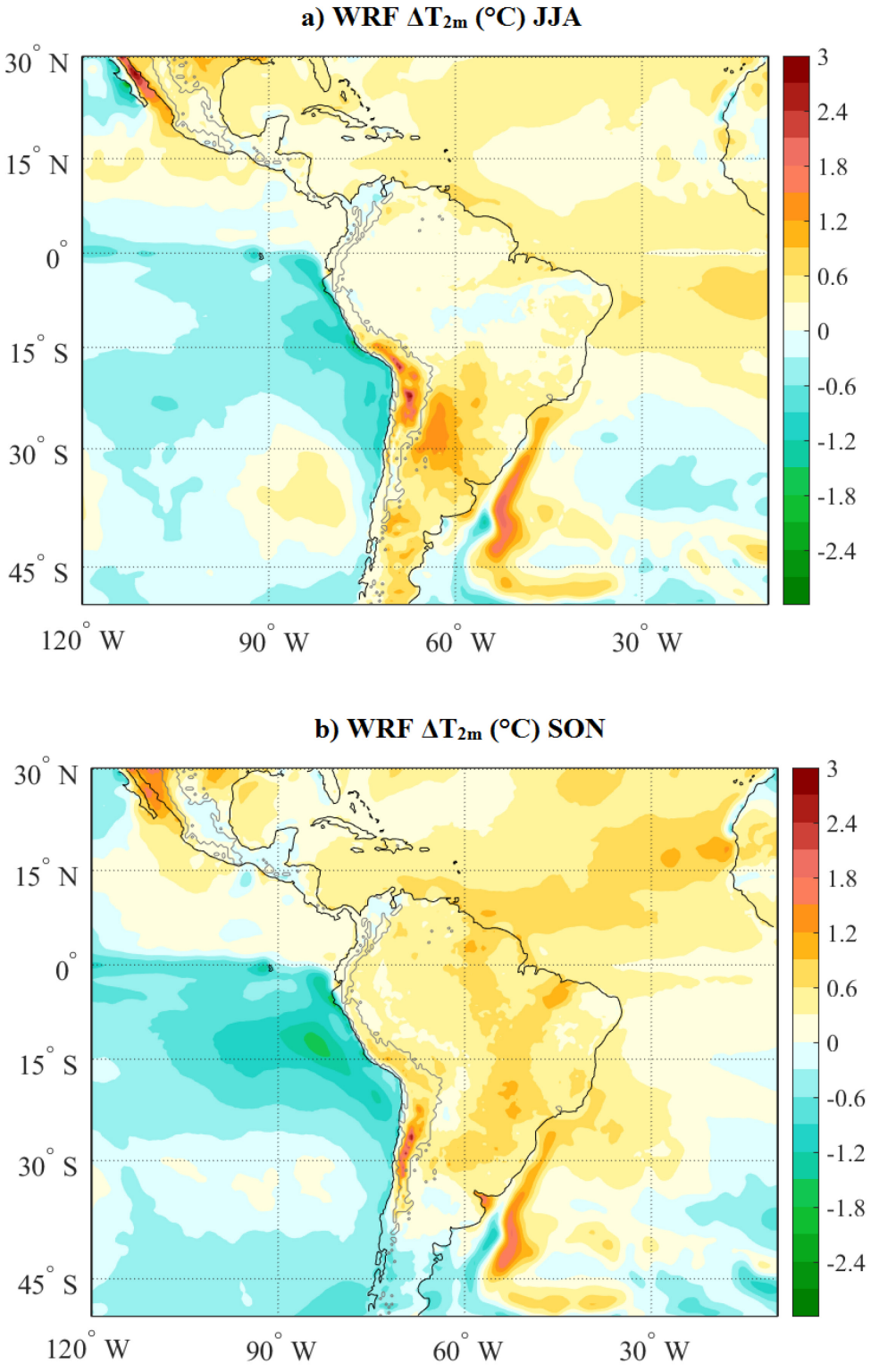


**Figure 3.13:** Difference in mean seasonal 2-meter temperature ($\Delta T_{2m}$) in °C generated by WRF between the two time periods 2006-2010 and 1980-1984 for the JJA season (a) and the SON season (b).

WRF-simulated OLR trends. Therefore, regional changes in the radiative balance may be linked to surface temperature trends in the Andes Mountains.

The technical reasons for WRF's improved performance compared to AMIP climate models in the simulation of OLR could be due to a number of reasons including 1) increased model resolution (both horizontally and vertically), 2) better parameterization of physical processes in this region of the globe, and 3) better forcing data. Yet what is perhaps more important is the dynamical reason for the improved performance of WRF over global AMIP climate model simulations. That is, what dynamical processes do the AGCMs miss due to their technical failings? In order to answer this question, changes in regional atmospheric circulation patterns are examined.

Figure 3.14 shows the difference in the mean seasonal wind vectors generated by WRF between the two time periods 2006-2010 and 1980-1984 in order to represent the change in winds over the last few decades. In JJA (Figure 3.14a), WRF simulates an intensification and northward shift, as well as a meridional tilt in, the South Eastern Pacific Anticyclone, which enhanced the coastal upwelling along the western coast of the Andes between 15°S and 30°S as well as a similar shift and potentially a slit in the South Western Atlantic Anticyclone. These changes in the semi-permanent low pressure systems over the oceans adjacent to the continent have the effect of creating an anomalously southward shift in the midlatitude westerlies progression across southern South America (as in Seager et al. 2010) which creates a general divergence over much of the central continent, and hence less uplift and less clouds.

In SON on the other hand (Figure 3.14b), there appears to be a weakening of the equatorial trade winds which may be due to either a northward shift or a delay in the

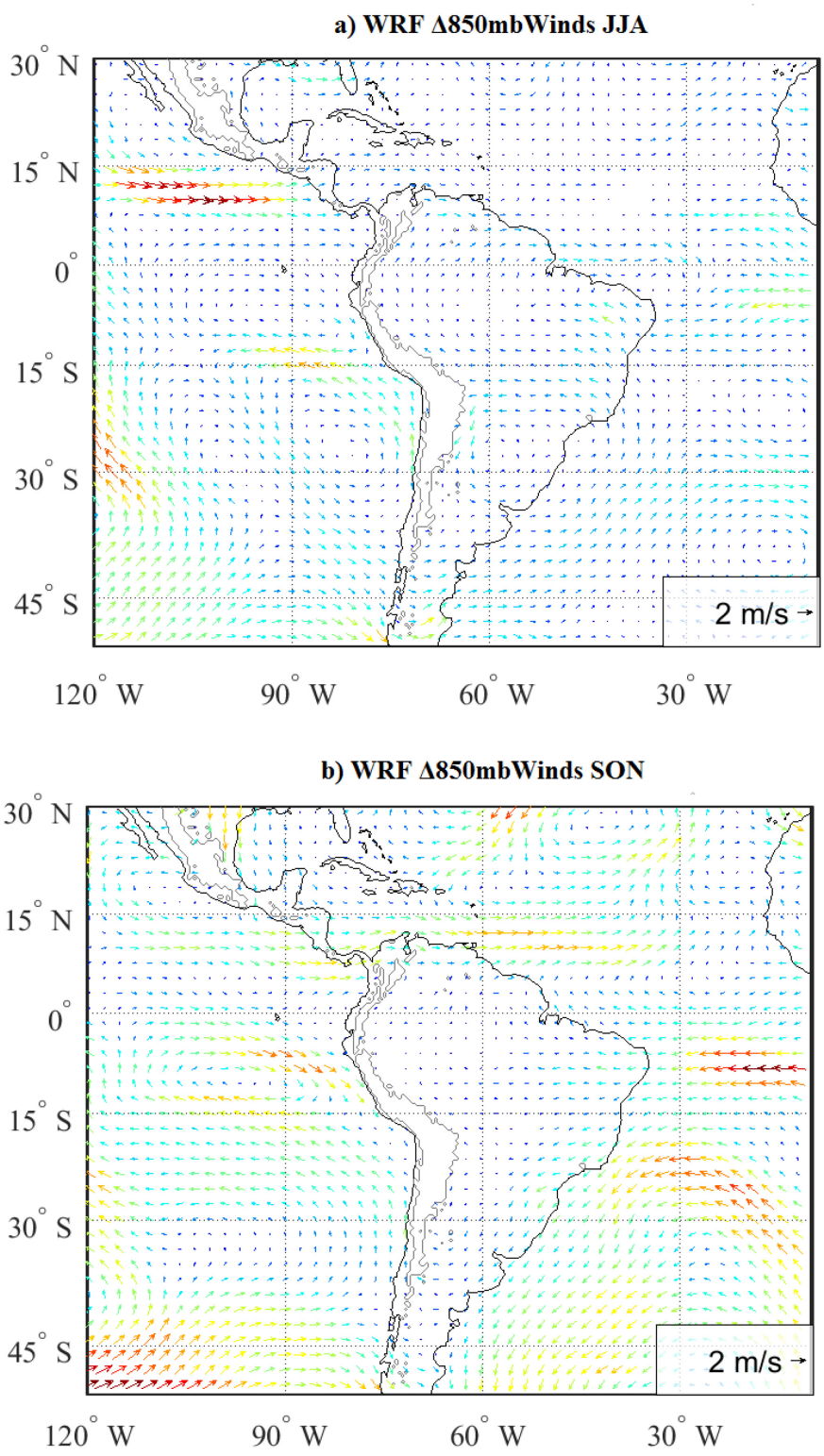


**Figure 3.14:** Difference in mean seasonal 850mb wind vectors generated by WRF between the two time periods 2006-2010 and 1980-1984 for the JJA season (a) and the SON season (b).

southward shift moving from JJA into SON. This pattern coupled with the anomalous southwestward flow along the southeastern portion of South America reduces the uplift that starts to occur in the South Atlantic Convergence Zone and brings cool dry air into the inner parts of the continent, which corresponds with less cloud cover. These trends may be related to the anomalously warm SSTs over the tropical Atlantic which resulted from a shift in the AMO into a positive phase, which has been shown to produce similar weakening of surface equatorial easterlies (Bell and Chelliah 2006). In addition, the patterns of OLR trends in SON also show decreased OLR over the tropics, which when coupled with the increases in OLR over the subtropics may be indicative of an intensification and/or northward shift in the regional Hadley cell circulation (Figure 3.9).

The simulated changes in regional circulation exhibited by WRF (Figure 3.14) are highly explanatory of the observation-based OLR trends (Figure 3.6), while the local intensification of OLR trends in particular in the southern Peruvian Andes, Bolivian Plateau, the western slopes of the Bolivian Andes and of the Central Argentinian Andes in JJA, and in the eastern slopes of the Chilean Andes in SON are likely the result of interactions between general divergent behavior and local topographically forced circulation patterns, and not due to elevation dependent warming (EDW) feedback mechanisms; see Russell et al. (2017) for a full exploration of EDW mechanisms in this region. Overall, the AGCMs are likely lacking the demonstrated trends in regional atmospheric circulation and future studies should diagnose inadequacies in the AGCM representation of changes in wind patterns in order to further understand the dynamical processes that play a part in the recent OLR trends.

## 3.4 SUMMARY AND DISCUSSION

Historical AGCM simulations generally fail to capture the historical changes in regional climate over South America over the past few decades. This is due to not only their course resolution which reduces the effect of topography on regional atmospheric circulation, but also due to their parameterization of physical processes. This is perhaps not surprising given that AGCMs must choose parameterization schemes that perform well on a global scale whereas certain parameterizations may not be well suited to the dynamics of a particular location. AGCMs may also suffer from uncertainties or deficiencies in the observational SST datasets used to force the models (e.g., Flannaghan et al. 2014). This study demonstrates that these technical issues can be overcome on a regional scale by using a high resolution, regionally-tuned mesoscale model such as WRF. WRF is used here to simulate changes in the regional climate of South America with more accuracy than AGCMs and results reveals that the previously documented increases in free-atmospheric temperatures in this region are strongly related to changes in regional atmospheric circulation patterns as hypothesized by Russell et al. (2017).

Furthermore, this study investigates the dynamical drivers for regional climate change over South America in the WRF simulations as follows. First, the opposite patterns of simulated changes in OLR over the tropics and subtropics by WRF (Figure 3.9) are consistent with the recent strengthening of the Hadley Cell circulation that has been documented by Lau and Kim (2015) and may be a primary candidate for driving regional climate change over the Andes Mountains of South America by drying out subtropical areas. Second, the recent shift of the AMO into a positive phase which is associated with

anomalously warm SSTs in the tropical Atlantic of about 0.15°K (e.g. Li et al. 2014) and anomalously weak equatorial surface trade winds (Bell and Chelliah 2006) can effectively weaken circulation patterns over South America. This shift in AMO combined with the fact that the tropical Pacific Ocean has entered a negative phase in its internal mode of multidecadal variability (e.g. PDO), may act to enhance these effects. In fact it may be this very opposite phasing between the Atlantic and Pacific Oceans which sets up a climate conducive to clear skies and warm free atmosphere in South America. Third, a shift in the midlatitude westerlies as simulated by WRF and corroborated by observational studies (Seager et al. 2010) may be the result of the southward shift in the midlatitude and/or subtropical jet which has been shown to be a robust response to the formation of the ozone hole with indirect impacts on Southeastern South American climate (e.g. Gonzalez et al. 2014).

Future studies should aim to quantitatively attribute the impact of each of these dynamical mechanisms discussed above to the changes in regional OLR and free-atmospheric temperature trends. A WRF simulation of the earlier 5-year time period 1980-1984 with an artificially imposed AMO-like SST warming in the tropical Atlantic Ocean would reveal the theoretical impact of AMO alone isolated from the other dynamical mechanisms that have manifested over the last few decades. An additional avenue to explore would be the impact of changes in the properties of the continental evapotranspiration (ET). For example, Zhang et al. (2016) report modeled trends in ET from 1981 to 2012 using the PML diagnostic model which exhibit a spatial pattern that looks broadly similar to that of the trends in OLR. Hence, changes in greenness or stomatal conductance may be resulting in less atmospheric water vapor which could be

contributing to increases in OLR. However, the 850mb wind trends (Fig. 3.14) suggest that most of the driving force is in the general atmospheric circulation over the oceans and Southern continent and not in the central part of the continent where there is a lot of vegetation. In any case, WRF simulations such as those performed in this study are highly useful for these types of investigations and should be expanded upon with manual manipulations of the lower and lateral boundary conditions to test certain hypotheses.

*Acknowledgements*

ISCCP D2 data were provided by the Integrated Climate Data Centre (ICDC), CliSAP/CEN, University of Hamburg, Hamburg, Germany, http://icdc.zmaw.de.

# Chapter 4. Understanding multidecadal variability in ENSO amplitude

**The work in this chapter has been published as a manuscript in the *Journal of Climate* (Russell and Gnanadesikan 2014) and is reproduced here.**

## 4.1 INTRODUCTION

El Niño – Southern Oscillation (ENSO) accounts for most of the interannual variability in global temperature and has links to global hydrological cycling and weather patterns (Philander 1989; Ropelewski and Halpert 1987; Hoerling et al. 1997; Cai et al. 2011). Nonlinear responses to ENSO have been seen in crop yields (Porter and Semenov 2005), ocean chlorophyll concentrations (Park et al. 2011) and the number of tropical cyclones formed (Wang and Chan 2002), among other things. Changes in ENSO amplitude produce changes in the long-period average behavior of environmental systems around the world. Therefore, it is important to understand how the amplitude of ENSO varies with time.

Representation of the variability of ENSO can differ widely between models, either due to differences in model formulation or due to climate change (e.g. Battisti and Hirst 1989; Timmermann et al. 1999). Differences in model parameterizations is one major source of inter-model differences in the mean state of the tropical Pacific – that is the

mean strength of the tropical Pacific zonal winds and SST gradients – such as whether the model includes cumulus momentum transport (CMT), which tends to shift the mean convection and trade winds eastward and enhance ENSO variability (Kim et al. 2007). Another source of inter-model differences is the varying strengths of the coupled atmosphere-ocean feedback loops which sustain ENSO. van Oldenborgh et al. (2005) used a linear regression of SST changes – based on Burgers and van Oldenborgh (2003) – in order to determine the strength of these processes in different models. A comprehensive review of the differences in the representation of ENSO in the CMIP3 and CMIP5 (Climate Model Intercomparison Project) models was performed by Bellenger et al. (2013).

It has been shown that ENSO behavior has large intrinsic, *unforced* variability, occurring on decadal and longer timescales, in both observations (Wang and Ropelewski 1995; Allan et al. 1996; Wang and Wang 1996; Kestin et al. 1998; Gershunov and Barnett 1998; Power et al. 1999; Mann et al. 2000; Hasegawa and Hanawa 2003; Kiem and Franks 2004; Kiem et al. 2003; Verdon et al. 2004) and in coupled climate models (Knutson and Manabe 1998; Walland et al. 2000; Vimont et al. 2002; Hunt and Elliott 2003; Power and Colman 2006; Wittenberg 2009). It is unclear what causes this long-period variation and what length of time is adequate to constrain this variability. In evaluating a 2000-yr control simulation of the Geophysical Fluid Dynamic Laboratory (GFDL) CM2.1 coupled global climate model (GCM), Wittenberg (2009) determined that ENSO amplitude varies on centennial timescales. He found that centennial spectra have extremes spanning a factor of 2 in power in the interannual band, with an even larger spread of spectra for 20-yr epochs. In the 4000-yr GFDL CM2.1 1860 control run

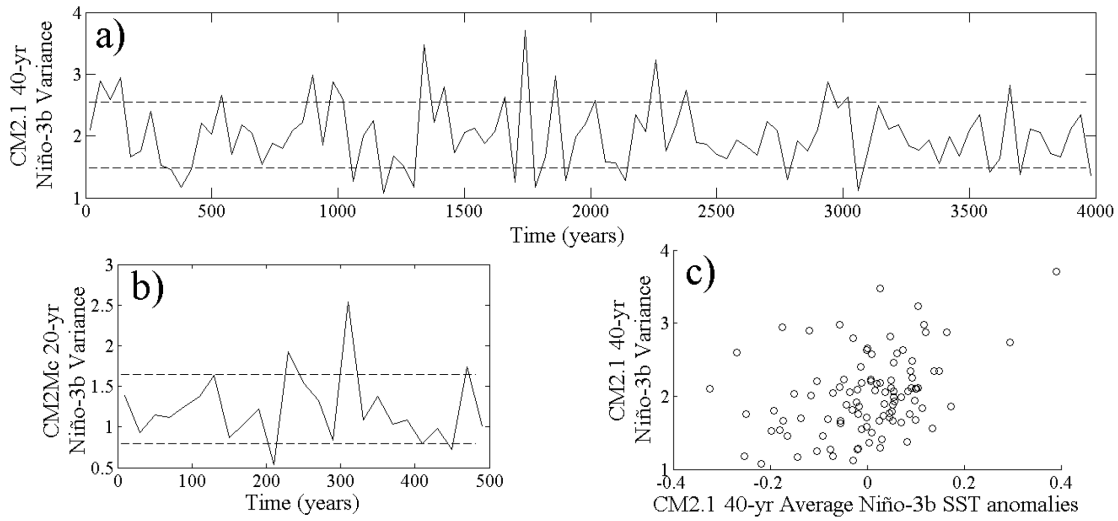


**Figure 4.1:** Variance of Niño-3b SST anomalies in (a) the CM2.1 model on 40-yr timescales and in (b) the CM2Mc model on 20-yr timescales where dashed lines mark the mean +/- the standard deviation, and (c) the 40-yr variance vs. the 40-yr average of the Niño-3b SST anomalies in the CM2.1 model.

the variance in the Niño-3b region (150W–90W, 3S–3N) ranges over a factor of 3 between different 40-yr epochs (Fig. 4.1a). In the 500-yr control run of the GFDL CM2Mc model – a lower-resolution descendant of CM2.1 described in Galbraith et al. (2011) – the variance ranges over a factor of 2 on 20-yr timescales (Fig. 4.1b).

The consequences of inherent long-period ENSO variability are not confined to the equatorial Pacific. ENSO has impacts on weather patterns around the globe, referred to as teleconnections (e.g. Ropelewski and Halpert 1987; Hoskins and Karoly 1981; Lau 1997; Trenberth et al. 1998). The teleconnections with ENSO are often nonlinear in nature (Hoerling et al. 1997). Figure 4.2 shows the regression of the log of the 40-yr smoothed precipitation onto the log of the 40-yr Niño-3 variance, which gives an idea of where ENSO holds sway over non-tropical climates. A one to one relationship would imply that the three-fold range in Niño-3b variance (Fig. 4.1a) would produce a three-fold change in precipitation, which is largely the case in the equatorial Pacific Ocean.

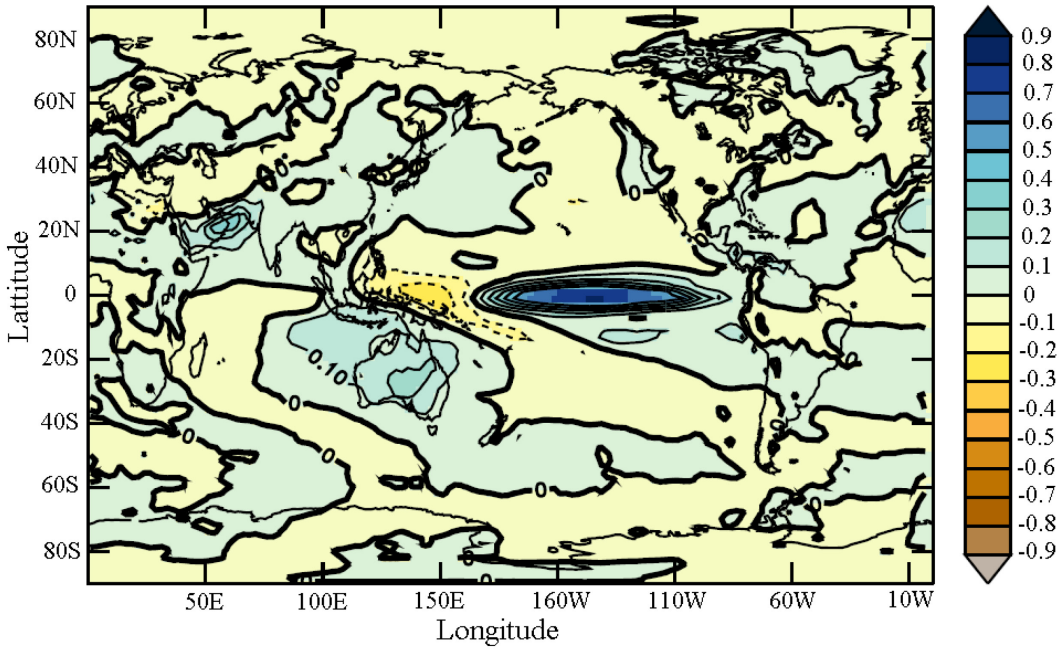


**Figure 4.2:** Regression of the logarithm of the 40-yr smoothed precipitation onto the logarithm of the 40-yr Niño-3 variance in the GFDL CM2.1 model.

A 0.1 value would imply that this change would be 30%, which is still potentially important for areas like Australia and Indonesia. For example, Power et al. (2006) found that the observed average rainfall over Australia exhibits a correlation with the Niño-4 SST anomaly index of -0.53, which ranges higher and lower with interdecadal variability. In addition, the zonal pattern of ENSO-related SST anomalies influences global circulation and precipitation. For example, Kim et al. (2009) showed that tropical storm tracks in the North Atlantic Basin are differently affected by central Pacific warming than by eastern Pacific warming. Ashok et al. (2007) found that ENSO-like events with a warm central tropical Pacific flanked by cooler waters to the east and west (referred to as El Niño Modoki) can, depending on the season, produce teleconnections that are the opposite of those from a conventional El Niño.

Because the ENSO system exhibits multidecadal to centennial variability in its amplitude as well as its zonal pattern, it will likely require multiple-century model runs to detect changes in the normal ENSO behavior due to anthropogenic forcing. Stevenson et al. (2012) evaluated CCSM4 Coupled Model Intercomparison Project phase 5 (CMIP5) model simulations and found that there are no statistically significant changes in ENSO variability with increases in $CO_2$, except at the highest $CO_2$ levels. They postulated that this lack of significance is due to the short length of the twenty-first-century simulations. In a more encompassing analysis of 27 CMIP5 models, Stevenson (2012) showed that the climate change signal is closely comparable to the naturally occurring centennial variations in ENSO in all the models. Therefore, it is important to characterize the long-period natural variability before we can try to tease out a climate change signal.

Wittenberg (2009) hypothesized that the slow variation of ENSO results from Poisson statistical behavior due to seasonal phase-locking in addition to interannual memory on short term scales of up to 10 years. Similar variability of the ENSO amplitude can be produced in delayed oscillator models simply as a result of integrating noise (e.g. Penland and Sardeshmukh 1995; Newman et al. 2011). This would lead one to expect the coupling between the ocean and the atmosphere to be constant in a control simulation, even as the amplitude changes. If, however, the coupling is not constant over different time periods, it might imply that there is a driving force behind the changes in coupling strength with time. Therefore, one of the goals of this paper is to identify potential driving mechanisms for long-period changes in ENSO amplitude.

There are a few possible simple explanations for the long-period variability of ENSO. One possibility is that the changes in Niño-3b anomalous SSTs are due to changes in the

mean SSTs. Battisti and Hirst (1989) proposed that under climate change the zonal asymmetries across the equatorial Pacific would reduce, which they argued would decrease ENSO variability. If true, this would have important implications for understanding the response of ENSO to climate change. However, in the CM2.1 model the temporal range of the 40-yr mean Niño-3b SST anomalies is small compared to the overall spatial variance of SSTs (Fig. 4.1c). This raises the question of whether such small changes in temperature can really drive the large changes in variance. Moreover, it is evident by looking at Figure 4.1c that there is not a strong relationship between the average SST and variance of the 40-yr Niño-3b SST anomalies (correlation coefficient of 0.374). Therefore, the mean temperature is not a particularly good predictor of the changes in variance. Timmerman et al. (1999) also rejected this possibility as the mechanism for enhanced interannual variability, in favor of changing ocean dynamics. They argued that the strengthening of the thermocline is the most important change in the mean state of the tropical Pacific Ocean under climate change and that it enhances interannual variability. Along similar lines, Anderson et al. (2009) proposed that decreased stratification due to increased shortwave penetration would reduce ENSO-related interannual variability.

Another possibility is that the changes in Niño-3b variance are the result of a change in the shape of ENSO (Fedorov and Philander 2000), which has implication for teleconnections like those shown by Kumar et al. (2006). We would expect from Fedorov and Philander's (2000) mechanism that epochs with low ENSO amplitude would see variance concentrated in the central tropical Pacific, while epochs with higher ENSO amplitude would be concentrated more in the eastern tropical Pacific. Instead we see that

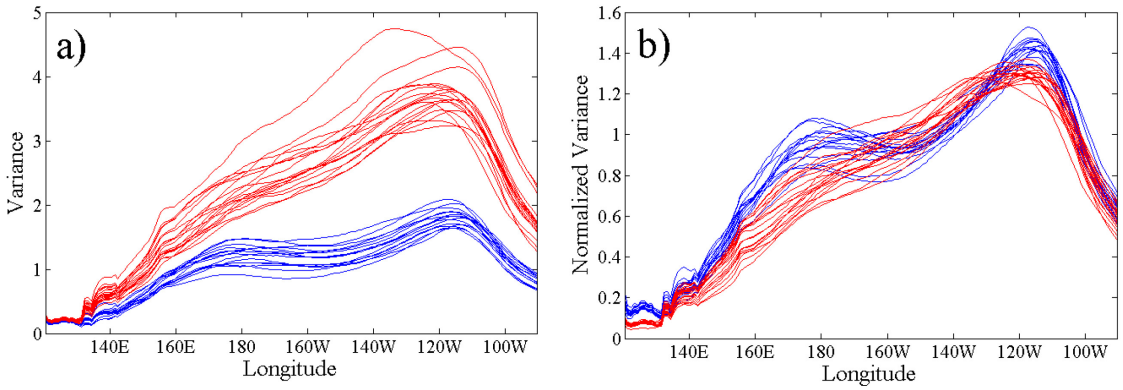


**Figure 4.3:** (a) Variance of SST anomalies (averaged over 3S-3N) during high (red) and low (blue) variance 40-yr periods and (b) variance normalized by its zonal mean in the CM2.1 model.

the shapes are quite similar (Fig. 4.3). In this paper, high (low) variance periods are defined as periods with Niño-3b variance greater than (less than) the mean plus (minus) the standard deviation of the Niño-3b variance time series over the total 4000-yr run (e.g. epochs above/below the dashed lines in Fig. 4.1a). Insofar that there is a difference between high and low amplitude ENSO epochs, it is that the low-amplitude epochs seem to show two distinct peaks, a phenomenon that does not map neatly onto the Fedorov and Philander (2000) theory.

The changes in SSTs (Fig. 4.1c), precipitation (Fig. 4.2) and ENSO shape (Fig. 4.3) are difficult to interpret in part because it is unclear whether they *result* from or *drive* changes in ENSO amplitude. Distinguishing between cause and effect requires an examination of the changes in the response of the ocean to the atmosphere as well as changes in the response of the atmosphere to the ocean. This paper examines these responses by building upon the framework proposed by van Oldenborgh et al. (2005) for examining inter-model differences in oceanic temperature responses. This is an

extremely useful method for characterizing the long-period variability in ocean-atmosphere coupling strengths.

The outline of this paper is as follows. Section 2 presents the models upon which the regression is performed. Section 3 describes the theory underlying the linear regression technique and the methodological application herein. The results of the linear regression on the models are presented and compared in Section 4a. In order to identify potential driving mechanisms of multidecadal variability, section 4b first investigates the connection between the model regression coefficients and ENSO variability (with a focus on the oceanic response to atmospheric forcing). Then the paper extends the regression technique to the individual temperature tendency components associated with specific transport mechanisms. Section 4c examines the atmospheric response to oceanic forcing, while section 5 summarizes our procedure and findings, while linking the results to implications for evaluating and using climate models.

## 4.2 MODELS AND DATA

This paper investigates the variability in ENSO amplitude and ocean-atmosphere coupling strengths on multidecadal timescales in three models, two of which are control runs. The first is the 4000-yr pre-industrial control run of the GFDL CM2.1 model which couples atmosphere, ocean, land, and sea ice components (Delworth et al. 2006). The atmospheric component has a horizontal resolution of 2.5° longitude by 2.0° latitude, with 24 vertical levels. The ocean component has a horizontal resolution of 1° in the extratropics, with zonal spacing reducing to 1/3° near the equator. The ocean has 50

vertical levels, the first 22 of which are evenly spaced by 10 meters. The CM2.1 model is ranked among the world's best GCMs in terms of its simulation of global climate as well as ENSO (van Oldenborgh et al. 2005; Wittenberg et al. 2006; Guilyardi 2006; Reichler and Kim 2008). The model does not use flux adjustments. The control run holds atmospheric composition, insolation and land cover constant at 1860 values, which means that all variability in the simulation is internally produced, as opposed to being driven by any anthropogenic (greenhouse gas, aerosol, land use change) or natural (solar variability, volcanic aerosol) climate forcings. The length of the 4000-yr simulation makes it a prime candidate for examining long-period variability.

However, the CM2.1 model did not save out all the temperature tendency components associated with radiative fluxes into the ocean's surface and large eddies within the mixed layer, which are essential for distinguishing between advective and diffusive changes. Therefore, we also present the results of the analogous 1860 control run of the 500-yr GFDL Climate Model version 2 with Modular Ocean Model version 4p1 at coarse resolution (CM2Mc; Galbraith et al. 2011), which saves out all the temperature tendency terms (advective, diffusive and eddy tendencies). CM2Mc is a lower-resolution version of the GFDL's CM2Mc model that uses no flux adjustments. It is very similar to the GFDL coupled model CM2.1 (in particular the column physics in the atmosphere are identical), but it has a coarser resolution in both atmosphere and ocean and uses an updated version of the Modular Ocean Model ocean code (MOM4p1) which includes a parameterization of mixed layer eddies as described in Fox-Kemper et al. (2011). The ocean meridional resolution in CM2Mc varies between 3 and 2/3 degrees, with sufficiently high resolution to resolve the equatorial wave guide and produce a reasonable

ENSO (Galbraith et al. 2011). Possible mechanisms controlling *unforced* changes in coupling strengths in these two models are explored in order to provide a baseline for comparison with 20$^{th}$ century, 21$^{st}$ century and future $CO_2$-forced changes.

This paper also analyzes the GFDL ensemble coupled data assimilation (ECDA) system, which was developed using the same basic model configuration as CM2.1 but strongly constrained by observations. ECDA uses CM2.1 to interpolate in data-poor regions and time periods. Therefore, differences between ECDA and CM2.1 are likely due to the addition of data constraints, rather than to some underlying difference in physical parameterizations. The ECDA has been shown to be a good representation of the ocean variability associated with ENSO and other climate modes (Chang et al. 2012). This study uses ECDA reanalyzed ocean temperatures and surface wind stresses for the period 1961–2010 (Zhang et al. 2007) in order to compare the two control runs to the observed variability of the tropical Pacific.

## 4.3 THEORY AND METHODOLOGY

Several phenomena play a role in the natural fluctuations associated with ENSO in the Niño-3b region: coastal and equatorial upwelling, zonal SST gradients, thermocline depth variations, and atmospheric circulation induced by east-west sea level pressure asymmetry. These various components determine the characteristics of ENSO. In essence, there is a positive feedback loop (Bjerknes 1966) whereby wind anomalies over the central equatorial Pacific cause wave propagation to the east in the top layers of the ocean which generate thermocline depth anomalies (Fig. 4.4). This results in coastal

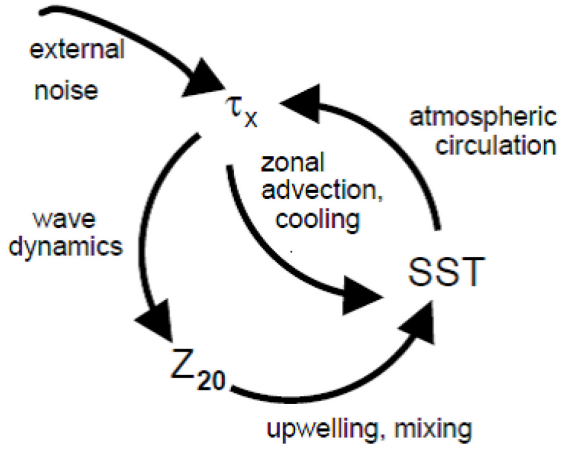


**Figure 4.4:** The main feedbacks in the ENSO cycle (van Oldenborgh et al. 2005) – licensed under a Creative Commons License 2.0.

upwelling which brings cooler seawater from depth up to the surface in the eastern equatorial Pacific, thereby producing a zonal SST gradient, which reinforces the pressure asymmetry along the equator and initiates further atmospheric circulation. The inner loop in Figure 4.4 portrays how the zonal winds push the cooler upwelled waters in the east toward the west, which cools the surface of the ocean in the central equatorial Pacific (Wyrtki 1975; Picaut et al. 1996). Given that the ocean is often assumed to modulate climate on long timescales (Hasselmann, 1976), it is reasonable to hypothesize that long-period changes in the structure of the ocean might produce changes in the strength of coupling that would modulate ENSO amplitude.

The relative strengths of the processes in Figure 4.4 in forcing SST anomalies can be modeled using a linear regression. van Oldenborgh et al. (2005) have shown that local changes in SSTs in the equatorial Pacific can be simulated as a linear function of thermocline depth anomalies, zonal wind stress anomalies and SST anomalies. The resulting linear regression equation is motivated by the linearized perturbation advection

equation for an incompressible flow in two dimensions (Eq. 4.1), assuming no meridional motion.

$$\frac{\partial T'}{\partial t} + \overline{u}T'_x + \overline{w}T'_z - (\overline{K}_v T'_z)_z + u'\overline{T}_x + w'\overline{T}_z - (K'_v\overline{T}_z)_z = Q' \qquad (4.1)$$

$T$ indicates the temperature and the subscripts indicate a derivative with respect to either the zonal ($x$) or vertical ($z$) direction and $K_v$ represents a diffusion coefficient. The zonal and vertical velocities are denoted by $u$ and $w$ respectively. Over-bars and primes indicate mean and perturbation quantities respectively. For the purposes of this paper, the means are calculated for each multidecadal epoch throughout the models and the perturbation quantities are the deviation from the mean of each epoch. The first term $\partial T'/\partial t$ is the change in temperature anomalies with time at a particular location, also called the local change. The second, third and fourth terms $\overline{u}T'_x + \overline{w}T'_z - (\overline{K}_v T'_z)_z$ represent the advection and mixing of anomalous temperatures by the mean flow. Insofar as vertical temperature perturbations and mean flow dominate this process, we expect a first order dependence on the upwelling and mixing of thermocline depth anomalies. Therefore, it is reasonable to hypothesize that these terms can be represented as a linear function of the thermocline depth anomaly. It is however worthwhile to note here that there need not be a strong relationship between $Z_{20}$ or the depth of maximum $N^2$ (buoyancy frequency squared) and integrated stratification above that depth. The fifth, sixth and seventh terms $u'\overline{T}_x + w'\overline{T}_z - (K'_v\overline{T}_z)_z$ represent the advection and mixing of the mean temperature by anomalous flow and mixing, which are expected to be related to the zonal wind stress. The final term $Q'$ is the perturbation heat flux from the atmosphere to

the ocean, including the feedback of SSTs on air-sea fluxes, which can be approximated by a linear relaxation of the temperature anomalies.

As a result, Equation 4.1 can be thus approximated as a linear regression equation (Eq. 4.2) where the changes in SST with time are regressed onto $Z_{20}$ (the depth of the 20°C isotherm – a useful approximation of the depth of the thermocline), $\tau_x$ (the zonal wind stress) and the local SST (Burgers and van Oldenborgh 2003).

$$\frac{\partial SST}{\partial t}(x,y,t) = \alpha(x,y)\cdot Z_{20}(x,y,t-\delta) + \beta(x,y)\cdot \tau_x(x,y,t) - \gamma(x,y)\cdot SST(x,y,t) \quad (4.2)$$

$$\text{where} \qquad \frac{\partial SST}{\partial t}(x,y,t) = SST(x,y,t+1) - SST(x,y,t)$$

The resulting weights/coefficients on each of the linear terms provide a first order estimate of the strength of atmosphere-ocean coupling. This simplification allows for the quantification of the complex processes involved in ENSO. The regression coefficient $\alpha$ determines the influence of the thermocline depth anomalies on the local change in SSTs, while $\beta$ determines the influence of the zonal wind stress anomalies on the local change in SSTs. The sign convention for zonal wind stress is that westerlies (wind blowing from west to east) are positive. The time $t$ indicates the time step in months; $x$ and $y$ indicate the zonal and meridional indices respectively. The regression coefficient $\gamma$ represents the damping time for SST anomalies. Thermocline depth anomalies are lagged by a factor $\delta$, which represents the finite upwelling time, because thermocline depth anomalies tend to lead SST anomalies with a delay ranging from 2 weeks in the eastern equatorial Pacific to 1 year in the central equatorial Pacific (Zelle et al. 2004). Although the finite upwelling time δ varies zonally, fitting a zonally variable δ produces unstable results when different time periods are considered; sharp changes in δ (e.g. from one month to two months) are

associated with sharp changes in the regression coefficients from one time period to another. Such correlated changes in regression coefficients are characteristic of a model which is over-fit, suggesting that zonal wind stress and lagged thermocline depth anomalies are not independent. Thus, in contrast to van Oldenborgh et al. (2005) we chose to keep $\delta$ constant at 1 month. Each of the variables (SST, $Z_{20}$ and $\tau_x$) is first reduced to monthly anomalies, the regression coefficients are computed as functions of both latitude and longitude and then they are averaged over 3S–3N.

van Oldenborgh et al. (2005) evaluated the performance of Equation 4.2 on climate models which were prepared for the Intergovernmental Panel on Climate Change (IPCC) Fourth Assessment Report (AR4) and on observations from the Tropical Atmosphere Ocean (TAO) array. The models exhibit varying sensitivities to the feedback processes captured by the regression coefficients. Of all the models tested, the CM2.1 model ($20^{th}$ century run) was among the top performers in exhibiting a realistic and balanced ENSO cycle as depicted by the regression coefficient strengths when compared to observations. However, the CM2.1 $20^{th}$ century run has climate-forcing built in and is relatively short in duration. One of the questions addressed here is how Equation 4.2 performs on the model when there is no climate forcing built in.

## 4.4 RESULTS

### 4.4.1 MODEL RESULTS AND COMPARISON WITH ECDA

The results of the linear regression (averaged over 3S–3N) are shown in Figure 4.5 for CM2.1 and in Figure 4.6 for CM2Mc. The CM2.1 regression coefficients are shown for 40-yr timescales (Fig. 4.5 column 1: thin gray lines), 200-yr timescales (Fig. 4.5 column 2: thin gray lines) and for the entire 4000-yr duration (Fig. 4.5: thick black lines). High variance periods are colored red while low variance periods are colored blue. It is clear that for 40-yr evaluation periods the CM2.1 control run produces widely ranging regression coefficients across epochs. The regression coefficients range within about a factor of 2 from the 4000-yr regressed amplitudes. Thus the atmosphere-ocean coupling strengths are not constant in the CM2.1 control run but in fact change on multidecadal timescales. Over longer evaluation periods, such as 200 years (Fig. 4.5 column 2), the regression coefficients are more well-constrained across different epochs.

The CM2Mc regression coefficients were only evaluated on 20-yr timescales (Fig. 4.6) due to the shorter duration of the model run. Although this produces very few samples (25 to be exact, of which only 2 are low variance and 3 are high variance), evaluating on any shorter timescales would run the risk of capturing interannual variations which would dilute the longer-term behavior. The CM2Mc regression coefficients exhibit qualitative agreement with those of CM2.1, which gives us some degree of confidence that the CM2Mc model can be used to decompose these regression coefficients into the individual temperature tendency terms that drive them.

In looking at the 40-yr CM2.1 regression coefficients in Figure 4.5, it is clear that there are large differences between how the system responds to the thermocline depth and wind stress anomalies in times of high and low variance. There are two main regions in the pattern of $\alpha$ where there is a distinguishable difference between high and low variance

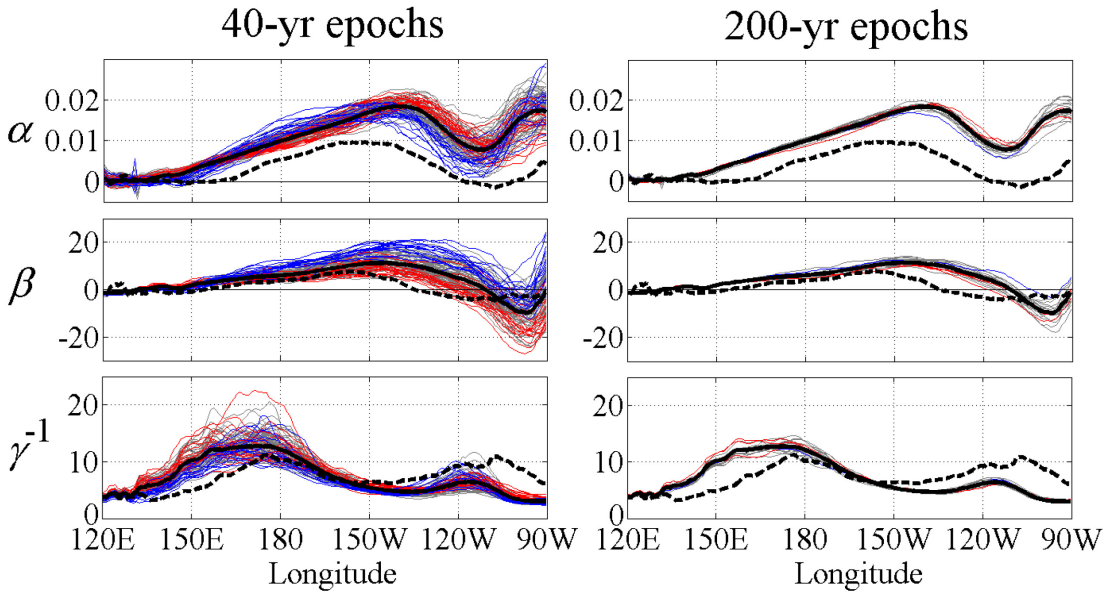


**Figure 4.5:** Regression coefficients $\alpha$ (km$^{-1}$ month$^{-1}$) – the thermocline depth parameter, $\beta$ (kPa$^{-1}$ month$^{-1}$) – the wind stress parameter and $\gamma^{-1}$ (months) – the damping time – averaged over 3S–3N in the CM2.1 model (bold black lines), in the ECDA reanalysis (dashed bold black lines), and in time periods of two different durations in the CM2.1 model (thin gray lines): 40-yr epochs and 200-yr epochs, where red (blue) lines indicate high (low) Niño-3b variance periods.

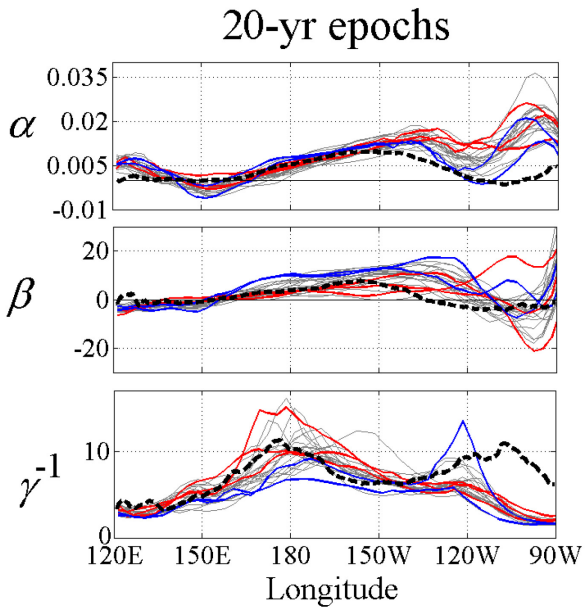


**Figure 4.6:** Regression coefficients $\alpha$ (km$^{-1}$ month$^{-1}$) – the thermocline depth parameter, $\beta$ (kPa$^{-1}$ month$^{-1}$) – the wind stress parameter and $\gamma^{-1}$ (months) – the damping time – averaged over 3S–3N, on 20-yr timescales in the CM2Mc model (thin gray lines), where red (blue) lines indicate high (low) Niño-3b variance periods, and in the ECDA reanalysis (dashed bold black lines).

periods: 170E–170W (hereafter referred to as the $\alpha_{west}$ region) and 138–118W (hereafter referred to as the $\alpha_{east}$ region). During high variance 40-yr periods there is weaker response of local SST changes to thermocline depth anomalies in the $\alpha_{west}$ region and a stronger response in the $\alpha_{east}$ region. Another way of looking at this is that $\alpha_{east} - \alpha_{west}$ (the difference between the 40-yr average $\alpha$ in each of those regions) tends to be negative during low variance periods and positive during high variance periods. In essence, $\alpha_{east} - \alpha_{west}$ can be used as a metric of the response of the SST to the slope of the thermocline in this model because it captures the relationship between ENSO amplitude variance and the thermocline depth fluctuations around an inflection point that is somewhere between those two regions. There is also a clear zonal shift in the shape of $\alpha$ between high and low variance periods, evident on both 40-yr and 200-yr timescales. In the CM2Mc model, there is a qualitatively similar trend in the $\alpha_{east}$ region such that there is higher response of local SST changes to thermocline depth anomalies during high variance periods. There does not appear to be a similarly strong separation in the $\alpha_{west}$ region, but it is difficult to tell given the small number of samples.

The pattern of the 40-yr CM2.1 $\beta$ exhibits differences in its magnitude between high and low variance periods over much of the equatorial Pacific (180–90W). Lower variance periods are associated with higher $\beta$ in the central equatorial Pacific, indicating a *stronger* response of the local SST change to wind stress anomalies, and lower $\beta$ in the eastern equatorial Pacific, indicating a *weaker* response to wind stress anomalies and of the opposite sign (and vice versa for high variance periods). The pattern of the CM2Mc $\beta$ shows a similar separation between high and low variance periods in much of the central equatorial Pacific, but the signal becomes ambiguous east of 120W.

The pattern of the 40-yr CM2.1 $\gamma^{-1}$ does not exhibit a clear difference between high and low variance 40-yr periods, except perhaps in the eastern most reaches of the equatorial Pacific basin. However, there does appear to be less damping in the western and central equatorial Pacific during times of low variance on 200-yr timescales. In the CM2Mc model, there is some evidence of separation in the pattern of $\gamma^{-1}$ in the western and central equatorial Pacific, although the high variance periods are not actually very different from normal variance periods (periods within one standard deviation of the mean). In both models in the region around 130–110W the low variance periods actually bracket the high variance periods.

These regression coefficients are not directly comparable to those calculated by the original study of van Oldenborgh et al. (2005) from the climate-forced CM2.1 simulation and from observations for three reasons. First, this study uses a constant finite upwelling time $\delta$ (from Eq. 4.2) as opposed to a variable one. Second, the CM2.1 20$^{th}$ century run has climate-forcings built in, while the 4000-yr control run keeps climate parameters constant at 1860 values. Third, van Oldenborgh et al. (2005) evaluated a single century, while we evaluate multiple centuries, in addition to multidecadal timescales. From our analysis, we can infer that a single century regression may produce regression coefficients that have very different amplitudes compared to other centuries.

Comparing the regression coefficients presented in this study to the observationally-derived regression coefficients in van Oldenborgh et al.'s (2005) paper is also complicated because it would be difficult to determine what amount of the differences are due to model inadequacies in representing the real-world, and what amount is due to the difference of including or excluding climate-forcing, not to mention the differences in

measurement locations. In an effort to address this issue, the regression is performed on the ECDA reanalysis, which has been shown to agree well with observations in both climatology and variability for the 50-yr period between 1961 and 2010. ECDA is ideal for comparison because it is on the same grid system as CM2.1.

The resulting ECDA regression coefficients, as shown in Figures 4.5 and 4.6 as the bold dashed black lines, display some qualitative similarities to the model-regressed coefficients. The shape of the CM2.1 $\alpha$ is very similar to that of ECDA, but with higher amplitude. In addition, there are slight zonal differences in the shape of $\alpha$ between CM2.1 and ECDA. The shape of $\beta$ differs largely between ECDA and CM2.1, with the CM2.1-regressed $\beta$ having higher amplitude. The peaks of the CM2.1 $\gamma^{-1}$ appear to be shifted slightly to the west when compared to the ECDA $\gamma^{-1}$, with higher amplitude in the western equatorial Pacific and lower amplitude in the eastern equatorial Pacific. The CM2Mc regression coefficients exhibit similar biases in zonal shape to those of CM2.1, but the CM2Mc amplitudes are much closer to those of ECDA.

It is difficult to determine a mechanism underlying the biases of the model given that ECDA does not conserve energy; that is ECDA adds spurious sources of heat where the CM2.1 model diverges from observations. However, we would conjecture that the overly strong response of the CM2.1 local change in SST anomalies to the thermocline depth anomalies ($\alpha$) is either due to upwelling from too great depths, overly strong upwelling, or too much ocean mixing. The overly strong response of the CM2.1's ocean surface to a given wind stress anomaly ($\beta$) could also be due to turbulent heat fluxes being too strong and/or upwelling coming from too great a depth. This may be because the model does not properly represent ocean eddy fluxes due to Tropical Instability Waves (Jochum and

Murtugudde 2006). The biases in the damping time ($\gamma^{-1}$) probably result from inadequacies in the parameterization of convection and clouds in the CM2.1 model (Wittenberg et al. 2006; Kim et al. 2007; Kim et al. 2011). For instance, Wittenberg et al. (2006) showed that the convective response in the CM2.1 is shifted too far to the west, which may explain the westward shift in the CM2.1 damping time peaks as compared to the ECDA. The regression coefficients lend themselves to understanding why the CM2.1 model produces an overly vigorous ENSO than has been seen over the past 50 years, a bias noted by Wittenberg et al. (2006). In the case of the coarser CM2Mc, the ocean's surface responds more realistically to wind stress and thermocline anomalies, which may produce more realistic ENSO amplitude.

### 4.4.2 CHANGES IN THE OCEANIC RESPONSE OF THE OCEAN TO THE ATMOSPHERE

If multidecadal variations in ENSO amplitude are caused by changes in the strength of ocean-atmosphere coupling, they will be reflected in the regression coefficients. In general, one would expect higher ENSO amplitude variance to be associated with an ocean surface that is more responsive to both thermocline depth anomalies (larger $\alpha$) and zonal wind stress anomalies (larger $\beta$), and less strongly damped (smaller $\gamma$). Figure 4.7 shows the correlation between the CM2.1 regression coefficients (the thin gray, blue and red lines in Figure 4.5) and the CM2.1 Niño-3b variance for each 40-yr epoch as a function of longitude. The dashed lines draw the eye to the regions that exhibit correlations above 0.5 and below -0.5, an arbitrary threshold for high correlation. The

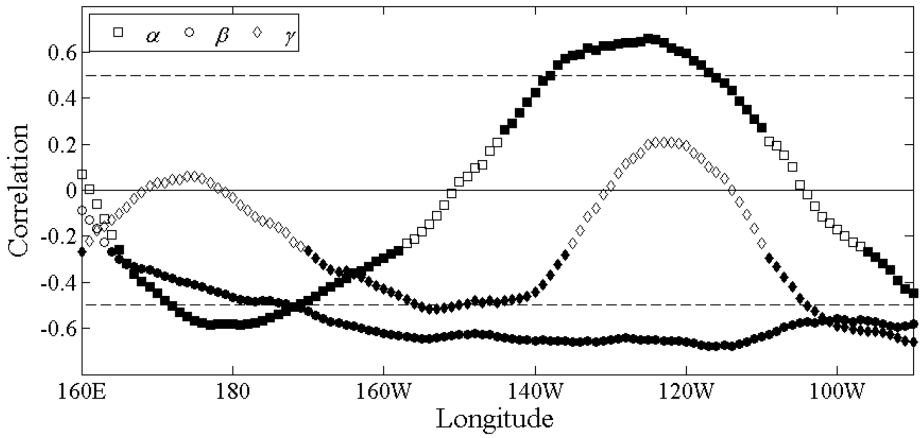


**Figure 4.7:** Correlation between the thermocline regression coefficient $\alpha$ (squares), the wind stress regression coefficient $\beta$ (circles) and the inverse damping time $\gamma$ (diamonds), and the Niño-3b variance on 40-yr timescales in the CM2.1 model. Dashed black lines draw attention to the 0.5 correlation coefficient level. Filled symbols are significant to the $p<0.01$ level.

filled symbols are significant to the $p < 0.01$ level. The inverse damping time $\gamma$ is not highly correlated with Niño-3b variance except in the eastern equatorial Pacific where there is a strongly negative correlation. This is expected because a larger $\gamma$ (shorter relaxation time) would be associated with more damping of temperature anomalies due to weaker winds and/or more longwave trapping, thus producing lower Niño-3b variance. The wind stress regression coefficient $\beta$ is highly anticorrelated with the Niño-3b variance on 40-yr timescales throughout most of the equatorial Pacific. This is the opposite of what one would expect if an increase in ENSO amplitude was due to a more responsive ocean surface. The thermocline depth regression coefficient $\alpha$ has a negative correlation with Niño-3b variance (also in the opposite direction to explain a stronger ENSO) in the $\alpha_{west}$ region, but a positive correlation in the $\alpha_{east}$ region.

In order to determine what processes could be driving the long-period variations in the responsiveness of the ocean's surface, we first examine the conceptual basis for the

regression (Eq. 4.1). As stated earlier, $\beta$ is expected to represent $u'\overline{T}_x + w'\overline{T}_z - (K_v'\overline{T}_z)_z -$ the transport of the mean temperature by the anomalous flow and mixing. Therefore, a possible source of the variability in SSTs could be changes in the mean background temperature gradient. Since the vertical temperature tendency is much larger than the zonal temperature tendency (by about a factor of 3 in the CM2Mc model), changes in $\beta$, and therefore a large amount of the changes in ENSO amplitude, are likely to reflect changes in vertical temperature stratification.

Indeed, the vertical temperature stratification in the subsurface equatorial Pacific is highly correlated with the Niño-3b variance on multidecadal timescales in both the CM2.1 model (Fig. 4.8a) and the CM2Mc model (Fig. 4.8b). For example, in the CM2.1 model the average $\beta$ over the region 170–110W exhibits a strong negative relationship (correlation coefficient of -0.69) with the average vertical temperature stratification at 45m depth (Fig. 4.12). Vertical temperature stratification is defined here as the difference between the ocean temperature at the surface box (5 m) and the temperature at any given depth. In the CM2.1 model, higher Niño-3b variance is concurrent with stronger vertical temperature stratification in the central equatorial Pacific, representing a shoaling of the thermocline, and weaker stratification in the eastern equatorial Pacific, representing a deepening of the thermocline. Hence, there is a strong indication that multidecadal epochs with high ENSO variance have generally flatter thermoclines and, as would be expected, less upwelling for a given wind stress in the eastern equatorial Pacific (Fig. 4.9a). The relationship between stratification and ENSO variance in the CM2Mc is not as strong because there are only 12 independent 40-yr epochs in the length of the 500-yr control run, but there is similar overall behavior.

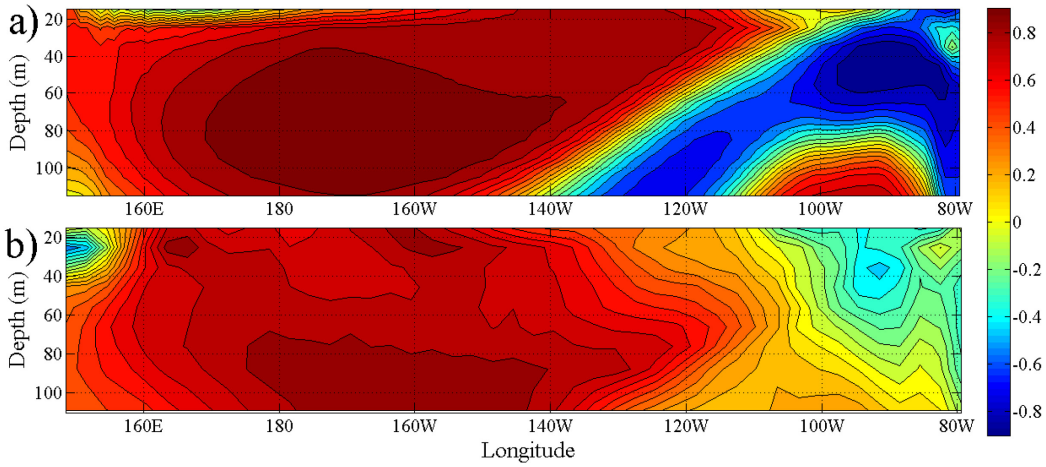


**Figure 4.8:** Correlation between the 40-yr average vertical stratification (temperature difference between 5m and the depth specified on the y-axis) averaged over 3S–3N and the 40-yr Niño-3b variance in the CM2.1 model (a) and in the CM2Mc model (b). Correlation starts at 15m because the surface bin is at 5m and next bins are incremented by 10m. Correlations > 0.2 are significant to the $p < 0.01$ level.

Turning to $\alpha$, from Equation 4.1 $\alpha$ is expected to represent $\overline{u}T'_x + \overline{w}T'_z - (\overline{K}_v T'_z)_z$ – the advection of anomalous temperatures by the mean flow and mixing. Since the most prominent advective tendencies are in the vertical direction, $\alpha$ is expected to represent the impact of $\overline{w}\partial T'/\partial z$ on $\partial T'/\partial t$. Therefore, changes in $\alpha$ may be due to changes in the mean vertical velocity field in the ocean, with strong upwelling resulting in a greater sensitivity to $Z_{20}$. However, in looking at the CM2.1 mean vertical ocean speeds ($w$) in the two regions where $\alpha$ exhibits a significant correlation with Niño-3b variance, there is an opposite relationship with Niño-3b variance. That is, in the $\alpha_{west}$ region there is a negative correlation (-0.48) between $\alpha$ and SST variability, but there is a positive correlation between $w$ and SST variability and vice versa for the $\alpha_{east}$ region where the correlation coefficient is 0.54 (correlation coefficients are significant to the $p<0.01$ level). Therefore, changes in the mean upwelling cannot be the reason for changes in variance.

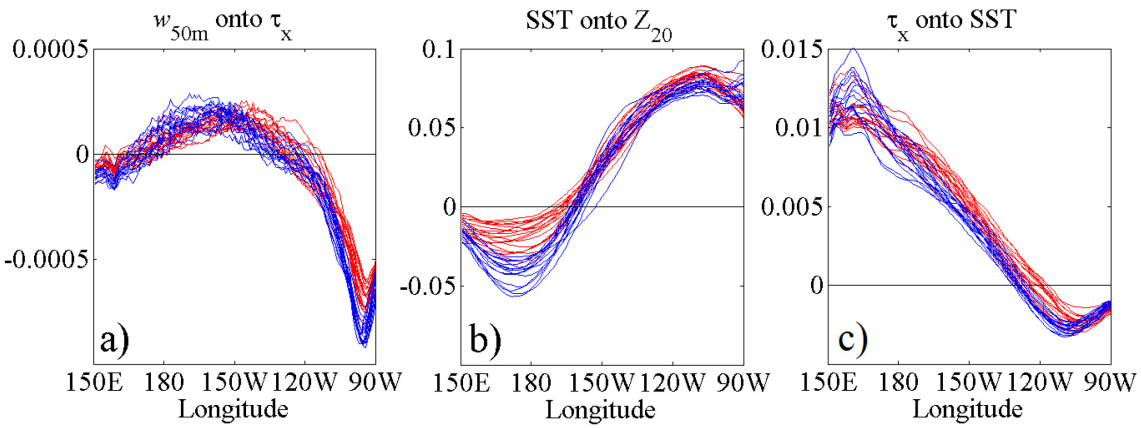


**Figure 4.9:** CM2.1 regression coefficients averaged over 3S–3N of (a) anomalous upwelling speeds at 50m ($w_{50m}$) onto anomalous $\tau_x$ (b) anomalous SSTs regressed onto anomalous $Z_{20}$ and (c) anomalous $\tau_x$ regressed onto anomalous SSTs in times of high (red) and low (blue) Niño-3b variance 40-yr periods.

Additionally, Figure 4.9b demonstrates that the influence of $Z_{20}$ on SST (as opposed to local SST change) is not necessarily the source of the change in the correlation with Niño-3b variance. We would expect that if changes in the responsiveness of the ocean's surface were driving changes in ENSO variance, SST anomalies would be more sensitive to thermocline depth anomalies during high variance periods. However, higher variance periods are associated with a smaller response of SST anomalies to thermocline depth anomalies in the $\alpha_{west}$ region, while in the $\alpha_{east}$ region there is not a strong relationship with variance. This implies that the relationship between $Z_{20}$ and SST is secondary to a more dominant source of variability.

The fact that there is a fairly high correlation between the average $\beta$ in the central equatorial Pacific and $\alpha_{east} - \alpha_{west}$ (Fig. 4.12), suggests there may be similar underlying drivers of variability. In fact, the response of the ocean's surface to thermocline depth anomalies, as indicated by $\alpha_{east} - \alpha_{west}$, is also highly correlated with ocean stratification (Fig. 4.12). This may point to a relationship whereby higher stratification in the $\alpha_{west}$ region shields the surface from the impact of thermocline variations. By contrast, higher

stratification in the $\alpha_{east}$ region amplifies the impacts of thermocline variability, thereby increasing the contrast between surface water and the waters upwelling from below.

Still, it is puzzling that the local SST change is less responsive both to a given wind stress perturbation in the central equatorial Pacific and to a given thermocline depth perturbation in the $\alpha_{west}$ region during high variance periods. This is not due to changes in the frequency of ENSO because the variance of the *change* in Niño-3b temperature anomalies $\partial T'/\partial t$ is highly correlated (>0.9) with the actual variance of the Niño-3b temperature anomalies and varies over the same relative range. Wittenberg (2009) also found little relationship between ENSO amplitude and frequency.

In order to better understand the multidecadal variability in the SST changes, we expand the linear regression equation to the individual temperature tendency components in a comparable model – the 500-yr CM2Mc model control run. Temperature tendency can be decomposed into three parts: the 3-D advective tendency, the vertical diffusive tendency – defined as the sum of the implicit vertical diffusive temperature tendency, the k-profile parameterization (KPP) nonlocal temperature tendency (Large et al. 1994) and the shortwave heating into the surface of the ocean – and the tendency due to parameterized subgrid-scale, mesoscale and sub-mesoscale eddies – henceforth collectively referred to as the "eddy tendency". In Figure 4.10, the anomalous temperature tendency terms summed over the top 50m of the ocean are regressed onto the anomalous thermocline depth, zonal wind stress and SST on 20-yr timescales in the CM2Mc model. Such a decomposition effectively separates out the physical processes that are contributing to $\alpha$, $\beta$ and $\gamma$. Not all terms have the same impact on variations. For example, the amplitudes of the eddy term regression coefficients are generally an order of

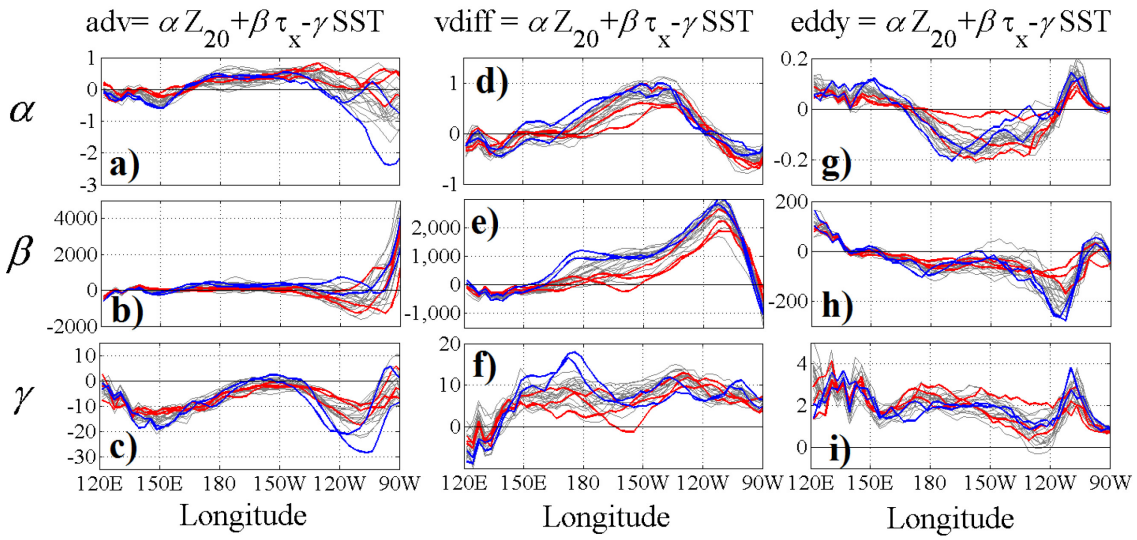


**Figure 4.10:** Regression coefficients averaged over 3S–3N of the anomalous temperature tendency terms: advective tendency, vertical diffusive tendency and eddy tendency (all summed over the top 50m of the ocean) onto the anomalous thermocline depth $Z_{20}$, anomalous zonal wind stress $\tau_x$ and anomalous SST in the CM2Mc model on 20-yr timescales, where red (blue) lines indicate high (low) Niño-3b variance.

magnitude smaller than those from the other two tendency components, which suggests that the eddy tendency is less important in modulating long-period variability.

Figure 4.10a reveals that advection responds in the opposite way to thermocline depth anomalies during high and low variance periods in the $\alpha_{east}$ region, such that a deeper thermocline is associated with advective warming (cooling) during high (low) variance periods. In the $\alpha_{west}$ region, there may be some distinguishability in the responses of both the advective and vertical diffusive tendency to thermocline depth anomalies, but it is not very clear (Fig. 4.10d&g). In the region 180–150W, the eddy and vertical diffusive tendencies exhibit responses of the opposite sign, which may account for the weak relationship between $\alpha$ and ENSO variance in that area.

Looking at the $\beta$ coefficients associated with the individual tendency terms, there is a clear signal in Figure 4.10e. During high variance periods there is a weaker response of vertical diffusion to zonal winds in the region 160E–120W and a somewhat stronger

response but of the opposite sign at the far eastern edge of the basin. This result helps explain the puzzling relationship between $\beta$ and stratification. We had originally expected that higher stratification would mean that mixing and upwelling would work on a larger temperature gradient and produce a larger change in SST. However, the response of mixing to winds actually becomes weaker under higher stratification; that is, all else being equal, the mixing coefficient drops as stratification increases. Hence, stratification is not a driver of variance, but appears to respond to it, and to some extent dampens it.

The $\gamma$ coefficients show how the individual tendency term anomalies respond to SST anomalies. During low variance periods, there is a stronger response of advection to SSTs in the region 130–110W (Fig. 4.10c) and a stronger response of diffusion to SSTs in the region 150E–170W (Fig. 4.10f). However, the response is of approximately the same magnitude and of the opposite sign between advective and vertical diffusive tendencies in those two regions, which explains why there is not a strong relationship between the inverse damping time and ENSO variance in those regions in Figure 4.7. There does not appear to be a significant signal in any of the other regions / terms, but that could be partly due to the limited number of samples.

### 4.4.3. CHANGES IN THE ATMOSPHERIC RESPONSE TO THE OCEAN

Figure 4.9c draws upon the ENSO feedback cycle in order to assess the response of the atmosphere to the ocean. During high variance periods there is a notably stronger response of the atmosphere – represented by zonal wind stress anomalies – to the ocean – represented by SST anomalies – over the central equatorial Pacific from about 170W to

130W, and a weaker response of the atmosphere to the ocean from about 120W to 110W. This is consistent with Anderson et al. (2009), who found that a warming of the eastern equatorial Pacific results in an increased wind response with a longer fetch, which amplifies ENSO amplitude. Additionally, as the center of action for the wind response moves east, the off-equatorial Rossby waves generated by the equatorial wind stress anomaly will also take longer to propagate to the west. In classical delayed oscillator type models this acts to increase the amplitude. Accordingly, during high variance periods when the precipitation is higher in the east, the winds penetrate further into the central part of the basin and the winds are more responsive to SSTs in the central equatorial Pacific. This indirect process provides an additional way in which changes in the atmospheric response to the ocean can feed back on the variance (Fig. 4.12).

The shifting state of the atmosphere may also play a role in reducing the responsiveness of the ocean to the atmosphere. There is a strong negative correlation (-0.78) between $\beta$ and precipitation over the central equatorial Pacific in the CM2.1 model (Fig. 4.12). This is likely due to the eastward shift of the center of convection during El Niño episodes, which produces heavier precipitation over the central and eastern equatorial Pacific, and consequently increases the near-surface temperature stratification (e.g. Li et al. 1998).

Interestingly, there is a much stronger response of $\tau_x$ to SSTs during El Niño than during La Niña throughout most of the central and eastern equatorial Pacific, as shown by the interannual regression between the wind stress anomalies and SST anomalies during the different phases of ENSO (Fig. 4.11). Here El Niño (La Niña) is defined as the times when the Niño-3b SST anomalies are greater than (less than) the mean + (-) the standard

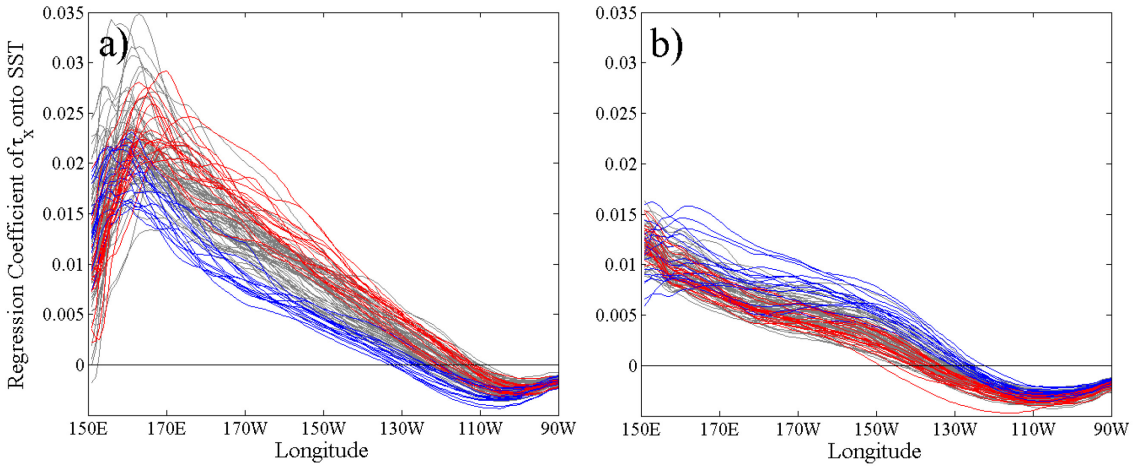


**Figure 4.11:** CM2.1 Regression coefficients averaged over 3S–3N for anomalous $\tau_x$ regressed onto anomalous SST for every 40-yr period during (a) El Niño months and (b) La Niña months; high (low) Niño-3b variance periods are in red (blue).

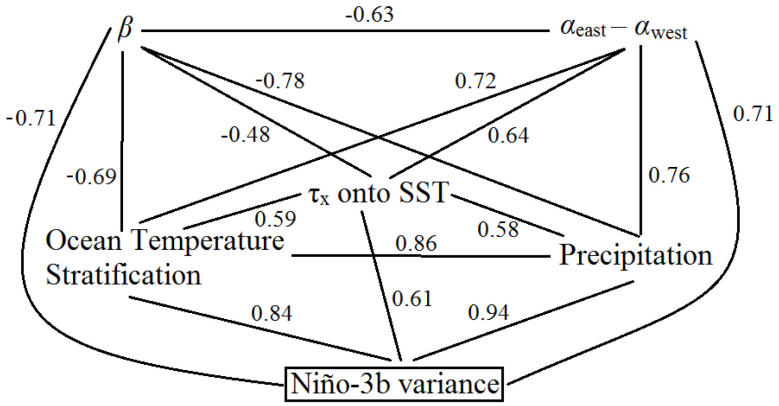


**Figure 4.12:** ENSO correlation coefficient network on 40-yr timescales in the CM2.1 model. Except for Niño-3b variance, which is averaged over the Niño-3b region, and $\alpha_{east} - \alpha_{west}$, which is the difference between the average over the $\alpha_{east}$ and the $\alpha_{west}$ regions, the other variables are averaged over the central equatorial Pacific (170–110W, 3S–3N). Correlation coefficients are significant to the $p < 0.01$ level.

deviation of the respective 40-yr average Niño-3b SST anomalies. Therefore, it seems that much of the variability in Niño-3b SST anomalies is dominated by a stronger response to warming during El Niño periods.

## 4.5 SUMMARY AND DISCUSSION

ENSO is a dynamic process which exhibits variability over a range of different timescales (e.g. Wittenberg 2009), making it difficult to detect and/or predict externally forced changes (Knutson et al. 1997; AchutaRao and Sperber 2002; Yukimoto and Kitamura 2003; Yeh et al. 2004; Yeh and Kirtman 2004; An et al. 2005a,b; Meehl et al. 2006; Power et al. 2006; Lin 2007). Multidecadal changes in ENSO amplitude variance do not seem to be largely explained by the relatively small changes in mean temperature or by changes in the shape of ENSO, making it difficult to determine what drives such long-period variability. This paper addresses these challenges and makes progress towards isolating the causes of multidecadal variability in Niño-3b variance found in the CM2.1 model.

A regression of local SST changes based on van Oldenborgh et al. (2005) is applied to the CM2.1 and CM2Mc control runs in order to examine the internal coupling strength variability associated with ENSO. The model regression coefficients are also compared to those produced by ECDA which gives insight into the physical biases of both models. CM2.1 and CM2Mc exhibit qualitatively similar regression coefficients to those of ECDA, with CM2Mc producing more realistic amplitudes than CM2.1. This analysis demonstrates that not only does ENSO amplitude range widely across multidecadal time periods, but the actual ocean-atmosphere coupling strengths exhibit large internal variability as well. In the CM2.1 model the regression coefficients change by about a factor of two on multidecadal timescales. These results suggest that it will require multiple decades to centuries-long model runs to characterize the internal long-period

variability in coupling strengths. In addition, one needs to be careful using only 40 years of data to constrain model physics. This highlights the importance of producing longer proxy records of tropical temperature variability, so that the mechanisms proposed here can be evaluated and compared to the real world.

In order to explain the long-period variability of coupling strengths (with a focus on oceanic responses to atmospheric forcing), the van Oldenborgh et al. (2005) framework was expanded in this paper to the temperature tendency components associated with 3-D advection, vertical diffusive processes and subgrid-scale eddy processes. This expansion revealed that increasing stratification in the central equatorial Pacific damps the response of the ocean to the atmosphere primarily through a decrease in vertical diffusion – highlighting the importance of mixed layer processes and potentially of salinity stratification as noted by Maes et al. (2005). An investigation of the response of the atmosphere to the ocean indicated that eastward shifts in precipitation are associated with a stronger atmospheric response to oceanic forcing in the central equatorial Pacific. Understanding such signatures of ENSO variability may contribute to the predictability of El Niño. Furthermore, the results suggest that when the CM2.1 model has a weaker (putatively more realistic) cold tongue, it ends up with a stronger (putatively less realistic) El Niño. While this result is unlikely to be true for all coupled models, it nonetheless shows how important it is to constrain all parts of the coupling cycle. Simply reducing the mean bias in one part of the system will not necessarily produce a more realistic model overall.

The analysis herein makes the assumption that a linear regression is sufficient to understand these processes. This is supported by the fact that when we use variable finite

upwelling delays, the regression model is in danger of over-fitting the data. However, when we look at the interannual regression between the wind stress anomalies and SST anomalies during the different phases of ENSO, some interesting patterns emerge that suggest the picture may not be so simple (Fig. 4.11). Not only is there a separation in the regression pattern between El Niño and La Niña periods, but there is a strong difference in the behavior of high variance 40-yr epochs between the different ENSO phases, indicating that the coupling may be nonlinear in nature. In summary, this paper confirms previous studies on long-period ENSO variability, while extending these results by identifying the driving mechanism as due to changes in coupling and describing the signature of these changes in the long-period mean states of the ocean and atmosphere.

*Acknowledgements*. The authors gratefully acknowledge NOAA's & GDFL's provision of both the CM2.1 model and Ensemble Coupled Data Assimilation. The authors thank Andrew Wittenberg for useful discussions and three anonymous reviewers for useful suggestions. AR acknowledges support from NSF through the Water, Climate and Health IGERT at Johns Hopkins University.

# Chapter 5. Conclusion

While future global changes are well constrained, regional climates are expected to change in a variety of ways due to the complex interactions between global influences, local physical dynamics and large scale phenomena and these interactions are inherently more difficult to simulate (Christensen et al. 2013). In fact, several studies have shown that regional climate change has been and will continue to be modulated by the fluctuations and phasings of internal modes of variability such as ENSO, AMO and PDO. For example, Murphey and Timbal (2007) describe the impacts of ENSO and internal variations in the Indian Ocean on the regional climate of Southeastern Australia and emphasize the need for a better understanding of the mechanisms by which these natural oscillations impact regional circulation features and how they interact with external forcings to determine future changes in climate parameters of interest. The analyses presented in this dissertation establish the importance of small temperature gradients associated with internal modes of variability, whether in the free-atmosphere or in the sea surface, in modulating regional climate variability in the tropics and the response of regional climatic parameters to global changes.

Chapter 2 demonstrates that the regional impacts of global warming tend to be controlled by local dynamics to the extent that certain areas of the world may respond to external forcings in different ways and to different extents. One such area that stands out as a hot spot of free-atmospheric warming in the Tropics is over the Andes Mountains of South America where 500mb temperature trends are 2-3 times stronger than other Pan-

Tropical land areas (Russell et al. 2017). Such regional variations in the expression of climate change emphasize the need to explicitly consider tropical temperature gradients instead of treating the tropical atmosphere as homogenous. In addition, this work underscores the major challenge of limited data availability in remote regions, which hinders the ability to accurately characterize regional climate variability and change. From a modeling perspective, there is also evidence to show that global climate models inadequately capture these regional effects and therefore fail to simulate regional climate trends in important variables. It is likely that coincident deficiencies in the simulation of radiative trends – namely top-of-the-atmosphere outgoing longwave radiation – by AGCMs are a primary source of the uncertainty in simulating free-atmospheric temperatures (Russell et al. 2017).

Chapter 3 shows that local changes in both free-atmospheric temperatures and radiation can be simulated using a regional climate model. The observed regional changes in OLR in the Andes Mountains in particular appear to be a major contributor to enhanced free-atmospheric temperature trends by inducing changes in regional atmospheric circulation patterns. This chapter indicates that long-term changes in the radiative balance over the Andes Mountains may be driven by the relatively small changes in SSTs that have occurred over the last few decades over the Atlantic and Pacific Oceans and/or by shifts in the position or strength of the midlatitude jet. An important outcome of this study is that the mechanisms which translate the SST gradients or atmospheric boundary conditions into local circulation changes are seasonally dependent, which is also likely to be the case elsewhere around the tropics. These mechanisms will be explored in more depth in future research efforts by performing

controlled numerical experiments which aim to isolate and quantify the effects of both SST gradients and jet positions/strength.

Chapter 4 examines the impacts of zonal SST gradients on the coupling strength between the atmosphere and the ocean on long time scales in a multicentennial control run of a global coupled climate model using an adapted regression technique. The model produces regression coefficients that vary widely on multidecadal timescales and these variations are strongly reflected in the long-period modulation of ocean stratification and surface precipitation. In fact, during high variance periods, when there is stronger stratification and precipitation in the central equatorial Pacific, the ocean's surface is less responsive to zonal wind stress perturbations, while the atmosphere is more responsive to SST perturbations. The mechanisms underlying this behavior are examined through an expansion of the linear regression equation to individual temperature tendency components. This analysis reveals that long-term changes in ENSO amplitude are due to changes in both the oceanic response to the atmosphere (which is predominantly driven by regional changes in the advective and vertical diffusive heat tendencies) and the atmospheric response to the ocean (which is primarily the result of the atmosphere being more responsive when SST gradients are smaller) (Russell and Gnanadesikan 2014).

Overall, the work presented herein documents the importance of horizontal temperature gradients in modulating regional climate. While the free-atmosphere exhibits gradients in regional temperature trends due to the interactions between local dynamics and global changes, these trends are poorly simulated by global climate models. The ability to model these trends can be improved through the use of high-resolution regionally-tuned numerical models and the potential role of SST gradients can

be assessed. Finally, the impact of SST gradients on regional climate has been shown to be more important when the gradients are small.

This dissertation builds upon the recent advances in the field which have helped to further our understanding of the Earth System. Namely, the current advances in computing and parameterizations of physical processes have allowed for better representation of both global and regional climate dynamics. In addition there have been many efforts to improve downscaling of global climate model projections for regional purposes. These efforts fall into two categories – empirical statistical downscaling and dynamical downscaling. While statistical downscaling produces higher resolution climatic information, it cannot usually improve deficiencies in the simulation of certain processes like wintertime precipitation over complex terrain as well as dynamical downscaling methods (e.g. Schmidli et al. 2007, Gutmann et al. 2012). Therefore, many current efforts are working towards the improvement of and reduction in the computational demands of regional climate downscaling. For example, the Intermediate Complexity Atmospheric Research Model (ICAR) – a linearized version of a numerical atmospheric model – significantly reduces computation demands while still allowing for sophisticated representation of physical processes (Gutmann et al. 2016).

While this dissertation makes significant progress towards the understanding and modeling of regional climate variability and change, there is much that remains to be done in the field. Future research efforts should focus on improving the parameterization of physical processes on a regional level as well as reducing the uncertainty in the expected future changes in the internal oscillations themselves (e.g. Kim et al. 2014, Cai et al. 2015). In addition, the impacts of horizontal temperature gradients need to be quantitatively defined in terms of their impact on regional climate elsewhere around the world.

# Appendix – WRF namelist

```
&time_control
 run_days                 = 244,
 run_hours                = 00,
 run_minutes              = 0,
 run_seconds              = 0,
 start_year               = 1981,
 start_month              = 04,
 start_day                = 01,
 start_hour               = 00,
 start_minute             = 00,
 start_second             = 00,
 end_year                 = 1981,
 end_month                = 12,
 end_day                  = 01,
 end_hour                 = 00,
 end_minute               = 00,
 end_second               = 00,
 interval_seconds         = 21600,
 input_from_file          = .true.,
 history_interval         = 360,
 frames_per_outfile       = 1,
 restart                  = .false.,
 restart_interval         = 14400,
 io_form_history          = 2,
 io_form_restart          = 2,
 io_form_input            = 2,
 io_form_boundary         = 2,
 debug_level              = 0,
 auxinput4_inname         = "wrflowinp_d<domain>",
 auxinput4_interval       = 360,
 io_form_auxinput4        = 2,
 io_form_auxinput2        = 2,
 history_outname          = "wrfout_d<domain>_<date>",
 /

 &domains
 time_step                = 180,
```

```
time_step_fract_num         = 0,
time_step_fract_den         = 1,
max_dom                     = 1,
e_we                        = 260,
e_sn                        = 200,
e_vert                      = 61,
p_top_requested             = 1000,
num_metgrid_levels          = 38,
num_metgrid_soil_levels     = 4,
dx                          = 50000,
dy                          = 50000,
grid_id                     = 1,
parent_id                   = 1,
i_parent_start              = 1,
j_parent_start              = 1,
parent_grid_ratio           = 1,
parent_time_step_ratio      = 1,
feedback                    = 0,
smooth_option               = 0
smooth_cg_topo              = .true.,
/

&physics
mp_physics                  = 6,
ra_lw_physics               = 4,
ra_sw_physics               = 1,
cam_abs_freq_s              = 21600,
radt                        = 50,
sf_sfclay_physics           = 2,
sf_surface_physics          = 2,
bl_pbl_physics              = 2,
bldt                        = 0,
cu_physics                  = 5,
cudt                        = 5,
isfflx                      = 1,
ifsnow                      = 1,
icloud                      = 1,
surface_input_source        = 1,
num_soil_layers             = 4,
sf_urban_physics            = 0,
num_land_cat                = 24,
tmn_update                  = 1,
lagday                      = 150,
sst_update                  = 1,
/
```

```
 &fdda
 /

&dynamics
 w_damping                = 0,
 diff_opt                 = 1,
 km_opt                   = 4,
 diff_6th_opt             = 0,
 diff_6th_factor          = 0.12,
 base_temp                = 290.,
 damp_opt                 = 0,
 zdamp                    = 5000.,
 dampcoef                 = 0.2,
 khdif                    = 0,
 kvdif                    = 0,
 non_hydrostatic          = .true.,
 moist_adv_opt            = 1,
 scalar_adv_opt           = 1,
 epssm                    = 0.1,
 /

 &bdy_control
 spec_bdy_width           = 5,
 spec_zone                = 1,
 relax_zone               = 4,
 spec_exp                 = 0.33,
 specified                = .true.,
 nested                   = .false.,
 /

 &grib2
 /

 &namelist_quilt
 nio_tasks_per_group      = 0,
 nio_groups               = 1,
 /

 &logging
/
```

# Bibliography

AchutaRao, K. M., and K. R. Sperber, 2002: Simulation of the El Niño Southern Oscillation: Results from the Coupled Model Intercomparison Project. *Climate Dyn.*, **19**, 191–209.

Allan, R. P., and A. Slingo, 2002: Can current climate model forcings explain the spatial and temporal signatures of decadal OLR variations? *Geophys. Res. Lett.*, **29**, 1141, doi:10.1029/2001GL014620.

Allan, R. J., J. Lindesay, and D. Parker, 1996: *El Niño Southern Oscillation and Climatic Variability*. CSIRO Publishing, 402 pp.

Amante, C., and B. W. Eakins, 2009: ETOPO1 1 Arc-Minute Global Relief Model: Procedures, Data Sources and Analysis. NOAA Tech. Memorandum NESDIS NGDC-24. 19 pp, doi:10.7289/V5C8276M.

An, S.-I., Y. G. Ham, J.-S. Kug, F.-F. Jin, and I. S. Kang, 2005: El Nino La Nina asymmetry in the Coupled Model Intercomparison Project Simulations. *J. Climate*, **18**, 2617–2627.

An, S.-I., W. W. Hsieh, and F.-F. Jin, 2005: A Nonlinear analysis of the ENSO cycle and its interdecadal changes. *J. Climate*, **18**, 3229–3239.

Anderson, W., A. Gnanadesikan, and A. Wittenberg, 2009: Regional impacts of ocean color on tropical Pacific variability. *Ocean Sci. Discuss.*, **6**, 243–275.

Andrews, T., J. M. Gregory, M. J. Webb, and K. E. Taylor, 2012: Forcing, feedbacks and climate sensitivity in CMIP5 coupled atmosphere-ocean climate models. *Geophys. Res. Lett.*, **39**, L09712, doi:10.1029/2012GL051607.

Ashok, K., S. K. Behera, S. A. Rao, H. Weng, and T. Yamagata, 2007: El Niño Modoki and its possible teleconnection. *J. Geophys. Res.*, **112**, C11007, doi:10.1029/2006JC003798.

Battisti, D. S., and A. C. Hirst, 1989: Interannual Variability in a Tropical Atmosphere–Ocean Model: Influence of the Basic State, Ocean Geometry and Nonlinearity. *J. Atmos. Sci., **46**,* 1687–1712.

Bell, G. D., and M. Chelliah, 2006: Leading tropical modes associated with interannual and multi-decadal fluctuations in North Atlantic hurricane activity. *J. Climate*, **19**, 590–612.

Bellenger H., E. Guilyardi, J. Leloup, M. Lengaigne, and J. Vialard, 2013: ENSO representation in climate models: from CMIP3 to CMIP5. *Climate Dyn.*, **42**, 1999–2018.

Bengtsson, L., S. Hagemann, and K. I. Hodges, 2004: Can climate trends be calculated from reanalysis data? *J. Geophys. Res.*, **109**, D11111, doi:10.1029/2004JD004536.

Bjerknes, J. 1966: A possible response of the atmospheric Hadley circulation to equatorial anomalies of ocean temperature, *Tellus*, **18**, 820–829.

Bony, S., and Coauthors, 2006: How well do we understand and evaluate climate change feedback processes? *J. Climate*, **19**, 3445–3482, doi:10.1175/JCLI3819.1.

Bosilovich, M. G., J. Chen, F. R. Robertson, and R. F. Adler, 2008: Evaluation of Global Precipitation in Reanalyses. *J. Appl. Meteor. Climatol.*, **47**, 2279–2299.

Bradley, R. S., F. T. Keimig, and H. F. Diaz, 2004: Projected temperature changes along the American cordillera and the planned GCOS network. *Geophys. Res. Lett.*, **36**, L16210, doi:10.1029/2004GL020229.

Bradley, R. S., M. Vuille, H. F. Diaz, and W. Vergara, 2006: Threats to water supplies in the tropical Andes. *Science*, **312**, 1755–1756, doi:10.1126/science.1128087.

Bradley, R. S., F. T. Keimig, H. F. Diaz, and D. R. Hardy, 2009: Recent changes in freezing level heights in the tropics with implications for the deglacierization of high mountain regions. *Geophys. Res. Lett.*, **36**, L17701, doi:10.1029/2009GL037712.

Burgers, G., and G. J. van Oldenborgh, 2003: On the Impact of Local Feedbacks in the Central Pacific on the ENSO cycle. *J. Climate*, **16**, 2396–2407.

Bury, J., B. G. Mark, M. Carey, K. R. Young, J. M. McKenzie, M. Baraer, A. French, and M. H. Polk, 2013: New Geographies of Water and Climate Change in Peru: Coupled Natural and Social Transformations in the Santa River Watershed. *Annals of the Association of American Geographers*, **103**, 363-374.

Cai, W., P. van Rensch, T. Cowan, and H. H. Hendon, 2011: Teleconnection pathways of ENSO and the IOD and the mechanisms for impacts on Australian rainfall. *J. Climate*, **24**, 3910–3923.

Cai, W., and Coauthors, 2015: ENSO and greenhouse warming. *Nature Climate Change*, **5**, 849–859, doi:10.1038/nclimate2743.

Chang, Y. -S., S. Zhang, A. Rosati, T. L. Delworth, and W. F. Stern, 2012: An assessment of oceanic variability for 1960–2010 from the GFDL ensemble coupled data assimilation. *Climate Dyn.*, doi:10.1007/s00382-012-1412-2.

Christensen, J.H., K. Krishna Kumar, E. Aldrian, S.-I. An, I.F.A. Cavalcanti, M. de Castro, W. Dong, P. Goswami, A. Hall, J.K. Kanyanga, A. Kitoh, J. Kossin, N.-C. Lau, J. Renwick, D.B. Stephenson, S.-P. Xie and T. Zhou, 2013: Climate Phenomena and their Relevance for Future Regional Climate Change. In: *Climate Change 2013: The Physical Science Basis. Contribution of Working Group I to the Fifth Assessment Report of the Intergovernmental Panel on Climate Change* [Stocker, T.F., D. Qin, G.-K. Plattner, M. Tignor, S.K. Allen, J. Boschung, A. Nauels, Y. Xia, V. Bex and P.M. Midgley (eds.)]. Cambridge University Press, Cambridge, United Kingdom and New York, NY, USA, pp. 1217–1308, doi:10.1017/CBO9781107415324.028.

Collins, M., et al., 2010: The impact of global warming on the tropical Pacific Ocean and El Niño. *Nat. Geosci.*, **3**, 391–397, doi:10.1038/NGEO868.

Compo, G. P., and Coauthors, 2011: The Twentieth Century Reanalysis Project. *Quart. J. Roy. Meteor. Soc.*, **137**, 1–28, doi:10.1002/qj.776.

Dee, D. P., and Coauthors, 2011: The ERA-Interim reanalysis: configuration and performance of the data assimilation system. *Quart. J. Roy. Meteor. Soc.*, **1370**, 553–597.

Dee, D., J. Fasullo, D. Shea, J. Walsh, and National Center for Atmospheric Research Staff, Last modified 23 Jul 2015: The Climate Data Guide: Atmospheric Reanalysis: Overview & Comparison Tables. Accessed 12 December 2015.

[Available online at https://climatedataguide.ucar.edu/climate-data/atmospheric-reanalysis-overview-comparison-tables]

Delworth, T. L., et al., 2006: GFDL's CM2 global coupled climate models. Part I: Formulation and simulation characteristics. *J. Climate*, **19**(5), 643–674.

Dijkstra, H. A., and G. Burgers, 2002: Fluid Dynamics of El Niño Variability. *Annu. Rev. Fluid Mech*., **34**, 531–558.

England, M. H., and Coauthors, 2014: Recent intensification of wind-driven circulation in the Pacific and the ongoing warming hiatus. *Nature Climate Change*, **4**, 222–227.

Falvey, M., and R. D. Garreaud, 2009: Regional cooling in a warming world: Recent temperature trends in the southeast Pacific and along the west coast of subtropical South America (1979–2006). *J. Geophys. Res.*, **114**, D04102, doi:10.1029/2008JD010519.

Fan, Y., and H. van den Dool, 2008: A global monthly land surface air temperature analysis for 1948-present. *J. Geophys. Res.*, **113**, doi:10.1029/2007JD008470.

Fasullo, J.T., 2011: A Mechanism for land-ocean contrasts in global monsoon trends in a warming climate, *Climate Dyn.*, **39**, 1137–1147, doi: 10.1007/s00382-011-1270-3.

Fedorov, A. V., and S. G. Philander, 2000: Is El Niño Changing? *Science*, **288**, 1997–2002.

Feeley, K. J., and Coauthors, 2011: Upslope migration of Andean trees. *J. Biogeogr.*, **38**, 783–791.

Fernandez J., J. P. Montavez, J. Saenez, J. F. Gonzalez-Rouco, and E. Zorita, 2007: Sensitivity of the MM5 mesoscale model to physical parameterizations for regional climate studies: Annual cycle. *J. Geophys. Res.*, **112**, D04101, doi:10.1029/2005JD006649.

Feser, F., B. Rockel, H. von Storch, J. Winterfeldt, and M. Zahn, 2011: Regional Climate Models Add Value to Global Model Data: A Review and Selected Examples. *Bull. Amer. Meteor. Soc.*, **92**,1181–1192, doi:10.1175/2011BAMS3061.1.

Flannaghan, T. J., S. Fueglistaler, I. M. Held, S. Po-Chedley, B. Wyman, and M. Zhao, 2014: Tropical temperature trends in Atmospheric General Circulation Model simulations and the impact of uncertainties in observed SSTs. *J. Geophys. Res.*, **119**, 13327–13337, doi:10.1002/2014JD022365.

Forero-Medina, G., J. Terborgh, S. J. Socolar, and S. L. Pimm, 2011: Elevational Ranges of Birds on a Tropical Montane Gradient Lag behind Warming Temperatures. *PLoS ONE*, **6**, e28535, doi:10.1371/journal.pone.0028535.

Fox-Kemper, B., R. Ferrari and R. Hallberg, 2008: Parameterization of mixed layer eddies, Part I: Theory and diagnosis. *J. Phys. Oceanogr.*, **38**, 1145–1165.

Fox-Kemper, B., G. Danabasoglu, R. Ferrari, S. M. Griffies, R. W. Hallberg, M. M. Holland, M. E. Maltrud, S. Peacock, and B. L. Samuels, 2011: Parameterization of mixed layer eddies. III: Implementation and impact in global ocean climate simulations. *Ocean Modelling*, **39**, 61–78.

Fu, Q., S. Manabe, and C. M. Johanson, 2011: On the warming in the tropical upper troposphere: Models versus observations. *Geophys. Res. Lett.*, **38**, doi:10.1029/2011GL048101.

Galbraith, E. D., E. Y. Kwon, A. Gnanadesikan, K. B. Rodgers, S. M. Griffies, D. Bianchi, J. L. Sarmiento, J. P. Dunne, J. Simeon, R. D. Slater, A. T. Wittenberg, and I. M. Held, 2011: Climate Variability and Radiocarbon in the CM2Mc Earth System Model. *J. Climate*, **24**, 4230–4254.

Garfinkel, C. I., M. M. Hurwitz, and L. D. Oman, 2015. Effect of recent sea surface temperature trends on the Arctic stratospheric vortex. *J. Geophys. Res. Atmos.*, **120**, 5404-5416, doi:10.1002/2015JD023284.

Garreaud, R. D., 2009: The Andes climate and weather. *Adv. Geosciences*, **7**, 1–9.

Garreaud, R. D., M. Vuille, R. Compagnucci, and J. Marengo, 2008: Present-day South American climate. *Paleogeography, Paleoclimatology, Paleoecology*, **281**, 180-195. doi: 10.1016/j.palaeo.2007.10.032.

Gershunov, A., and T. P. Barnett, 1998: Interdecadal modulation of ENSO teleconnections. *Bull. Amer. Meteor. Soc.*, **79**, 2715–2725.

Gnanadesikan, A., K. A. Emanuel, G. A. Vecchi, W. G. Anderson, and R. W. Hallberg, 2010: How ocean color can steer Pacific tropical cyclones. *Geophys. Res. Lett.*, **37**, L18802, doi:10.1029/2010GL044514.

Gonzalez, P. L. M., L. M. Polvani, R. Seager, and G. J. P. Correa, 2014: Stratospheric ozone depletion: a key driver of recent precipitation trends in South Eastern South America. *Climate Dyn.*, **42**, 1775–1792, doi:10.1007/s00382-013-1777-x.

Guilyardi E., 2006: El Niño–mean state–seasonal cycle interactions in a multi-model ensemble. *Climate Dyn.*, **26**, 329–348.

Guilyardi, E., A. Wittenberg, A. Fedorov, M. Collins, C.Z. Wang, A. Capotondi, G.J. van Oldenborgh, and T. Stockdale (2009a): Understanding El Niño in ocean-atmosphere

General Circulation Models: Progress and challenges. *Bull. Amer. Met. Soc.*, **90**, 325–340.

Guilyardi, E., P. Braconnot, F.-F. Jin, S. T. Kim, M. Kolasinski, T. Li, and I. Musat, 2009: Atmosphere feedbacks during ENSO in a coupled GCM with a modified atmospheric convection scheme. *J. Clim*ate, **22**, 5698–5718.

Gutmann, E., and Coauthors, 2012: A Comparison of Statistical and Dynamical Downscaling of Winter Precipitation over Complex Terrain. *J. Climate*, **25**, 262–281, doi:10.1175/2011JCLI4109.1.

Gutmann, E., I Barstad, M. Clark, J. Arnold, and R. Rasmussen, 2016: The Intermediate Complexity Atmospheric Research Model (ICAR). *J. Hydrometeor.*, **17**, 957–973.

Hasegawa, T., and K. Hanawa, 2003: Decadal-scale variability of upper ocean heat content in the tropical Pacific. *Geophys. Res. Lett.*, **30**, 1272, doi:10.1029/2002GL016843.

Hasselmann, K., 1976: Stochastic climate variability. *Tellus*, **28**, 473–484.

Hoerling, M., A. Kumar, and M. Zhong, 1997: El Niño, La Niña, and the nonlinearity of their teleconnections. *J. Climate*, **10**, 1769–1786.

Hoskins, B. J., and D. J. Karoly, 1981: The Steady Linear Response of a Spherical Atmosphere to Thermal and Orographic Forcing. *J. Atmos. Sci., **38**, 1179–1196.*

Hunt, B. G., and T. I. Elliott, 2003: Secular variability of ENSO events in a 1000-year climatic simulation. *Climate Dyn.*, **20**, 689–703.

IPCC, 2013: Climate Change 2013: *The Physical Science Basis. Contribution of Working Group I to the Fifth Assessment Report of the Intergovernmental Panel on Climate Change* [Stocker, T.F., D. Qin, G.-K. Plattner, M. Tignor, S.K. Allen, J. Boschung, A.

Nauels, Y. Xia, V. Bex and P.M. Midgley (eds.)]. Cambridge University Press, Cambridge, United Kingdom and New York, NY, USA, 1535 pp, doi:10.1017/CBO9781107415324.

Jochum, M., and R. Murtugudde, 2006: Temperature Advection by Tropical Instability Waves. *J. Phys. Oceanogr., **36**, 592–605.*

Kalnay, E., and Coauthors, 1996: The NCEP/NCAR 40-year reanalysis project. *Bull. Amer. Meteor. Soc.*, **77**, 437-470.

Kanamitsu, M., W. Ebisuzaki, J. Woollen, S.-K. Yang, J. J. Hnilo, M. Fiorino, and G. L. Potter, 2002: NCEP-DOE AMIP-II Reanalysis (R-2). *Bull. Amer. Meteor. Soc.*, 1631–1643.

Kaser, G., I. Juen, C. Georges, J. Gomez, and W. Tamayo, 2003: The impact of glaciers on the runoff and the reconstruction of mass balance history from hydrological data in the tropical Cordillera Blanca, Peru. *J. Hydrol.*, **282**, 130–144.

Kaser, G., C. Georges, I. Juen, and T. Mölg, 2005: Low-latitude glaciers: unique global climate indicators and essential contributors to regional fresh water supply. A conceptual approach. *Global Change and Mountain Regions: An Overview of Current Knowledge*, U. Huber, H. K. M. Bugmann, and M. A. Reasoner, Eds., Springer, Vol. 23, 185–196.

Kestin, T. S., D. J. Karoly, J.-I. Yano, and N. A. Rayner, 1998: Time–frequency variability of ENSO and stochastic simulations. *J. Climate*, **11**, 2258–2272.

Kiem, A. S., and S. W. Franks, 2004: Multidecadal variability of drought risk, eastern Australia. *Hydrol. Processes*, **18**, 2039–2050.

Kiem, A. S., S. W. Franks, and G. Kuczera, 2003: Multi-decadal variability of flood risk. *Geophys. Res. Lett.*, **30**, 1035, doi:10.1029/2002GL015992.

Kim, D., J.-S. Kug, I. S. Kang, F. F. Jin, and A. T. Wittenberg, 2007: Tropical Pacific impacts of convective momentum transport in the SNU coupled GCM. *Climate Dyn.*, doi:10.1007/s00382-007-0348-4.

Kim, D., Y.-S. Jang, D.-H. Kim, Y.-H. Kim, M. Watanabe, F.-F. Jin, and J.-S. Kug, 2011: El Niño–Southern Oscillation sensitivity to cumulus entrainment in a coupled general circulation model. *J. Geophys. Res.*, 116, D22112, doi:10.1029/2011JD016526.

Kim, H.-M., P. J. Webster, and J. A. Curry, 2009: Impact of Shifting Patterns of Pacific Ocean Warming on North Atlantic Tropical Cyclones. *Science*, **325**, 77–80.

Kim, S. T., W. Cai, F.-F. Jin, A. Santoso, L. Wu, E. Guilyardi, and S.-I. An, 2014: Response of El Niño sea surface temperature variability to greenhouse warming. *Nature Climate Change*, **4**, 786–790, doi:10.1038/nclimate2326.

Kistler, R., W. Collins, S. Saha, G. White, J. Woollen, E. Kalnay, M. Chelliah, W. Ebisuzaki, M. Kanamitsu, V. Kousky, H. van den Dool, R. Jenne, and M. Fiorino, 2001: The NCEP–NCAR 50–Year Reanalysis: Monthly Means CD–ROM and Documentation. *Bull. Amer. Meteor. Soc.*, **82**, 247–268.

Knutson, T.R., S. Manabe, and D. Gu, 1997: Simulated ENSO in a global coupled ocean-atmosphere model: Multidecadal amplitude modulation and CO2 sensitivity. *J. Climate*, **10**, 131–161.

Knutson, T. R., and S. Manabe, 1998: Model assessment of decadal variability and trends in the tropical Pacific Ocean. *J. Climate*, **11**, 2273–2296.

Kosaka, Y., and S.-P. Xie, 2013: Recent global-warming hiatus tied to equatorial Pacific surface cooling. *Nature*, **501**, 403–407.

Kumar, K. Krishna, et al., 2006: Unraveling the Mystery of Indian Monsoon Failure During El Niño. *Science*, **314**, 115–119.

Large, W. G., J. C. McWilliams, and S. C. Doney, 1994: Oceanic vertical mixing: a review and a model with a nonlocal boundary layer parameterization. *Rev. Geophys.*, **32**, 363–403.

Lau, N.-C., 1997: Interactions between Global SST Anomalies and the Midlatitude Atmospheric Circulation. *Bull. Amer. Met. Soc.*, **78**, 21–33.

Lau, W. K. M., and K.-M. Kim, 2015: Robust Hadley Circulation changes and increasing global dryness due to CO2 warming from CMIP5 model projections. *Proceedings of the National Academy of Sciences*, **112**, 3630–3635.

Lejeune, Y., L. Bouilloud, P. Etchevers, P. Wagnon, P. Chevallier, J.-E. Sicart, E. Martin, and F. Habets, 2007: Melting of Snow Cover in a Tropical Mountain Environment in Bolivia: Processes and Modeling. *J. Hydrometeor.*, **8**, 922–937, doi:10.1175/JHM590.1.

Li, L., and Coauthors, 2013: The flexible global ocean-atmosphere-land system model, Grid-point Version 2: FGOALS-g2. *Adv. Atmos. Sci.*, **30**, 543–560.

Li, X., C.-H. Sui, D. Adamec, and K.-M. Lau, 1998: Impacts of precipitation in the upper ocean in the western Pacific warm pool during TOGA-COARE. *J. Geophys. Res.*, **103**, 5347–5359.

Li, X., D. M. Holland, E. P. Gerber, and C. Yoo, 2014: Impacts of the north and tropical Atlantic Ocean on the Antarctic Peninsula and sea ice. *Nature*, **505**, 538–542, doi:10.1038/nature12945.

Liebmann, B., and C.A. Smith, 1996: Description of a Complete (Interpolated) Outgoing Longwave Radiation Dataset. *Bull. Amer. Meteor. Soc.*, **77**, 1275–1277.

Lin, J.-L., 2007: Interdecadal variability of ENSO in 21 IPCC AR4 coupled GCMs. *Geophys. Res. Lett.*, **34**, L12702, doi:10.1029/2006GL028937.

Maes, C., J. Picaut, and S. Belamari, 2005: Importance of salinity barrier layer for the buildup of El Niño, *J. Climate*, **18**, 104–118.

Mann, H. B., 1945: Nonparametric tests against trend. *Econometrica*, **13**, 245–259.

Mann, M. E., R. S. Bradley, and M. K. Hughes, 2000: *Long-term variability in the El Niño/Southern Oscillation and associated teleconnections. El Niño and the Southern Oscillation: Multiscale Variability and Global and Regional Impacts*, H. F. Diaz and V. Markgraf, Eds., Cambridge University Press, 357–412.

Mark, B. G., J. M. McKenzie, and J. Gomez, 2005: Hydrochemical evaluation of changing glacier meltwater contribution to stream discharge: Callejon de Huaylas, Peru. *Hydrol. Sci. J.*, **50**, 975–87.

Masiokas, M. H., R. Villalba, B. H. Luckman, C. Le Quesne, and J. C. Aravena, 2006: Snowpack Variations in the Central Andes of Argentina and Chile, 1951–2005: Large-Scale Atmospheric Influences and Implications for Water Resources in the Region. *J. Climate*, **19**, 6334–6352.

Masiokas, M. H, R. Villalba, D. A. Christie, E. Betman, B. H. Luckman, C. Le Quesne, M. R. Prieto, and S. Mauget, 2012: Snowpack variations since AD 1150 in the

Andes of Chile and Argentina (30°–37°S) inferred from rainfall, tree-ring and documentary records. *J. Geophys. Res.*, **117**, doi:10.1029/2011JD016748.

McPhaden, M. J., S. E. Zebiak, and M. H. Glantz, 2006: ENSO as an integrating concept in earth science. *Science*, **314**, 1739–1745.

Meehl, G., H. Teng, and G. Branstator, 2006: Future changes of El Niño in two global coupled climate models. *Climate Dyn.*, **26**, 549–566.

Meehl, G. A., A. Hu, J. M. Arblaster, J. Fasullo, and K. E. Trenberth, 2013: Externally Forced and Internally Generated Decadal Climate Variability Associated with the Interdecadal Pacific Oscillation. *J. Climate*, **26**, 7298–7310.

Meehl, G. A., H. Teng, and J. M. Arblaster, 2014: Climate model simulations of the observed early-2000s hiatus of global warming. *Nature Climate Change*, **4**, 898–902.

Met Office, 2006: Met Office Global Radiosonde Data. NCAS British Atmospheric Data Centre, Accessed 4 January 2016. [Available online at https://badc.nerc.ac.uk/data/radiosglobe/southamerica.html]

Mitchell, D. M., P. W. Thorne, P. A. Stott, and L. J. Gray, 2013: Revisiting the controversial issue of tropical tropospheric temperature trends. *Geophys. Res. Lett.*, **40**, 2801–2806, doi:10.1002/grl.50465.

Morrissey, M. L., 1986: A Statistical Analysis of the Relationships among Rainfall, Outgoing Longwave Radiation and the Moisture Budget during January–March 1979. *Mon. Weather. Rev.*, **114**, 931–942.

Mountain Research Initiative EDW Working Group, 2015: Elevation-dependent warming in mountain regions of the world. *Nature Climate Change*, **5**, 424–430, doi:10.1038/nclimate2563.

Murphy, B. F., and B. Timbal, 2007: A review of recent climate variability and climate change in southeastern Australia. *International Journal of Climatology*, **28**, 859–879, doi:10.1002/joc.1627.

Newman, M., S.-I. Shin, and M. A. Alexander, 2011: Natural variation in ENSO flavors. *Geophys. Res. Lett.*, **38**, L14705, doi:10.1029/2011GL047658.

Nogues-Bravo, D., M. B. Araujo, M. P. Errea, and J. P. Martinez-Rica, 2007: Exposure of global mountain systems to climate warming during the 21st Century. *Global Environmental Change*, **17**, 420–428.

Norris, J. R., 2005: Multidecadal changes in near-global cloud cover and estimated cloud cover radiative forcing. *J. Geophys. Res.*, **110**, D08206, doi:10.1029/2004JD005600.

Oliver, E., 2015: Blind use of reanalysis data: apparent trends in Madden–Julian Oscillation activity driven by observational changes. *Int. J. Climatol.*, doi:10.1002/joc.4568.

Park, J.-Y., J.-S. Kug, J. Park, S.-W. Yeh, and C. J. Jang, 2011: Variability of chlorophyll associated with El Niño–Southern Oscillation and its possible biological feedback in the equatorial Pacific. *J. Geophys. Res.*, **116**, C10001, doi:10.1029/2011JC007056.

Penland, Cécile, and P. D. Sardeshmukh, 1995: The Optimal Growth of Tropical Sea Surface Temperature Anomalies. *J. Climate*, **8**, 1999–2024.

Pepin, N. C., and J. D. Lundquist, 2008: Temperature trends at high elevations: patterns across the globe. *Geophys. Res. Lett.*, **35**, doi:10.1029/2008GL034026.

Philander, S. G. 1989: *El Niño, La Niña, and the Southern Oscillation*. Academic Press, 293 pp.

Philipona, R., B. Dürr, A. Ohmura, and C. Ruckstuhl, 2005: Anthropogenic greenhouse forcing and strong water vapor feedback increase temperature in Europe. *Geophys. Res. Lett.*, **32**, L19809.

Picaut, J., M. Ioulalen, C. Menkes, T. Delcroix, and M. J. McPhaden, 1996: Mechanism of the Zonal Displacement of the Pacific warm pool: implications for ENSO. *Science*, **274**, 1486–1489.

Po-Chedley, S., and Q. Fu, 2012: Discrepancies in tropical upper tropospheric warming between atmospheric circulation models and satellites. *Environ. Res. Lett.*, **7**, doi:10.1088/1748-9326/7/4/044018.

Porter, J. R., and M. A. Semenov, 2005: Crop responses to climatic variation. *Phil. Trans. Roy. Soc. B*, **360**, 2021–2035.

Power, S. B., and R. Colman, 2006: Multi-year predictability in a coupled general circulation model. *Climate Dyn.*, **26**, 247–272.

Power, S., M. Haylock, R. Colman, and X. Wang, 2006: The Predictability of Interdecadal Changes in ENSO Activity and ENSO Teleconnections. *J. Climate*, **19**, 4755–4771.

Power, S. B., T. Casey, C. Folland, A. Colman, and V. Mehta, 1999: Interdecadal modulation of the impact of ENSO on Australia. *Climate Dyn.*, **15**, 319–324.

Prieto, R., R. Herrera, P. Doussel, L. Gimeno, P. Ribera, R. Garcia, and E. Hernandez, 2001: Interannual oscillations and trend of snow occurrence in the Andes region since 1885. *Australian Meteorological Magazine*, **50**, 164–168.

Quadro, M. F. L., E. H. Berbery, M. A. F. Silva Dias, D. L. Herdies, and L. G. G. Gonçalves, 2013: The atmospheric water cycle over South America as seen in the new generation of global reanalyses. *AIP Conf. Proc.*, **1531**, doi:10.1063/1.4804874.

Rabatel, A., and Coauthors, 2013: Current state of glaciers in the tropical Andes: a multi-century perspective on glacier evolution and climate change. *The Cryosphere*, **7**, 81–102.

Rangwala, I., 2013: Amplified water vapour feedback at high altitudes during winter. *Int. J. Climatol.*, **33**, 897–903.

Rangwala, I., J. Miller, and M. Xu, 2009: Warming in the Tibetan Plateau: possible influences of the changes in surface water vapor. *Geophys. Res. Lett.*, **36**, L06703.

Rangwala, I., J. Miller, G. L. Russell, and M. Xu, 2010: Using a global climate model to evaluate the influences of water vapor, snow cover and atmospheric aerosol on warming in the Tibetan Plateau during the twenty-first century. *Climate Dyn.*, **34**, 859–872.

Rapp, J. M., M. R. Silman, J. S. Clark, C. A. J. Girardin, D. Galiano, and R. Tito, 2012: Intra- and interspecific tree growth across a long altitudinal gradient in the Peruvian Andes. *Ecology*, **93**, 2061–2072.

Reichler, T., and J. Kim, 2008: How Well do Coupled Models Simulate Today's Climate? *Bull. Amer. Meteor. Soc.*, **89**, 303–311.

Ropelewski, C. F., and M. S. Halpert, 1987: Global and regional scale precipitation associated with El Niño/Southern Oscillation. *Mon. Wea. Rev.*, **115**, 985–996.

Rossow, W. B., and Schiffer, R. A., 1999: Advances in Understanding Clouds from ISCCP. *Bull. Amer. Meteor. Soc.*, **80**, 2261–2288.

Ruiz, J. J., C. Saulo, and J. Nogues-Paegle, 2010: WRF Model Sensitivity to Choice of Parameterization over South America:Validation against Surface Variables. *Mon. Weather. Rev.*, **138**, 3342–3355, doi:10.1175/2010MWR3358.1.

Russell, A. M., A. Gnanadesikan, 2014: Understanding Multidecadal Variability in ENSO Amplitude. *J. Climate*, **27**, 4037–4051, doi:10.1175/JCLI-D-13-00147.1.

Russell, A. A. Gnanadesikan, and B. Zaitchik, 2017: Are the Central Andes a warming hotspot? *Journal of Climate*, doi:10.1175/JCLI-D-16-0268.1, in press.

Saha, S., and Coauthors, 2010. The NCEP climate forecast system reanalysis. *Bull. Amer. Meteor. Soc.*, **910**, 1015–1057.

Santer, B. D., J. J. Hnilo, T. M. L. Wigley, J. S. Boyle, C. Doutriaux, M. Fiorino, D. E. Parker, and K. E. Taylor, 1999: Uncertainties in observationally based estimates of temperature change in the free atmosphere. *J. Geophys. Res.*, **104**, 6305–6333.

Schauwecker, S., and Coauthors, 2014: Climate trends and glacier retreat in the Cordillera Blanca, Peru, revisited. *Global Planet. Change*, **119**, 85–97.

Schiffer, R. A., and Rossow, W. B., 1983: The International Satellite Cloud Climatology Project (ISCCP): The First Project of the World Climate Research Programme. *Bull. Amer. Meteor. Soc.*, **64**, 779–784.

Schmidli, J., C. M. Goodess, C. Frei, M. R. Haylock, Y. Hundecha, J. Ribalaygua, and T. Schmith, 2007: Statistical and dynamical downscaling of precipitation: An

evaluation and comparison of scenarios for the European Alps. *Climate and Dynamics*, **112**, D04105, doi:10.1029/2005JD007026.

Schulz, N., J. P. Bosier, and P. Aceituno, 2012: Climate change along the arid coast of northern Chile. *Int. J. Climatol.*, **32**, 1803–1814, doi:10.1002/joc.2395.

Scoccimarro E., and Coauthors, 2011: Effects of Tropical Cyclones on Ocean Heat Transport in a High Resolution Coupled General Circulation Model. *J. Climate*, **24**, 4368–4384.

Seager, R. and M. Ting, **2017**: Decadal drought variability over North America: Mechanisms and predictability. *Curr. Clim. Change Rep.*: in press.

Seager R., N. Naik, W. Baethgen, A. Robertson, Y. Kushnir, J. Nakamura, S. Jurburg, 2010: Tropical oceanic causes of interannual to multidecadal precipitation variability in Southeast South America over the past century. *J. Climate*, **23**, 5517–5539, doi:10.1175/2010JCLI3578.1.

Seidel, D. J., Q. Fu, W. J. Randel, and T. J. Reichler, 2008: Widening of the tropical belt in a changing climate. *Nature Geoscience* **1**, 21–24, doi:10.1038/ngeo.2007.38.

Sen, P. K., 1968: Estimates of the regression coefficient based on Kendall's Tau. *Am. Stat. Assoc. J.*, **63**, 1379–1389.

Shook, K., and J. W. Pomeroy, 2012: Changes in the hydrological character of rainfall on the Canadian prairies. *Hydrol. Processes*, **26**, 1752–1766, doi:10.1002/hyp.9383.

Skamarock, W. C., and Coauthors, 2008: *A Description of the Advanced Research WRF Version 3*. NCAR Technical Note NCAR/TN-475+STR, doi:10.5065/D68S4MVH.

Sobel, A. H., and C. S. Bretherton, 2000: Modeling tropical precipitation in a single column. *J. Climate*, **13**, 4378–4392.

Sobel, A. H., J. Nilsson, and L. M. Polvani, 2001: The weak temperature gradient approximation and balanced tropical moisture waves. *J. Atm. Sci.*, **58**, 3650–3665.

Solman, S., 2013: Regional Climate Modeling over South America: A Review. *Adv. Meteor.*, **2013**, doi:10.1155/2013/504357.

Solman, S. A., and N. L. Pessacg, 2012: Evaluating uncertainties in regional climate simulations over South America at the seasonal scale. *Climate Dyn.*, **39**, 59–76.

Solman, S. A., and Coauthors, 2013: Evaluation of an ensemble of regional climate model simulations over South America driven by the ERA-Interim reanalysis: model performance and uncertainties. *Climate Dyn.*, **41**, doi:10.1007/s00382-013-1667-2.

Soruco, A., C. Vincent, A. Rabatel, B. Francou, E. Thibert, J. E. Sicart, and T. Condom, 2015: Contribution of glacier runoff to water resources of La Paz city, Bolivia (16° S). *Annals of Glaciology*, **56**, doi: 10.3189/2015AoG70A001.

Steinman, B. A., M. E. Mann, and S. K. Miller, 2015: Atlantic and Pacific multidecadal oscillations and Northern Hemisphere temperatures. *Science*, **347**, 998–991.

Stevenson, S., B. Fox-Kemper, M. Jochum, R. Neale, C. Deser, and G. Meehl, 2012: Will There Be a Significant Change to El Niño in the Twenty-First Century? *J. Climate*, **25**, 2129–2145.

Stevenson, S. L., 2012: Significant changes to ENSO strength and impacts in the twenty-first century: Results from CMIP5. *Geophys. Res. Lett.*, **39**, L17703, doi:10.1029/2012GL052759.

Stocker, T. F., and Coauthors, 2013: Technical Summary. In: *Climate Change 2013: The Physical Science Basis. Contribution of Working Group I to the Fifth Assessment Report of the Intergovernmental Panel on Climate Change* [Stocker, T.F., D. Qin, G.-K. Plattner, M. Tignor, S.K. Allen, J. Boschung, A. Nauels, Y. Xia, V. Bex and P.M. Midgley (eds.)]. Cambridge University Press, Cambridge, United Kingdom and New York, NY, USA.

Taylor, K. E., R. J. Stouffer, and G. A. Meehl, 2012: An overview of CMIP5 and the experiment design. *Bull. Amer. Meteor. Soc.*, **93**, 485–98.

Timmermann, A., J. Oberhuber, A. Bacher, M. Esch, M. Latif, and E. Roeckner, 1999: Increased El Niño frequency in a climate model forced by future greenhouse warming. *Nature*, **398**, 694–697.

Trenberth, K.E., and J. T. Fasullo, 2013: An apparent hiatus in global warming? *Earth's Future*, **1**, 19–32.

Trenberth, K. E., D. P. Stepaniak, J. W. Hurrell, and M. Fiorino, 2001: Quality of reanalyses in the Tropics. *J. Climate*, **14**, 1499–1510.

Trenberth, K. E, G. W. Branstator, D. Karoly, A. Kumar, N.-C. Lau, and C. Ropelewski, 1998. Progress during TOGA in understanding and modeling global teleconnections associated with tropical sea surface temperatures. *J. Geophys. Res.*, **103**, 14291–14324.

Unden, P., and Coauthors, 2002: HIRLAM-5 Scientific Documentation, Swedish Meteorological and Hydrological Institute Tech. Report, S-601 76, 144 pp.

Urrutia, R., and M. Vuille, 2009: Climate change projections for the tropical Andes using a regional climate model: Temperature and precipitation simulations for the end of the 21st century. *J. Geophys. Res.*, **114**, D02108, doi:10.1029/2008JD011021.

van Oldenborgh, G.J., et al., 2005: El Niño in a Changing Climate. *Ocean Science*, **1**, 81–95.

Vecchi, G. A., and B. J. Soden, 2007: Increased tropical Atlantic wind shear in model projections of global warming. *Geophys. Res. Lett.*, **34**, L08702, doi:10.1029/2006GL028905.

Verdon, D. C., A. M. Wyatt, and S. W. Franks, 2004: Multi-decadal variability of rainfall and streamflow: Eastern Australia. *Water Resour. Res.*, **40**, W10201, doi:10.1029/2004WR003234.

Vergara, W., A. M. Deeb, A. M. Valencia, R. S. Bradley, B. Francou, A. Zarzar, A. Grunwalt, and S. M. Haeussling, 2007: Economic Impacts of Rapid Glacier Retreat in the Andes. Eos Trans. AGU, **88**, 261–264.

Vimont, D. J., D. S. Battisti, and A. C. Hirst, 2002: Pacific interannual and interdecadal equatorial variability in a 1000-yr simulation of the CSIRO coupled GCM. *J. Climate*, **15**, 160–178.

Volodin, E. M., N. A. Dianskii, and A. V. Gusev, 2010: Simulating present-day climate with the INMCM4.0 coupled model of the atmospheric and oceanic general circulations. *Izv., Atmos. Oceanic Phys.*, **46**, 414–431.

Vuille, M., and R. S. Bradley, 2000: Mean annual temperature trends and their vertical structure in the tropical Andes. *Geophys. Res. Lett.*, **27**, 3885–3888, doi:10.1029/2000GL011871.

Vuille, M., R.S. Bradley, and F. Keimig, 2000a. Interannual climate variability in the Central Andes and its relation to tropical Pacific and Atlantic forcing. *J. Geophys. Res.*, **105**, 12447–12460.

Vuille, M., R.S. Bradley, and F. Keimig, 2000b: Climate variability in the Andes of Ecuador and its relation to tropical Pacific and Atlantic sea surface temperatures anomalies. *J. Climate*, **13**, 2520–2535.

Vuille, M., R. S. Bradley, M. Werner, and F. Keimig, 2003: 20th century climate change in the tropical Andes: observations and model results. *Climatic Change*, **59**, 75–99.

Vuille, M., B. Francou, P. Wagnon, I. Juen, G. Kaser, B. G. Mark, and R. S. Bradley, 2008: Climate change and tropical Andean glaciers: Past, present and future. *Earth-Sci. Rev.*, **89**, 79–96.

Vuille, M., E. Franquist, R. Garreaud, W. S. Lavado Casimiro, and B. Caceres, 2015: Impact of the global warming hiatus on Andean temperature. *J. Geophys. Res.*, **120**, 3745–3757.

Walland, D. J., S. B. Power, and A. C. Hirst, 2000: Decadal climate variability simulated in a coupled GCM. *Climate Dyn.*, **16**, 201–211.

Wang, B., and Y. Wang, 1996: Temporal structure of the Southern Oscillation as revealed by waveform and wavelet analysis. *J. Climate*, **9**, 1586–1598.

Wang, X. L., C. F. Ropelewski, 1995: An Assessment of ENSO-Scale Secular Variability. *J. Climate*, **8**, 1584–1599.

Wang, B., and J. C. L. Chan, 2002: How Strong ENSO Events Affect Tropical Storm Activity over the Western North Pacific. *J. Climate*, **15**, 1643–1658.

Watanabe, M., H. Shiogama, H. Tatebe, M. Hayashi, M. Ishii, and M. Kimoto, 2013: Contribution of natural decadal variability to global warming acceleration and hiatus. *Geophys. Res. Lett.*, **40**, 3175–3179.

Watanabe, M., and Coauthors, 2010: Improved Climate Simulation by MIROC5: Mean States, Variability, and Climate Sensitivity. *J. Climate*, **23**, 6312–6335, doi:10.1175/2010JCLI3679.1.

Wittenberg, A. T., A. Rosati, N.-C. Lau, and J. J. Ploshay, 2006: GFDL's CM2 global coupled climate models. Part III: Tropical Pacific climate and ENSO. *J. Climate*, **19**, 698–722.

Wittenberg, A. T., 2009: Are historical records sufficient to constrain ENSO simulations? *Geophys. Res. Lett.*, **36**, L12702, doi:10.1029/2009GL038710.

Wyrtki, K. 1975: El Niño – The dynamic response of the equatorial Pacific Ocean to atmospheric forcing. *J. Phys. Oceanogr.*, **5**, 572–584.

Yeh, S.-W., and B. P. Kirtman, 2004: The impact of internal atmospheric variability on the North Pacific SST variability. *Climate Dyn.*, **22**, 721– 732.

Yeh, S.-W., B. P. Kirtman, and S.-I. An, 2004: Local versus non-local atmospheric weather noise and the North Pacific SST variability. *Geophys. Res. Lett.*, **34**, L14706, doi:10.1029/2007GL030206.

Yeh, S.-W., J.-S. Kug, B. Dewitte, M.-H. Kwon, B. P. Kirtman, and F.-F. Jin, 2009: El Niño in a changing climate. *Nature*, **461**, 511–514.

Yue, S., and P. Pilon, 2004: A comparison of the power of the t test, Mann–Kendall and bootstrap tests for trend detection. *Hydrol. Sci. J.*, **49**, 21–37.

Yukimoto, S., and Y. Kitamura, 2003: An investigation of the irregularity of El Niño in a coupled GCM. *J. Meteor. Soc. Japan.*, **81**, 599– 622.

Zelle, H., G. Appeldoorn, G. Burgers, and G. J. van Oldenborgh, 2004: The relationship between sea surface temperature and thermocline depth in the eastern equatorial Pacific. *J. Phys. Oceanogr.*, **34**, 643–655.

Zhang S., M.J. Harrison, A. Rosati, and A.T. Wittenberg, 2007: System design and evaluation of coupled ensemble data assimilation for global oceanic climate studies. *Mon. Weather. Rev.*, **135**, 3541–3564.

Zhang, Y., and Coauthors, 2016: Multi-decadal trends in global terrestrial evapotranspiration and its components. *Nature*, **6**, 19124, doi: 10.1038/srep19124.

Zhao, M., I. M. Held, S.-J. Lin, and G.A.Vecchi, 2009: Simulations of global hurricane climatology, interannual variability, and response to global warming using a 50-km resolution GCM. *J. Climate*, **22**, 6653–6678.

# Vita

Alexandria ("Alexi") M. Russell was born in Detroit, Michigan in 1989 and grew up in Broomfield, Colorado. In 2011 she received a B. S. degree in Environmental Science from the University of Oregon where she was also a student of the Robert D. Clark Honors College. In 2014, Alexi received a M. A. in Earth and Planetary Science from Johns Hopkins University and then continued on in the department to complete a Ph. D. in 2017. Her research interests lie in the fields of numerical weather prediction, remote sensing and precipitation dynamics. Starting in spring 2017, Alexi will work as an Atmospheric Modeler at Northrop Grumman Corporation, where she will work toward improving the modeling of cloud interference for optical communications and imaging applications.